UNIVERSITAT POLITÈCNICA DE VALÈNCIA

INSTITUTO INTERUNIVERSITARIO DE INVESTIGACIÓN DE RECONOCIMIENTO MOLECULAR Y DESARROLLO TECNOLÓGICO

Development of molecular and nanostructured sensors for illicit drug detection

PhD THESIS

Submitted by

Eva María Garrido García

PhD Supervisors:

Prof. María Dolores Marcos Martínez

Prof. Félix Sancenón Galarza

Prof. Ramón Martínez Máñez

Valencia, July 2022

MARÍA DOLORES MARCOS MARTÍNEZ, PhD in Chemistry and Professor at the *Universitat Politècnica de València*, FÉLIX SANCENÓN GALARZA PhD in Chemistry and Professor at the *Universitat Politècnica de València* and RAMÓN MARTINÉZ MÁÑEZ PhD in Chemistry and Professor at the *Universitat Politècnica de València*.

CERTIFY:

That the work *"**Development of molecular and nanostructured sensors for illicit drug detection.**"* has been developed by Eva María Garrido García under their supervision in the Instituto Interuniversitario de Investigación de Reconocimiento Molecular y Desarrollo Tecnológico (IDM) of the *Universitat Politècnica de València*, as a Thesis Project in order to obtain the degree of PhD in Chemistry at the *Universitat Politècnica de València.*

Valencia, July 2022.

Prof. María Dolores Marcos Martínez

Prof. Félix Sancenón Galarza

Prof. Ramón Martínez Máñez

A mi familia por darle sentido a mi vida.

A ti por darle sentido a todo.

*«Soy de las que piensan que **la ciencia tiene una gran belleza**. Un científico en su laboratorio no es sólo un técnico: **es también un niño colocado ante fenómenos naturales** que le impresionan como un cuento de hadas.»*

Marie Curie

*«Sería posible describir todo científicamente, **pero no tendría ningún sentido**; carecería de significado el que usted describiera a la sinfonía de **Beethoven como una variación de la presión de la onda auditiva.**»*

Albert Einstein

*«Son nuestras **elecciones** las que muestran lo que somos, mucho más que nuestras **habilidades**.»*

Albus Dumbledore

«El auténtico valor es vivir y sufrir por lo que uno cree.»

Christopher Paolini

ACKNOWLEDGEMENTS

Aún no me puedo creer que después de 5 años haya llegado al final de una etapa que desde luego marcará un antes y después en mi vida. No solo por el gran crecimiento personal y profesional, sino por la enorme cantidad de personas que se han cruzado en mi camino para enriquecerlo con grandes momentos y recuerdos que sé, serán para toda la vida.

En primer lugar, me gustaría agradecer al Prof. Ramón Martínez Máñez por confiar en mí, darme la oportunidad de desarrollar esta PhD Tesis en su fantástico grupo de investigación y por siempre apoyar mis ideas. Además, agradecer a mis otros dos directores de tesis, la Prof. María Dolores Marcos Martínez y el Prof. Félix Sancenón Galarza por ayudarme a sumergirme en este "nanomundo" y aprender de ellos.

Agradecer al Prof. Knut Rurack por darme la oportunidad de realizar mi estancia predoctoral en su grupo y motivarme a indagar en este gran mundo de la investigación. Gracias Estela, por ayudarme a exprimir al máximo esos tres meses de estancia que fueron una bocada de aire fresco en el momento perfecto. Gracias por estar tan pendiente de mí, por enseñarme Berlín y por hacer aún más especial esta experiencia.

Por otro lado, todo esto no habría sido posible sin las increíbles personas que forman este grupo y que me han ayudado a superarme día tras día en el Lab 2.6, os voy a llevar siempre conmigo. Desde Eva Brun, Enrique, Tania y Arantxa que ponen orden en todo ese caos de pedidos, facturas, trámites y papeleos que nos vuelven locos en muchos momentos y que, sin ellos, hubiera sido imposible sacar adelante. De verdad, gracias. Y qué decir de mis chicxs que me han acompañado durante a veces incluso 10 horas o más al día entre esas cuatro paredes que nos han unido en momentos de estrés, de risas (son la mayoría), de lluvias y achicar agua, en fin, en miles y miles de momentos que recordaré siempre. Me gustaría hacer especial mención a algunos de ellos que sin duda se han convertido en personas muy importante para mí, por no decir familia.

Borja y María, gracias por todo vuestro apoyo desde el primer momento, por hacer que esta tesis sea posible y, sobre todo, gracias por aconsejarme y estar siempre ahí para mí. Gracias Borja por los momentos de risas con la música de Bricomanía en bucle, por las carreras de sillas, por el rafting, por la san silvestre y por todos los momentos de estos años. Gracias María por las charlas interminables, por darle luz a mis rayadas y por calmarme y escucharme siempre.

Andrea B. fuiste la primera persona con la que empecé en este mundo de la nanotecnología y la primera que me ayudó al llegar al laboratorio en esos primeros días de adaptación. Gracias por enseñarme, dedicarme tiempo y, sobre todo, gracias por las cenas llenas de risas y de mucho vino 😊.

Xente y Bea de Luis, mil gracias a los dos porque habéis sido pilares fundamentales para mí en estos años de tesis. Me llevo mil momentos con vosotros y cualquier cosa que pueda decir se queda corta. Así que, simplemente os quiero y ha sido un placer compartir esta experiencia con vosotros.

Gracias al equipo comunicación, Paula, Andrea E., Javi y Yoel (dímelo tú 😜) por los cotilleos, las conversaciones en la bancada, por ayudarme siempre, aconsejarme, por todos los momentos, comidas, cenas, en definitiva, gracias por todo. Paula, gracias por escucharme siempre, por las conversaciones hasta las mil, por las excursiones buscando vestido, por todas nuestras charlas políticas y por un sinfín de cosas más. Te quiero un montón, amiga. Javi, sin duda, un gran descubrimiento como amigo, gracias por el apoyo, los consejos y por siempre estar ahí. Gracias, por tanto.

Gracias al equipo de sensores, Guillermo, Giovanni, Marcia y JuanFran, por todo el apoyo, ayuda y por soportar mis charlas interminables en las reuniones. A Giovanni gracias por hacerme desconectar en momentos estresantes con esos partidos de pádel y haciéndome reír en el lab, no sabes cuánto te lo agradezco.

Guille, ¿qué decirte?, aunque tu nerviosismo y locura a veces me estrese más de la cuenta, gracias por todo lo que me has enseñado con todas nuestras charlas y, sobre todo, gracias por simplemente estar.

Gracias de corazón a Blanca y Elena L. por los viajes, las confidencias, el apoyo, las multas jajaja. En definitiva, gracias por estar siempre ahí.

Además, gracias a mis chicas de la CPI, Angy y a la brava de Serena, sois lo más. Edgar, Cris T., Sameh, Carol, Elena, Carmen, Amelia, Santi, Lorena, Ismael, Hazem, Toni, Vicente, Luis Villaescusa, Luis Pla, Bea Lozano, Adrián, Elisa, Andy, Ismael, Marta, Pablo, Miguel, Sara R., Sara Santiago, Araceli, Alejandra, Alba G., Gema, Javi M., Iris, Isa, Nieves, Marina, Alba L., Mari Carmen, Gonçalo, Molud, Kobra, en definitiva, muchísimas gracias a todxs y cada una de las personas que me han acompañado en estos años.

Gracias a mis amigas andaluzas, Miriam, Belén y Ana por apoyarme en todo y estar siempre ahí. Todo lo que os diga es poco, os quiero divas 😊.

Gracias infinitas a mis padres, Juan y Eva, y a mi hermano por ser mi fuente inagotable de ánimos, de apoyo, de cariño y por darme la oportunidad de llegar hasta donde he llegado. Sin duda, nada de esto sería posible sin cada uno de vosotros.

Gracias a Oliver por tus palabras de apoyo y tus consejos. Gracias India 😊.

Gracias abuelxs, os quiero.

Gracias a ti, Miki, porque esta aventura te puso en mi camino y no he podido ser más afortunada de compartirla contigo. Gracias por cada día darme una parte de ti, hacerme mejorar y permitirme compartir todo contigo.

Gracias Max y Kiara porque distéis luz a mi oscuridad.

ABSTRACT

RESUMEN

La presente tesis titulada “Desarrollo de sensores moleculares y nanoestructurados para la detección de estupefacientes” es una tesis realizada por compendio de artículos de investigación que se centran en la síntesis, caracterización, evaluación y aplicación en ensayos de *lateral-flow* de sensores moleculares, así como, de distintos sistemas híbridos orgánicos-inorgánicos basados en nanopartículas de sílice mesoporosa (MSNs) capaces de producir una respuesta fluorogénica ante la presencia de estímulos exógenos específicos como serían las drogas de abuso para su detección en diferentes medios competitivos.

En el primer capítulo, se establece una visión general de los tipos de drogas de abuso existentes, así como, sus principales características y la importancia del desarrollo de nuevos métodos para detectarlas debido a que, en los últimos años, su consumo ha crecido de forma exponencial convirtiéndose en un problema que preocupa tanto a gobiernos como a instituciones internacionales. Además, se presenta una visión general del campo de la nanotecnología, más particularmente de los materiales mesoporosos de sílice funcionalizados con puertas moleculares (basadas en anticuerpos y complejos supramoleculares receptor-sustrato) capaces de controlar la liberación de diferentes moléculas encapsuladas y su potencial aplicación como herramientas multifuncionales en el campo de los sensores, así como, una descripción general de sistemas de detección basados en complejos de metales de transición.

A continuación, en el segundo capítulo se enumeran los principales objetivos generales a conseguir durante el desarrollo de la presente tesis doctoral y que se abordan en los siguientes capítulos experimentales.

En el tercer capítulo se presenta un nanodispositivo para la detección fluorimétrica del estupefaciente 25I-NBOMe (25I-N-metoxibencil) en golosinas. El sistema consta de MSNs cargadas con un fluoróforo (rodamina B) y funcionalizadas

en su superficie externa con un derivado de serotonina. Finalmente, los poros son bloqueados completamente por la interacción del derivado de serotonina anclado en la superficie con el anticuerpo del receptor 5-HT_{2A} que actúa como puerta molecular. La liberación selectiva del colorante encapsulado se produce en presencia de 25I-NBOMe debido a una competencia entre el derivado de serotonina anclado y el analito por la coordinación con el anticuerpo del receptor 5-HT_{2A}. La respuesta obtenida con el nanosensor es muy selectiva y con límites de detección bajos. Además, el nanosensor se ha empleado con éxito para detectar 25I-NBOMe en dulces adulterados.

En el cuarto capítulo se llevó a cabo la preparación y caracterización de un nanosensor híbrido orgánico-inorgánico para la detección fluorogénica selectiva y sensible de 3,4-metilendioxipirovalerona (MDPV), comúnmente conocida como droga caníbal. El nanodispositivo está basado en MSNs cargadas con un colorante fluorescente (rodamina B), y funcionalizadas en su superficie externa con un derivado de dopamina, que interactúa específicamente con el transportador de dopamina (DAT), bloqueando los poros. En presencia de MDPV, se produce la inhibición del reconocimiento entre el derivado de dopamina y el DAT que se desprende consecuentemente de las MSNs, provocando la liberación de rodamina B y permitiendo la detección de la droga. El nanodispositivo se ha empleado con éxito para la detección de MDPV en muestras de saliva y plasma sanguíneo.

El quinto capítulo muestra el diseño de una sencilla tira portátil de doble canal usando nanomateriales híbridos para la detección *in situ* y simultánea de escopolamina y MDPV. La detección de estas drogas en saliva se lleva a cabo mediante la cuantificación del colorante liberado empleando un dispositivo smartphone. El nanosensor se basa en MSNs cargadas con un colorante fluorescente (rodamina B) y con la superficie externa funcionalizada con betanecol (agonista del receptor muscarínico de acetilcolina M2/CM2 (M_2-AChR)). Al añadir el receptor M_2-AChR se produce el tapado de los poros debido a la interacción

específica con el derivado de betanecol. El mecanismo de detección se basa en la coordinación selectiva de la escopolamina con el receptor M_2-AChR abriéndose los poros y liberando el fluoróforo atrapado. El nanodispositivo se integró en un ensayo de *lateral-flow*, junto con el sensor desarrollado para MDPV, para la detección de ambos analitos en muestras de saliva.

En el sexto capítulo se presenta un sensor molecular para la detección de GHB en bebidas alcohólicas, basado en un complejo de Cu^{2+} coordinado con un ligando tetradentado y un colorante fluorescente, cumarina 343. El mecanismo de detección se basa en un ensayo de desplazamiento del indicador (*IDA*) donde en ausencia de GHB, la fluorescencia del colorante cumarina 343 se encuentra desactivada mientras que en presencia de GHB se produce el desplazamiento de la cumarina 343 del complejo, recuperando, por tanto, la fluorescencia. Este sistema se incorporó a una tira reactiva en un ensayo de *lateral-flow* capaz de detectar GHB en refrescos y bebidas alcohólicas en menos de 1 minuto en presencia de otras drogas comunes.

Por último, en el capítulo 7 se presentan las conclusiones generales. Los estudios realizados mostraron que estas sondas (que pueden ser simples moléculas o sistemas más sofisticados que involucran biomoléculas en materiales híbridos orgánico-inorgánicos) proporcionan excelentes ventajas sobre las técnicas analíticas tradicionales, tales como su simplicidad química, facilidad de uso, respuestas rápidas adecuadas para la detección *in situ* en tiempo real haciendo que la aplicación de estos sistemas suponga un prometedor avance para la detección precoz de casos de sumisión química o de adulteración de muestras con drogas de abuso difícilmente detectables.

RESUM

La present tesi titulada “Desenvolupament de sensors moleculars i nanoestructurats per a la detecció d'estupefaents” és una tesi realitzada per compendi d'articles d'investigació que se centren en la síntesi, caracterització, avaluació i aplicació en assajos tipus *lateral-flow* de sensors moleculars, així com, de diferents sistemes híbrids orgànics-inorgànics basats en nanopartícules de sílice mesoporosa (MSNs) capaços de produir una resposta fluorogénica davant la presència d'estímuls exògens específics com serien les drogues d'abús per a la seua detecció en diferents medis competitius.

En el primer capítol, s'estableix una visió general dels tipus de drogues d'abús existents, així com, les seues principals característiques i la importància del desenvolupament de nous mètodes per a detectar-les a causa del creixement exponencial del seu consum en els últims anys, que s'ha convertit en un problema que preocupa tant a governs com a institucions internacionals. A més, es presenta una visió general del camp de la nanotecnologia, més particularment dels materials mesoporosos de sílice funcionalitzats amb portes moleculars basades en anticossos i complexos supramoleculars receptor-substrat capaços de controlar l'alliberament de diferents molècules encapsulades i la seua potencial aplicació com a eines multifuncionals en el camp dels sensors, així com, una descripció general de sistemes de detecció basats en complexos de metalls de transició.

A continuació, en el segon capítol s'enumeren els principals objectius generals a aconseguir durant el desenvolupament de la present tesi doctoral i que s'aborden en els següents capítols experimentals.

En el tercer capítol es presenta un nanodispositiu per a la detecció fluorimètrica de l'estupefaent 25I-NBOMe (25I-N-metoxibencil) en llepolies. El sistema consta de MSNs carregades amb un fluorofore (rodamina B) i funcionalitzades en la seua superfície externa amb un derivat de serotonina.

Finalment, els porus són bloquejats completament per la interacció del derivat de serotonina ancorat a la superfície amb l'anticòs del receptor 5-HT_{2A} que actua com a porta molecular. L'alliberament selectiu del fluorofore encapsulat es produeix en presència de 25I-NBOMe a causa d'una competència entre el derivat de serotonina ancorat i l'anàlit per la coordinació amb l'anticòs del receptor 5-HT_{2A}. La resposta obtinguda es molt selectiva i amb limits de detecció baixos. Per altra banda, el nanosensor ha estat utilitzat amb exit per a detectar 25I-NBOMe en llepolies adulterades.

En el quart capítol es va dur a terme la preparació i caracterització d'un nanosensor híbrid orgànic-inorgànic per a la detecció fluorogénica selectiva i sensible de 3,4-metilendioxipirovalerona (MDPV), comunament coneguda com a droga caníbal. El nanodispositiu està basat en MSNs carregades amb un colorant fluorescent (rodamina B), i funcionalitzades en la seua superfície externa amb un derivat de dopamina, que interactua específicament amb el transportador de dopamina (DAT), bloquejant els porus. En presència de MDPV, es produeix la inhibició del reconeixement entre el derivat de dopamina i el DAT que es desprén conseqüentment de les MSNs, provocant l'alliberament de rodamina B permetent la detecció de la droga. El nanodispositiu ha estat utilitzat amb exit per a detectar MDPV en mostres de saliva i plasma sanguini.

En el cinqué capítol s'ha dissenyat una senzilla tira portàtil de doble canal usant nanomaterials híbrids per a la detecció in situ i simultània de escopolamina i MDPV. La detecció de aquestes drogues en saliva es du a terme mitjançant la utilització d'un dispositiu *smartphone*. El nanosensor es basa en MSNs carregades amb un colorant fluorescent (rodamina B) i amb la superfície externa functionalitzada amb un derivat de betanecol (agonista del receptor muscarínic d'acetilcolina M2/CM2 (M_2-AChR)). En presencia de M_2-AChR es tapen els porus a causa de la interacció específica amb el derivat de betanecol. El mecanisme de detecció es basa en el desplaçament del receptor M_2-AChR induït per la presència

d'escopolamina que produeix la apertura dels porus i l'alliberament de la rodamina B. El nanodispositiu es va integrar en un assaig *lateral-flow*, juntament amb el sensor desenvolupat per a MDPV, per a la detecció de tots dos anàlits en mostres de saliva.

En el sisé capítol es presenta un sensor molecular per a la detecció de GHB en begudes alcohòliques, basat en un complex de Cu^{2+} coordinat amb un lligand tetradentat i un colorant fluorescent, cumarina 343. El mecanisme de detecció es basa en un assaig de desplaçament de l'indicador (*IDA*) on en absència de GHB, la fluorescència del colorant cumarina 343 es troba desactivada mentre que en presència de GHB es produeix el desplaçament de la cumarina 343 del complex recuperant, per tant, la fluorescència. Aquest sistema es va incorporar a una tira reactiva en un assaig *lateral-flow* capaç de detectar GHB en refrescos i begudes alcohòliques en menys d'1 minut en presència d'altres drogues comunes.

Finalment, en el capítol setè es presenten les conclusions generals. Els estudis realitzats van mostrar que aquestes sondes (que poden ser simples molècules o sistemes més sofisticats que involucren biomolècules en materials híbrids orgànic-inorgànics) proporcionen excel·lents avantatges sobre les tècniques analítiques tradicionals, com son la seua simplicitat química, facilitat d'ús, respostes ràpides i adequades per a la detecció in situ en temps real fent que l'aplicació d'aquests sistemes supose un prometedor avanç per a la detecció precoç de casos de submissió química o d'adulteració de mostres amb drogues d'abús difícilment detectables.

ABSTRACT

This PhD thesis entitled "Development of molecular and nanostructured sensors for the detection of illicit drugs" is a compendium by research articles that focus on the synthesis, characterisation, evaluation and application in lateral-flow assays of molecular sensors, as well as different hybrid organic-inorganic systems based on mesoporous silica nanoparticles (MSNs) able to generate a fluorogenic response in the presence of specific exogenous stimuli such as abuse drugs for their detection in different competitive environments.

In the first chapter, an overview about the different types of abuse drugs is given, as well as their main characteristics and the importance of new detection methods due to the exponential growth of their consumption in recent years, which has become a serious issue for governments and international institutions. In addition, a general view relate to metal complexes as sensor and nanotechnology is presented, more particularly about mesoporous silica materials functionalised with molecular gates based on antibodies and supramolecular receptor-substrate complexes capable of controlling the release of a wide variety encapsulated molecules and their potential application as multifunctional tools in the field of sensors.

Then, the second chapter describes the main general objectives to be achieved during the development of this PhD thesis, which are addressed in the following experimental chapters.

The third chapter presents a nanodevice for the fluorimetric detection of 25I-NBOMe (25I- N-methoxybenzyl) in candies. The system consists of MSNs loaded with a fluorophore (rhodamine B) and functionalised on their external surface with a serotonin derivative. Finally, the pores are completely capped by the interaction of the surface-anchored serotonin derivative with the 5-HT_{2A} receptor antibody

acting as a molecular gate. In the presence of 25I-NBOMe, the encapsulated rhodamine B is selectively released due to the competition between the anchored serotonin derivative and the analyte for coordination with the 5-HT_{2A} receptor antibody. The response obtained with the nanosensor is quite selective and with low detection limits. Besides, the nanodevice was successfully used to detect 25I-NBOMe in adulterated candies.

In the fourth chapter, the preparation, and characterisation of a hybrid organic-inorganic nanosensor for the highly selective and sensitive fluorogenic detection of 3,4-methylenedioxypyrovalerone (MDPV), commonly known as cannibal drug, was carried out. The nanodevice is based on MSNs loaded with a fluorescent reporter (rhodamine B) and functionalised on their outer surface with a dopamine derivative, which specifically interacts with the dopamine transporter (DAT), capping the pores. In the presence of MDPV, recognition inhibition occurs between the dopamine derivative and the DAT that is consequently detached from the MSNs, leading to the release of rhodamine B and the drug detection. The nanosensor was successfully used for MDPV detection in saliva and blood plasma samples.

In the fifth chapter, a straightforward portable dual-track strip using nanomaterials has been designed for *in situ* and simultaneous detection of scopolamine and MDPV. Detection of both drugs in saliva samples was achieved by quantifying the released dye using a smartphone device. The nanosensor for MDPV detection is based on MSNs loaded with a fluorescent dye (rhodamine B) and a bethanechol derivative (an agonist of the muscarinic acetylcholine receptor M2/CM2 (M_2-AChR)) grafted onto the external surface of the nanoparticles. Pores were capped after addition of M_2-AChR due to its preferential coordination with the grafted bethanechol. The detection mechanism is based on the inhibition of the bethanechol derivative coordination because scopolamine forms a strong complex

with M_2-AChR receptor. The nanodevice was integrated into a lateral-flow assay, together with the MDPV sensor for both analytes detection in saliva samples.

The sixth chapter presents a molecular sensor for the GHB detection in alcoholic beverages, based on a Cu^{2+} complex coordinated with a tetradentate ligand and a fluorescent dye, coumarin 343. The detection mechanism is based on an indicator displacement assay (*IDA*) where in the absence of GHB, the fluorescence of the coumarin 343 dye is quenched while in the presence of GHB, coumarin 343 is displaced from the complex, thus recovering the fluorescence. This system was incorporated into a test strip in a lateral-flow assay capable of detecting GHB in soft drinks and alcoholic beverages in less than 1 minute in the presence of other common drugs.

Finally, general conclusions are presented in Chapter seven. The studies performed showed that these probes (which can be from simple molecules to more sophisticated systems involving biomolecules in organic-inorganic hybrid materials) provide excellent advantages over traditional analytical techniques, such as their chemical simplicity, ease of use, rapid responses suitable for real-time *in situ* detection whereby the application of these systems is a promising advance for the early detection of chemical submission cases or adulteration of samples with hardly detectable abuse drugs.

PUBLICATIONS

The results obtained in this PhD thesis belong to the following scientific publications.

Lozano-Torres, B., Galiana, I., Rovira, M., **Garrido, E.**, Chaib, S., Bernardos, A., Muñoz-Espín, D., Serrano, M., Martínez-Máñez, R., Sancenón, F. "An OFF−ON Two-Photon Fluorescent Probe for Tracking Cell Senescence in Vivo." *Journal of de American Chemical Society*, **2017**, *139*, 8808-8811.

Garrido, E., Pla, L., Lozano-Torres, B., El Sayed, S., Martínez-Máñez, R., Sancenón, F. "Chromogenic and Fluorogenic Probes for the Detection of Illicit Drugs." *ChemistryOpen*, **2018**, *7*, 401-428.

Alfonso, M., **Garrido, E.**, Sancenón, F., Martínez-Máñez, R. "Metal complexes as sensors." *Reference Module in Chemistry, Molecular Sciences and Chemical Engineering*, **2020**.

Garrido, E., Alfonso, M., Díaz de Greñu, B., Lozano-Torres, B., Parra, M., Gaviña, P., Marcos, M. D., Martínez-Máñez, R., Sancenón, F. "Nanosensor for Sensitive Detection of the New Psychedelic Drug 25I-NBOMe." *Chemistry-A European Journal*, **2020**, *26*, 2813-2816.

Garrido, E., Alfonso, M., Díaz de Greñu, B., Marcos, M. D., Costero, A. M., Gil, S., Sancenón, F., Martínez-Máñez, R. "A Sensitive Nanosensor for the In Situ Detection of the Cannibal Drug." *ACS Sensors*, **2020**, *5*, 2966-2972.

Garrido, E., Hernández-Sigüenza, G., Climent, E., Marcos, M. D., Rurack, K., Sancenón, F., Martí-Centelles, V., Martínez-Máñez, R. "GHB sensing in strips by lateral flow test using a dye-displacement assay." Submitted. **2022**

Garrido, E., Climent, E., Marcos, M. D., Sancenón, F., Rurack, K., Martínez-Máñez, R. "Selective dualplex lateral flow assay for simultaneous scopolamine and cannibal drug detection based on receptor-gated mesoporous nanoparticles." Submitted. **2022**

ABBREVIATIONS AND ACRONYMS

5-HT	5-hydroxytryptamine
AChE	Acetylcholine
AMF	Alternating magnetic field
APTES	3-aminopropyltriethoxysilane
BET	Brunauer-Emmet-Teller
BJH	Barret-Joyner-Halenda
CB1	Cannabinoid type 1 receptor
CB2	Cannabinoid type 2 receptor
CTAB	Cetyltrimethylamonium bromide
^{13}C-NMR	Carbon-13 nuclear magnetic resonance
DA	Dopamine
DFP	Diisopropyl fluorophosphate
DLS	Dynamic light scattering
DMT	N,N-dimethyltryptamine
EA	Elemental Analysis
EMCDDA	European Monitoring Centre for Drug Addiction
FDA	Food and Drug Administration
FTIR	Fourier-transform infrared spectroscopy
GABA	γ-aminobutyric acid
GC-MS	Gas Chromatography-Mass Spectrometry
GHB	Gamma-hydroxybutyric acid
HCl	Hydrochloric acid
^{1}H-NMR	Hydrogen-1 nuclear magnetic resonance
IR	Infrared
IUPAC	International Union of Pure and Applied Chemistry
LC-MS	Liquid chromatography-mass spectrometry
LFA	Lateral flow assay
LOD	Limit of detection
LSD	Lysergic acid diethylamide
MCM	Mobile Composition of Matter

MDMA	3,4-methylenedioxymethamphetamine
MDPV	Methylenedioxypyrovalerone
MSNs	Mesoporous Silica Nanoparticles
M41S	Molecular 41 sieves
NDMA	Dimethylnitrosamine
NPS	Nanoparticles
PBS	Phosphate buffer saline
PCP	Phencyclidine
PMOs	Periodic mesoporous organosilicas
PXRD	Powder x-ray diffraction
QTOF	Quadrupole Time of Flight
Rh	Rhodamine
SDAS	Structural-directing agents
TEM	Transmission electron microscopy
TEOS	Tetraethyl orthosilicate
TGA	Thermogravimetric analysis
THC	Tetrahydrocannabinol
TMOS	Tetramethyl orthosilicate
UHPLC-MS/MS	Ultra-high-performance liquid chromatography-mass spectrometer
UNODC	United Nations Office on Drugs and Crime
VMAT-2	Vesicular monoamine transporter 2
WHO	World Health Organization
λ_{exc}	Excitation wavelength
λ_{em}	Emission wavelength

Table of Contents

CHAPTER 1

GENERAL INTRODUCTION

1.1. New Psychoactive Drugs

According to FDA, new psychoactive substances (NPS) are a complex, heterogeneous, and ever-growing group of compounds often known as either designer or synthetic drugs and more popular referred to as *legal highs*, *bath salts* and *research chemicals*.[1,2] Furthermore, NPS are legal or illegal abuse drugs, structurally analogues of existing controlled drugs, pharmaceutical products or newly synthesised chemicals, that have been typically consumed for their psychoactive effects and are often associated with dependence and addiction. Since the late 1980s, these substances were well-known as *designer drugs*, to refer to various synthetic opioid drugs, based mostly on the fentanyl molecule. However, it was not until 2005 when the term *new psychoactive drugs* was coined by the

[1] World drug report United Nations Office on Drugs and Crime (UNODC). Inform; **2020**.
[2] European drug report Trends and Developments. European Monitoring Centre for Drugs and Drug addition (EMCDDA). Inform; **2020**.
[3] Feng, L.-Y.; Battulga, A.; Han, E.; Chung, H.; Li, J.-H. *J Food Drug Anal*, **2017**, *25*, 461-471.

European community.[3] Clearly, *new* does not necessarily relate to an innovative compound but can also refer to those substances synthesized some years ago and recently come back to the limelight in the trafficking of abuse drugs.

Consequently, because of their number, nature and composition assumes a significant challenge for the worldwide forensic community and, more broadly, researchers, toxicologists, healthcare systems and drug control policy. Among these substances, marijuana, tobacco, cocaine, heroin, steroids, methamphetamine, as well as prescription drugs like opioids, dextromethorphan, and stimulants can be highlighted for their widespread use as well as their impact on public health.

1.1.1. Occurrence, control, and consumption of NPS

Notwithstanding the strict control on designer drugs worldwide, a great variety (in type and number) of NPS are continuously emerging in the recreational drug market, in the deliberate attempt of manufacturers to evade drug legislation. This fact combined with the flexibility of modern chemistry allows for an almost inexhaustible supply of alternative illicit drugs. In the 1920s, Second International Opium Convention specifically banned morphine and the diacetyl ester of morphine, heroin, as well as a number of alternative morphine esters quickly started to be manufactured and sold. This then led the Health Committee of the League of Nations to pass several resolutions attempting to bring these new drugs under control, ultimately leading in 1930 to the first broad analogues provisions extending legal control to all esters of morphine, oxycodone, and hydromorphone.[4]

[4] King, L. A.; Kicman, A. T. *Drug Test Anal*, **2011**, *3*, 401-403.

Later, during the 1960s and 1970s, several new synthetic hallucinogens were introduced.

Thus, *Comprehensive Drug Abuse Prevention and Control Act* of 1970 was promulgated in the United States whereby the manufacture, importation, possession, and distribution of certain drugs were regulated. In addition, the legislation established five categories depending on the acceptable medical use of the drug and the drug's potential for abuse or dependence. The abuse rate is a determinate factor in the scheduling of the drug; for example, Schedule I drugs have a high potential for abuse and the potential to create severe psychological and/or physical dependence. As the drug schedule changes-Schedule II, Schedule III, etc., so does the abuse potential-Schedule V drugs represents the least potential for abuse. Some examples of drugs in each classification would be:[5]

- **Schedule I.** Heroin, lysergic acid diethylamide (LSD), marijuana (cannabis), 3,4-methylenedioxymethamphetamine (MDMA or ecstasy), methaqualone, and peyote.
- **Schedule II.** Cocaine, methamphetamine, methadone, hydromorphone, meperidine, oxycodone, fentanyl, Dexedrine, Adderall, and Ritalin.
- **Schedule III.** Ketamine, anabolic steroids, testosterone.
- **Schedule IV.** Xanax, Soma, Darvon, Darvocet, Valium, Ativan, Talwin, Ambien, Tramadol.
- **Schedule V.** Cough preparations with less than 200 milligrams of codeine as Lomotil, Motofen, Lyrica, Parepectolin.

During the last 30 years, international control has been extended from plant-based drugs (heroin, cocaine, and cannabis) to synthetic drugs (amphetamines, 3,4-methylenedioxymethamphetamine, etc.) and pharmaceutical

[5] Peacock, A.; Bruno, R.; Gisev, N.; Degenhardt, L.; Hall, W.; Sedefov, R.; White, J.; Thomas, K. V.; Farrell, M.; Griffiths, P. *Lancet*, **2019**, *394*, 1668-1684.

drugs (buprenorphine, methadone, benzodiazepines, etc.). Until mid-2012, the majority of the identified NPS were synthetic cannabinoids (23 per cent), phenethylamines (23 per cent) and synthetic cathinones (18 per cent), followed by tryptamines (10 per cent), plant-based substances (8 per cent) and piperazines (5 per cent). Particularly, the single most widespread substances were JWH-018 and JWH-073 among the synthetic cannabinoids; mephedrone, MDPV and methylone among the synthetic cathinones; and *m*-chlorophenylpiperazine, *N*-benzylpiperazine and 1-(3-trifluoromethylphenyl)piperazine among the piperazines. Plant-based substances included mostly kratom, khat and Salvia divinorum.

In this way, between 2009 and 2017, 111 countries and territories reported a total of 803 individual NPS to the United Nations Office on Drugs and Crime (UNODC) and European Monitoring Centre for Drugs and Drug Addiction (EMCDDA) (see Figure 1). At the same time, popular compounds as synthetic cannabinomimetics, psychostimulant derivatives of cathinone (β-ketamines) and new benzodiazepines have gained attention on the recreational drug market. Hence, NPS are a major challenge for laboratories, not only because of the large numbers of NPS, but also due to the continuous chemical development of the substances and thus, the rapid turnover of the drug market.[6]

Therefore, the consumption has risen drastically since the late 2000s worldwide. According to World Drug Report 2020 around 269 million people have used drugs in 2018, which corresponds to 5.4% global population aged 15-64.[1] Amongst these, around 35.6 million people are estimated to suffer from drug-associated disorders which correspond to a global prevalence of drug-use disorders

[6] Evans-Brown, M.; Hughes, B.; Sedefov, R. *Novel Psychoactive Substances (Second Edition), Academic Press*, **2022**, 3-56.

[7] Tracy, D. K.; Wood, D. M.; Baumeister, D. *Bmj*, **2017**, *356*, i6848.

of 0.7% of the population aged 15-64 (see Figure 2).[7] The problematic use of these illicit drugs is associated with considerable mortality, morbidity and several health disorders.

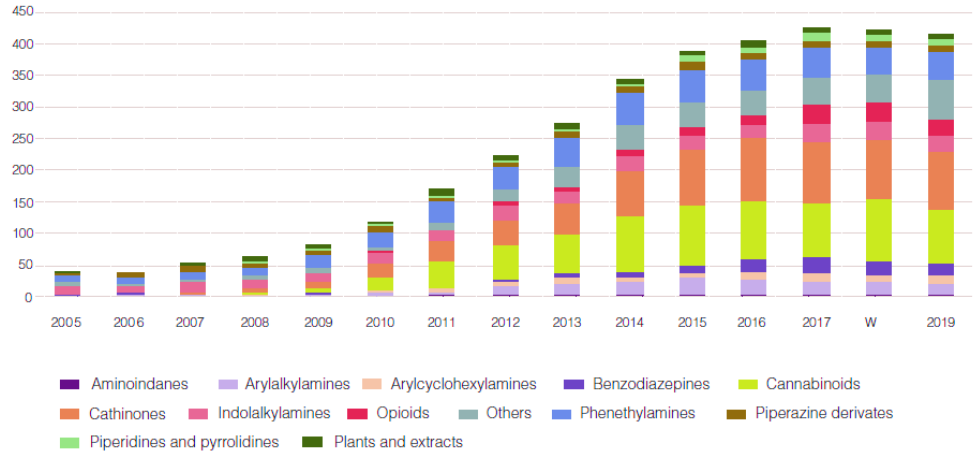

Figure 1. Growth in each category of controlled illicit drug in the 2000s. *Reprinted from Legal classification and international systems for monitoring and responding to novel psychoactive substances, Copyright (2022), with permission from Elsevier.*

Besides the public health problems of traditional illicit drugs, NPS pose an additional serious public health threat, mainly because of the huge lack of knowledge about their toxicity, about the limit between a "safe" dose and a fatal dose, and about the unknown adverse health effects they produce.[8] Furthermore, the identity of the NPS is generally unknown by the drug users because the new products containing NPS provide no or little information about their composition.[9] In addition, specially concerning but common cases involve the consumption of NPS

[8] Kraemer, M.; Boehmer, A.; Madea, B.; Maas, A. *Forensic Sci Int*, **2019**, *298*, 186-267.
[9] Lavelle, S. *Arch Psychiatr Nurs*, **2016**, *30*, 447-448.
[10] Pelletier, R.; Le Daré, B.; Grandin, L.; Couette, A.; Ferron, P. J.; Morel, I.; Gicquel, T. *Clin Toxicol (Phila)*, **2021**, 1-4.

in combination with other drugs (including other NPS and/or traditional illicit drugs) either consciously or unconsciously (as "adulterants" of these drugs of abuse).[10]

Nonetheless, the number of new NPS detections has decreased in recent years and, in addition, the nature of the market has changed, with a relative decrease in the number of new stimulants and synthetic cannabinoids detected, and an increase in the numbers of new opioids and benzodiazepines available.[11] The rapidly changing profile of the NPS market raises concerns over uncertainty and ambiguity regarding their chemical, metabolic and toxicity profiles, and the associated physical, social and mental health harms.[12]

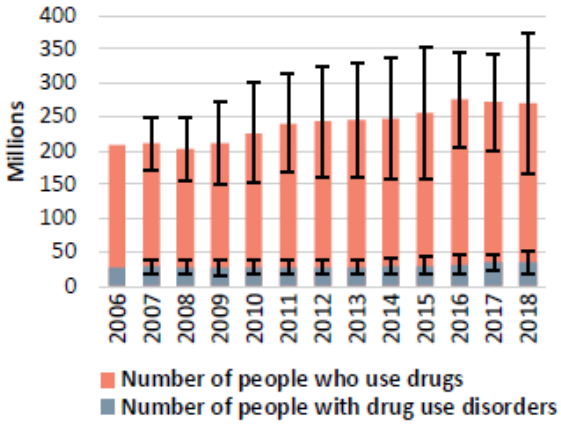

Figure 2. Global use of new psychoactive substances, 2006-2018. *Adapted from World drug report United Nations Office on Drugs and Crime (UNODC). Inform; 2020.*

1.1.2. Types, mechanism of action and effects of NPS

According to UNODC and EMCDDA, new psychoactive substances can be classified according to their psychoactive effects as stimulants or hallucinogens as

[11] Madras, B. K. *Curr Top Behav Neurosci*, **2017**, *32*, 1-18.
[12] Ahmed, S. H.; Badiani, A.; Miczek, K. A.; Müller, C. P. *Neurosci Biobehav Rev*, **2020**, *110*, 3-27.

well as according to their chemical family.[13] Currently, compounds are classified on the basis of their common pharmacological action rather than by their similar chemical structures. The substances have a fairly broad spectrum of dopaminergic, noradrenergic or serotonergic action, even within their chemical family. Consequently, the clinical psychotropic and toxicological effects are also very diverse and vary considerably from one drug to another. Based on this, NPS can be classified into four main groups namely stimulants (e.g., cocaine and amphetamine), synthetic cannabinoids or antipsychotics (e.g., Δ^9-tetrahydrocannabinol), hallucinogens (e.g., lysergic acid diethylamide and tryptamines) and depressants (e.g., benzodiazepines and opiates) (see Figure 3).[14,15]

Subsequently, the main characteristics, the mode of action and the main effects of each of the different types of NPS are shown.

[13] Zapata, F.; Matey, J. M.; Montalvo, G.; García-Ruiz, C. *Microchem J*, **2021**, *163*, 105877.
[14] Shafi, A.; Berry, A. J.; Sumnall, H.; Wood, D. M.; Tracy, D. K. *Ther Adv Psychopharmacol,* **2020**, *10*, 2045125320967197-2045125320967197.
[15] Langman, L. J.; Snozek, C. L. H. *Chapter 6-Critical Issues in Alcohol and Drugs of Abuse Testing (Second Edition)*, Dasgupta, A. Ed.; Academic Press, **2019**, 71-78.

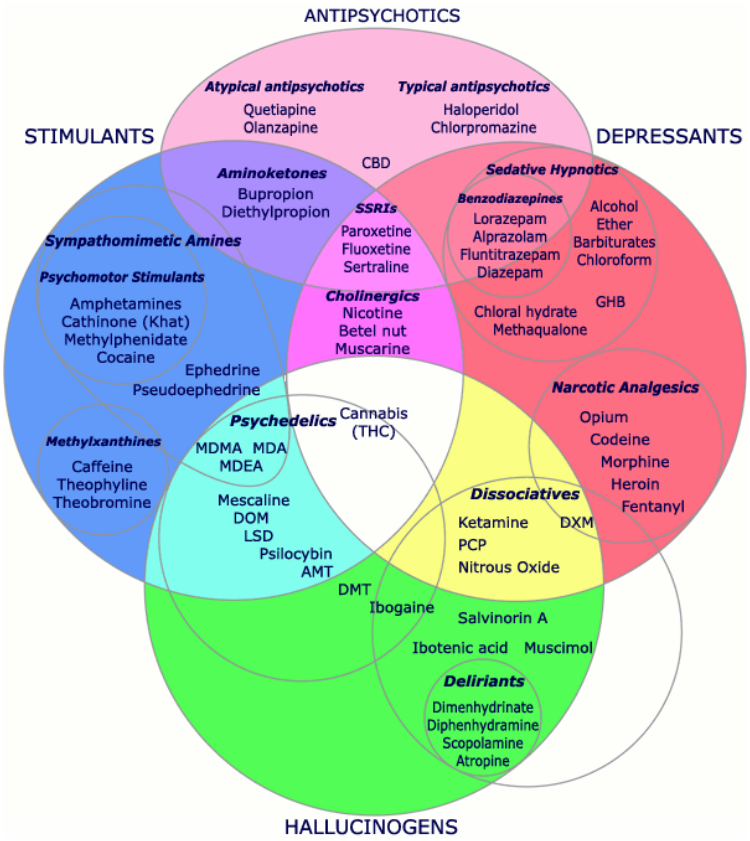

Figure 3. Representative chart of the most relevant psychoactive substance types.

STIMULANTS

Since 2009, stimulants have comprised the main category (36%) of NPS reported to the UNODC early warning advisory.[16] They are a diverse illicit drug class that act on the central nervous system and enhances the function of the three main monoamine neurotransmitters: serotonin, dopamine and/or noradrenaline. Inside this substances group are traditional stimulant controlled drugs, such as cocaine, MDMA and amphetamines as well as some NPS as cathinones (mephedrone, methylenedioxypyrovalerone (MDPV) and methylone), aminoindanes,

[16] Luethi, D.; Liechti, M. E. *Arch Toxicol*, **2020**, *94*, 1085-1133.

phenethylamines (NBOMe and 2C-series), piperazines and tryptamines (see Figure 4).[17]

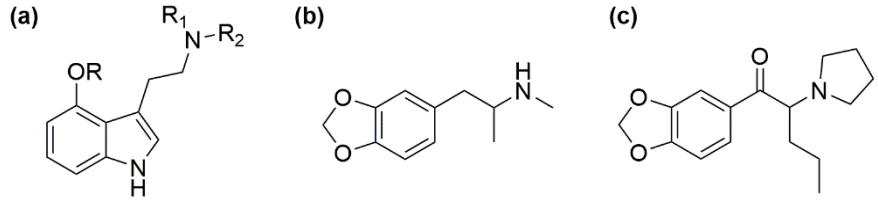

Figure 4. Chemical structure of the principal stimulant drugs, (a) tryptamines, (b) MDMA and (c) MDPV.

Metabolically, synthetic stimulants promote an increase in synaptic activity of neurotransmitters, mainly dopamine (DA) and serotonin (5-HT). DA plays an important role in motivation, arousal, learning and reward, whereas 5-HT is a contributor to feelings of happiness and a sense of emotional connectedness (entactogenic). Two distinct mechanisms are responsible for the increase in monoamine concentration in the synaptic cleft. Firstly, there is stimulation of non-exocytotic neurotransmitter release by inhibiting the vesicular monoamine transporter-2 (VMAT-2) and reversing the transporter influx, thereby stimulating neurotransmitter release from the cytosolic pool or synaptic vesicles. Secondly, there is an inhibition of the uptake of neurotransmitters from the synaptic cleft by inhibiting the plasma membrane transporters, which are responsible for the uptake of DA, 5-HT and NE.[18,19]

As a result of this, stimulants speed up mental and physical processes, which can produce desirable effects in the short-term by increasing levels of dopamine in the brain. Particularly, the main effects are euphoric, agitation, nausea, vomiting, headache, palpitations, tachycardia, hypertension, and

[17] Graddy, R.; Buresh, M. E.; Rastegar, D. A. *Med Clin North Am*, **2018**, *102*, 697-714.
[18] Iversen, L.; White, M.; Treble, R. *Neuropharmacology*, **2014**, *87*, 59-65.
[19] Schifano, F.; Papanti, G. D.; Orsolini, L.; Corkery, J. M. *Expert Rev Clin Pharmacol*, **2016**, *9*, 943-954.

hyperthermia, and less frequently as paranoia, hallucinations, seizures, and collapse (see Figure 5).[20,21]

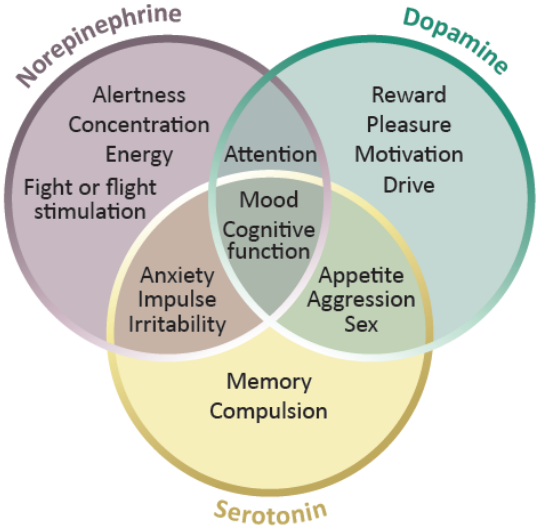

Figure 5. Effects produced by altering the activity of the three major neurotransmitters. *Adapted from World drug report United Nations Office on Drugs and Crime (UNODC). Inform; 2019.*

SYNTHETIC CANNABINOIDS

Cannabis is the most widely psychoactive product obtained from the plant *Cannabis Sativa* used established recreational drug for over 4000 years. This substance is controlled under the Single Convention on Narcotic Drugs of 1961 as amended by the 1972 Protocol (Schedules I and IV) which includes Δ^9-tetrahydrocannabinol (THC) as major psychoactive component.[22]

[20] Mohamed, W. M.; Ben Hamida, S.; Cassel, J. C.; de Vasconcelos, A. P.; Jones, B. C. *Pharmacol Biochem Behav*, **2011**, *99*, 759-774.
[21] Ross, E. A.; Reisfield, G. M.; Watson, M. C.; Chronister, C. W.; Goldberger, B. A. *Am J Med*, **2012**, *125*, 854-858.
[22] Zawilska, J. B.; Andrzejczak, D. *Drug Alcohol Depend*, **2015**, *157*, 1-17.

In the last decades, the composition of these herbal products seems to have substantially changed to include potent NPS known as synthetic cannabinoids. Some of the most noteworthy synthetic analogues of THC are HU-210, that is considered to have a potency of at least 100 times, and aminoalkylindoles such as naphthoylindoles (JWH-018), phenylacetylindoles (JWH-250), and benzoylindoles (AM-2233). Another group of synthetic cannabinoids termed non-classical include cyclohexylphenols or 3-arylcyclohexanols (see Figure 6). [23] While cannabis and THC are controlled under the international drug control treaties, none of the synthetic cannabinoids are currently regulated.

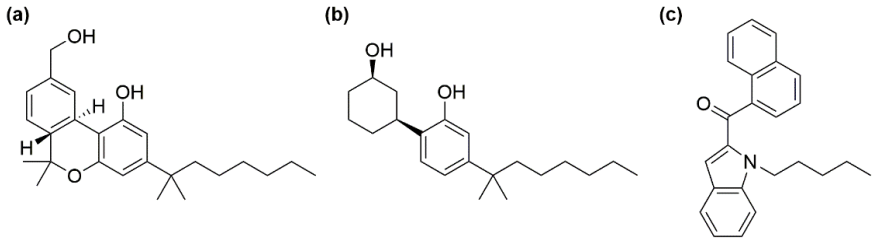

Figure 6. Chemical structure of the most common synthetic cannabinoids: (a) HU-210 (classical cannabinoid), (b) CP-47,497 (non-classical cannabinoid), (c) JWH-018 (aminoalkylindoles).

In this regard, the most frequent adverse effects reported from users are nausea, prolonged vomiting, agitation, drowsiness, dizziness, confusion, hypertension, tachycardia, and chest pain, which are usually of limited duration. The reason for this is that synthetic cannabinoids interact primarily with the endocannabinoid system and its two specific G-protein-coupled receptors: predominantly with the cannabinoid receptor type 1 (CB1) and to a lesser extent with the cannabinoid receptor type 2 (CB2).[24]

- **HALLUCINOGENS**

[23] Lafaye, G.; Karila, L.; Blecha, L.; Benyamina, A. *Dialogues Clin Neurosci*, **2017**, *19*, 309-316.
[24] Tamama, K.; Lynch, M. J. *Handb Exp Pharmacol* **2020**, *258*, 463-502.

Hallucinogens are a broad group of naturally occurring and synthetic drugs that induce distorted states of consciousness, perception, thinking and feeling, accompanied by different degrees of auditory or visual hallucinations. Synthetic hallucinogens include two main subcategories: classic hallucinogens (LSD, mescaline, psilocybin, bufotenine and DMT) and dissociatives (ketamine, phencyclidine (PCP), methoxetamine and diarylethylamine) (see Figure 7).[25]

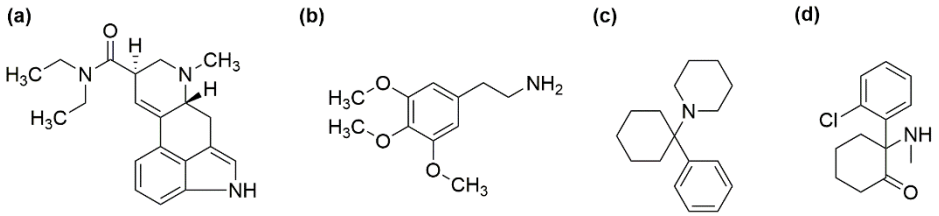

Figure 7. Chemical structure of main hallucinogen and dissociative drugs: (a) LSD, (b) Mescaline, (c) PCP and (d) ketamine.

Historically, some of these drugs have been used in religious rituals because they cause the user to see and hear things that are non-existent and unreal, making them feel out of control or disconnected from their body and environment. In particular, some of their most prominent effects are produced in the prefrontal cortex, an area involved in mood, cognition and perception, as well as in other areas of the brain important in the regulation of arousal and physiological responses. These drugs can be found in some plants, mushrooms or can be man-made. LSD, psilocybin and DMT produce their effects through interaction with serotonin (5-HT) receptors. Others, the most common dissociative drugs, affect the *N*-methyl-d-aspartate receptor (NDMA receptor), the *k*-opioid receptor and the neurotransmitter acetylcholine.[26]

[25] De Gregorio, D.; Enns, J. P.; Nuñez, N. A.; Posa, L.; Gobbi, G. *Chapter 3-Progress in Brain Research*, Calvey, T. *Elsevier*, **2018**, *242*, 69-96.
[26] Evan J. Kyzar; Allan V. Kalueff, *Zebrafish*, **2016**, *13*, 379-390.

Most of the common hallucinogens are controlled under the Convention on Psychotropic Substances of 1971, although some synthetic hallucinogens are not currently under international control and are labelled as NPS. Ketamine is an example of non-controlled substance that is included in the World Health Organization (WHO) list of essential medicines.

- **DEPRESSANT**

The last group of NPS are depressant drugs. Depressant drugs account for a wide variety of compounds that decrease the central nervous system activity resulting in a sedative effect.[27] Thus, they can be classified into two major subcategories: benzodiazepines and opiates including compounds such as γ-hydroxybutyrate (GHB), fentanyl, heroin, barbiturates, among others (see Figure 8).[28]

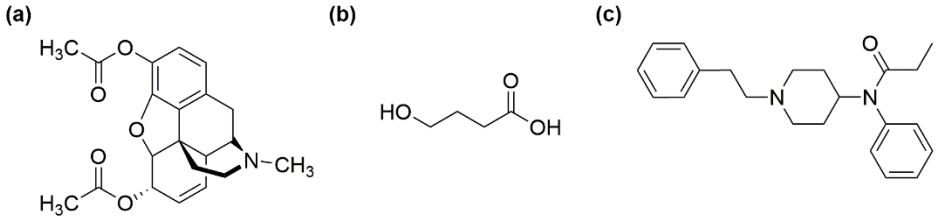

Figure 8. Chemical structure of (a) heroin, (b) GHB and (c) fentanyl.

Pharmacologically, depressants exert their effects through a number of different mechanisms, the most prominent of which include facilitation of GABA, and inhibition of glutamatergic or monoaminergic activity. Specifically, benzodiazepines mediate their effects through interactions with gamma-aminobutyric acid (GABA-A) receptors. GABA-A receptors are ion channels consisting of different subunits that respond to the inhibitory neurotransmitter

[27] Janis, G. *Chapter 15-Toxicology Cases for the Clinical and Forensic Laboratory*, Ketha, H., Garg, U. Eds.; *Academic Press*, **2020**, 269-276.
[28] Zawilska, J. B.; Wojcieszak, J. *NeuroToxicology*, **2019**, *73*, 8-16.

GABA. In this way, synthetic benzodiazepines can potentiate the effects of GABA as positive allosteric modulators by binding to a receptor site that is different from the GABA binding site leading to sedative, hypnotic (sleep-inducing), anxiety, anticonvulsant, and muscle relaxant effects.[29]

Unlike synthetic benzodiazepines, opioids are able to interact with G protein-coupled receptors in the brain and spinal cord as partial to full agonists at mu, delta and kappa opioid receptor subtypes, with selectivity for the mu opioid receptor.

In brief, the main mechanisms of action of the drug groups identified are shown in Figure 9.

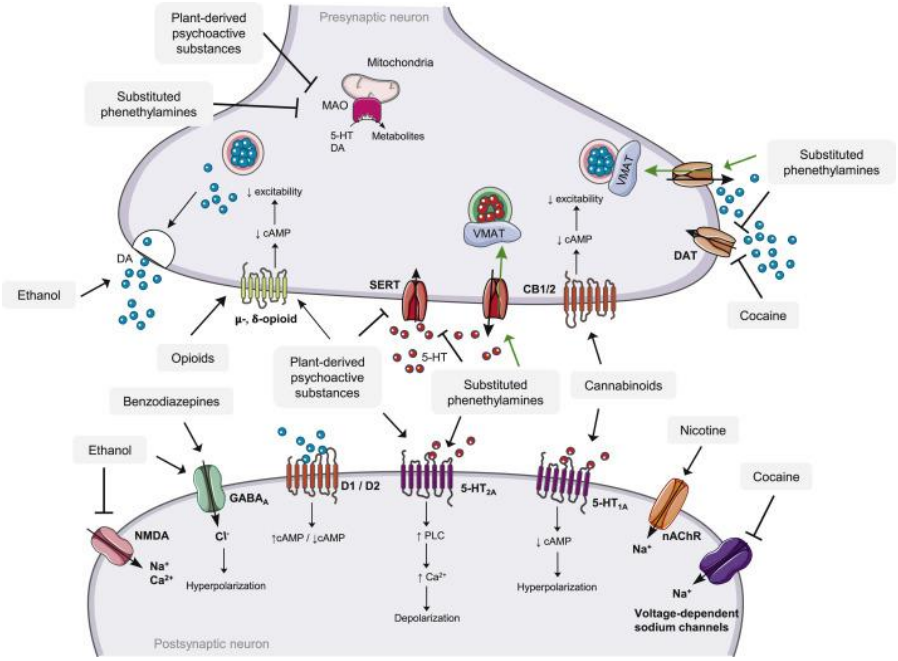

Figure 9. Representative diagram of the pharmacodynamic pathways of the most common substances of abuse. *Reprinted from Current Opinion in Toxicology* ***2021****, 28, 76-83, Copyright (2021), with permission from Elsevier.*

[29] Dias da Silva, D.; Silva, J. P.; Carmo, H.; Carvalho, F. *Current Opinion in Toxicology*, **2021**, *28*, 76-83.

1.1.3. NPS Detection Methods

Based on the above, the development of highly sensitive and selective methods capable of detecting recreational substances in different biological samples (urine, saliva, hair, or plasma blood) as well as in complex matrices (urban wastewater, sweet or alcoholic beverages) has become a challenging task in order to reduce the non-responsible use of substances with a high impact on health and society.[30]

Over the last years, several analytical methods have been developed and published for the identification and/or quantification of a wide range of NPS belonging to different chemical classes. Colorimetric tests based on gold-nanoparticles,[31,32] metal transition complexes or molecular probes,[33] immunoassays[34] and mass spectrometry-based techniques[35] have been employed in the detection of NPS. In this regard, liquid chromatography with quadrupole time of flight mass spectrometry (LC-QTOF-MS) has demonstrated better selectivity, with lower detection limits in the range 0.01-3.00 ng/mL, than gas chromatography mass spectroscopy (GC-MS) in detecting most forms of NPS within serum, blood and hair samples.[36] Another method for the analysis of NPS in whole blood after protein precipitation was automated solid phase extraction (SPE) and dispersive liquid-liquid microextraction coupled to ultra-high-performance liquid

---

[30] Smith, J. P.; Sutcliffe, O. B.; Banks, C. E. *Analyst*, **2015**, *140*, 4932-4948,
[31] Bahram, M.; Madrakian, T.; Alizadeh, S. *J Pharm Anal,* **2017**, *7*, 411-416.
[32] Masemola, D. P.; Mafa, P. J.; Nyoni, H.; Mamba, B. B.; Msagati, T. A. M. *J Environ Sci Health B,* **2020**, *55*, 455-461.
[33] Rodríguez-Nuévalos, S.; Costero, A. M.; Arroyo, P.; Sáez, J. A.; Parra, M.; Sancenón, F.; Martínez-Máñez, R. *Chem Commun (Camb),* **2020**, *56*, 12600-12603.
[34] Graziano, S.; Anzillotti, L.; Mannocchi, G.; Pichini, S.; Busardò, F. P. S. *J. Pharm. Biomed*, **2019**, *163*, 170-179.
[35] Garrido, E.; Pla, L.; Lozano-Torres, B.; El Sayed, S.; Martínez-Máñez, R.; Sancenón, F. *ChemistryOpen,* **2018**, *7*, 401-428.
[36] Mercolini, L. *Chapter 20-Critical Issues in Alcohol and Drugs of Abuse Testing (Second Edition)*, Dasgupta, A. Ed.; *Academic Press*, **2019**, 247-258.

chromatography tandem mass spectrometry (UHPLC-MS/MS), using minimal amount of organic solvent as a miniaturized alternative blood sample preparation.

Likewise, colorimetric methods based on lateral flow assay integrated smartphone-based portable device (LFA) have emerged currently as an innovative technique for the simultaneous NPS detection in complex matrix. Similarity, nanomaterials are bringing important advances in the design of these novel biosensing systems or improvements of the existing devices. The principal advantages are easy to use, portable, point-of-use tests, with limited need for sample pre-preparation. On the other hand, the main disadvantages include user variability in detecting colour-changes, cross-reactivity (associated with false-positive results), in addition to the limited range of individual NPS compounds that may be tested for in a single sample.[37,38,39]

Compared with the traditional analysis method, the developed LFA reader is easier operated, lower cost, no qualified personnel required and more portable, which provided an on-site quantitative analysis tool.

[37] Fojtíková, L.; Šuláková, A.; Blažková, M.; Holubová, B.; Kuchař, M.; Mikšátková, P.; Lapčík, O.; Fukal, L. *Toxicol Rep*, **2018**, *5*, 65-75.
[38] Qriouet, Z.; Cherrah, Y.; Sefrioui, H.; Qmichou, Z. *Molecules*, **2021**, *26*.
[39] McNeill, L.; Megson, D.; Linton, P. E.; Norrey, J.; Bradley, L.; Sutcliffe, O. B.; Shaw, K. J. *Forensic Chem.*, **2021**, *26*, 100370.

1.2. Nanotechnology

Nanotechnology has emerged as a promising alternative that enables, in a controllable way, not only to create nanomaterials but also to operate them. Conceptually, nanotechnology is the term given to those areas of science and engineering aimed at the development, control, and implementation of materials at nanoscale dimensions (1-100 nm) with unique properties that are used in the design, characterisation, production and application of structures, devices and systems in multiples science fields and daily life. To get an idea, a nanometre is equivalent to one billionth of a metre (1 nm = 10^{-9} m); a sheet of paper is approximately 100,000 nanometres thick.[40] As a result, the application of nanotechnology has studded every nook and corner of human life with multiple value-added products. In the natural world, there are many examples of structures that exist with nanometre dimensions, including from essential molecules within the human body such as cells, DNA, atoms, to some components of foods (see Figure 10). Although many technologies have incidentally involved nanoscale structures for many years, it has only been in the last quarter of a century that it has been possible to actively modify molecules and structures within this size range.

[40] Khan, S.; Mansoor, S.; Rafi, Z.; Kumari, B.; Shoaib, A.; Saeed, M.; Alshehri, S.; Ghoneim, M. M.; Rahamathulla, M.; Hani, U.; et al. *J Mol Liq*, **2021**, 118008.

It is this control at the nanometre scale that distinguishes nanotechnology from other areas of technology.

The first mention of purposely created and applied technological processes and means, which were subsequently termed nanotechnology, is usually connected with the well-known conference of Mr. Richard Feynman (Nobel Prize Laureate in Physics in 1965), professor in Institute of technology at Californian University, delivered in 1959 at the meeting of the American Physical Society.[41] In this lecture called "*There is a lot of space down there*" for the first time the possibility to create nanosized products with the use of atoms as building particles was considered. Currently, this lecture is referred to as the origin of the nanotechnological paradigm.

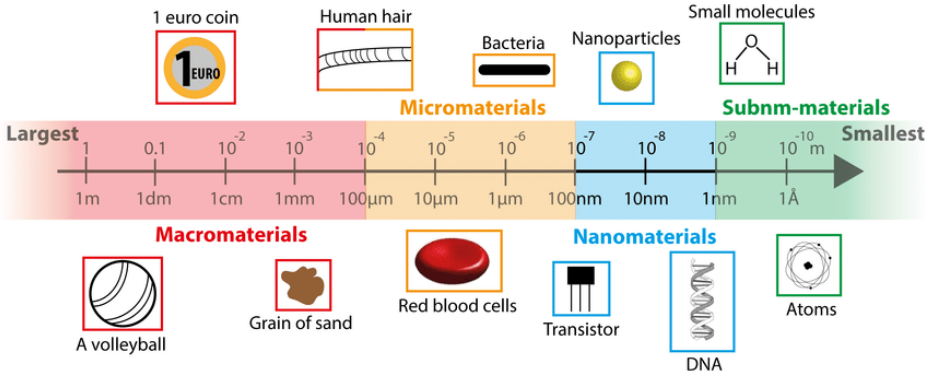

Figure 10. Illustration of the size range from macromaterials to nanomaterials. *Adapted from Brullot Ward, Development, synthesis and characterization of multifunctional nanomaterials, PhD Dissertation, Ku Leuven, 2014.*

On the other hand, in 1974 the word *nanotechnology* was introduced for the first time into a scientific world by Norio Taniguchi at the international conference about industrial production in Tokyo in order to describe semiconductor processes with nanometer accuracy and the creation of nano-sized

[41] Hulla, J. E.; Sahu, S. C.; Hayes, A. W. *Hum Exp Toxicol*, **2015**, *34*, 1318-1321.

mechanisms. His definition still stands as the basic statement today: *"Nanotechnology mainly consists of the processing of separation, consolidation, and deformation of materials by one atom or one molecule."*.[42]

Nanomaterials have been with us since the beginning of mankind. The first evidence of nanomaterials was when cementite nanowires were discovered in the microstructure of wootz steel made in ancient India. Later, the science of nanotechnology was advanced further when Iijima, a Japanese scientist, developed carbon nanotubes.[43] Another key factor has been the development of fullerenes in the 1980s by Kroto, Smalley and Curl.[44] Nevertheless, it was not until the beginning of 21st century when an increased interest in the emerging nanoscience and nanotechnology fields was observed.[45] For example, materials in the form of very thin films used in catalysis and electronics, two-dimensional nanotubes and nanowires for optical and magnetic systems, as well as nanoparticles used in cosmetics, pharmaceuticals and coatings. The industrial sectors most readily embracing nanotechnology are the information and communications sector, including electronic and optoelectronic fields, food technology, energy technology and the medical products sector, including many different facets of pharmaceuticals and drug delivery systems, diagnostics, and medical technology, where the terms nanomedicine and bio-nanotechnology are already commonplace. Noteworthy in this field, biosensors based on nanomaterials, which represent the integration of materials science, molecular engineering, chemistry, and biotechnology that can significantly improve the sensitivity and specificity of biomolecule detection, have the ability to detect or manipulate atoms and

[42] Bayda, S.; Adeel, M.; Tuccinardi, T.; Cordani, M.; Rizzolio, F. *Molecules*, **2019**, *25*.
[43] Aqel, A.; El-Nour, K. M. M. A.; Ammar, R. A. A.; Al-Warthan, A. *Arab J Chem*, **2012**, *5*, 1-23.
[44] Kroto, H. W., Heath, J. R., O'Brien, S.C., Curl, R. F., Smalley, R. E. *Nature*, **1985**, *318*, 162-163.
[45] Goroff, N. S. *Acc Chem Res*, **1996**, *29*, 77-83.

molecules, and great potential in applications such as biomolecule recognition, pathology diagnostics and environmental monitoring.

Clearly the various forms of nanotechnology possess the potential to generate a very significant impact on society. In general, it may be assumed that the application of nanotechnology will be very beneficial to individuals and organisations. Many of these applications involve new materials which provide physical, chemical, and biological radically unusual properties through functioning at the nanoscale, where new phenomena are associated with the very high surface area-volume ratios experienced at these dimensions and with quantum effects that are not seen with larger sizes. These properties may differ significantly from that of bulk materials and single atoms or molecules. In this sense, composites made from particles of nano-size ceramics or metals smaller than 100 nanometers can suddenly become much stronger than predicted by existing materials-science models.[46] This can be an advantage for some applications, such as catalysing reactions on their surface or functionalising them with a high percentage of biomolecules to develop more sensitive biosensors.[47] Additionally, due to their small size, nanoparticles can penetrate inside cells to perform certain functions such as drug delivery or localised heating when external light is applied.[48]

Thereby, nanoscience and nanotechnology display a multidisciplinary approach and can be applied in practically all fields, from chemistry to physics, from biology to medicine, from industry to agriculture, from the environment to the organism, and from earth to outer space. The reality is that nanotechnology is changing the world in many fundamental ways, making *nano* one of the most exciting scientific research fields.

---

[46] Keçili, R.; Büyüktiryaki, S.; Hussain, C. M. *TrAC Trends Anal Chem*, **2019**, *110*, 259-276.
[47] Zhang, X.; Guo, Q.; Cui, D. *Sensors (Basel)*, **2009**, *9*, 1033-1053.
[48] Sahu, T.; Ratre, Y. K.; Chauhan, S.; Bhaskar, L. V. K. S.; Nair, M. P.; Verma, H. K. *J Drug Delivery Sci Technol*, **2021**, *63*, 102487.

1.2.1. Supramolecular Chemistry

Chemistry is the science that studies the nature, properties, and structure of matter. In this case, the fundamental principle is the creation of molecular assemblies through the controlled formation of covalent bonds. According to Nobel Laureate Jean-Marie Lehn (who received this prize in 1987 together with Donald J. Cram and Charles J. Pedersen), supramolecular chemistry can be defined as the science that bridges the gap between the world of molecules and nanotechnology. Although the term supramolecular had already appeared in Webster's Dictionary in 1903, the word *übermoleküle* was coined in 1937 to describe species of higher organization derived from the association of smaller molecular entities. Is not until 1960, due to pioneering work Lehn, that supramolecular chemistry was defined as *the chemistry beyond molecules*. Hence, supramolecular chemistry plays an essential role in the design and synthesis of nanostructured materials and nanoparticles as well as in the development of hybrid nanomaterials with advanced functionalities.[49]

Numerous examples of supramolecular assembly can be found in nature, such as the chemical interactions between a protein and a drug, or a catalyst and its substrate, or a macrocyclic host and a guest; the self-assembly of nanomaterials and even some chemical reactions are dominated by non-covalent interactions. Moreover, the use of a scaffold for self-assembly is an especially interesting option, because a scaffold can guide the organisation of weakly interacting molecules into well-defined self-assembled architectures. These supramolecules possess broad functionality, such as catalytic, photophysical, electronic or redox properties, and are ideal building blocks for sensors, information storage materials and nanodevices.[50]

---

[49] Albrecht, M. *Naturwissenschaften*, **2007**, *94*, 951-966.
[50] Ling, X. Y.; Reinhoudt, D. N.; Huskens, J. *Pure Appl Chem*, **2009**, *81*, 2225-2233.

In this respect, non-covalent interactions, molecular recognition and self-assembly are thereby key features that distinguish between molecular chemistry and supramolecular chemistry (see Figure 11). Regarding **non-covalent bonds**, these interactions are crucial for the reversible formation of supramolecular aggregates and thus, for molecular recognition and self-assembly mechanisms. Subsequently, **molecular recognition** is the preferential interaction between a host molecule with a specific guest which are complementary as the lock-key principle that characterises the enzyme-substrate interaction. Another important characteristic is **self-assembly**, spontaneous organization of smaller subunits to form larger, well-organized patterns. For nanoparticles, this spontaneous assembly is a consequence of interactions between the particles aimed at achieving a thermodynamic equilibrium and reducing the system's free energy.[51,52]

Thus, in the development of new nanomaterials is crucial that the molecular building blocks able to produce an effective aggregation by non-covalent interactions, which in reversible self-assembly processes leads to stable and well-defined supramolecular species through molecular recognition processes. Aggregation of the components might result in innovative properties, which are expressed in a supramolecular function. As mentioned above, by the use of this principle to construct large ensembles of molecules, supramolecular chemistry bridges the gap between the picometer dimensions of molecules and the nanoworld. Therefore, the understanding of its fundamental basics is crucial for a successful chemical “bottom–up” approach toward nanotechnology.[53]

[51] Descalzo, A. B.; Martínez-Máñez, R.; Sancenón, F.; Hoffmann, K.; Rurack, K. *Angew Chem Int Ed.*, **2006**, *45*, 5924-5948.
[52] Menger, F. M. *PNAS*, **2002**, *99*, 4818.
[53] Fukuhara, G. *J Photochem Photobiol, C* , **2020**, *42*, 100340.

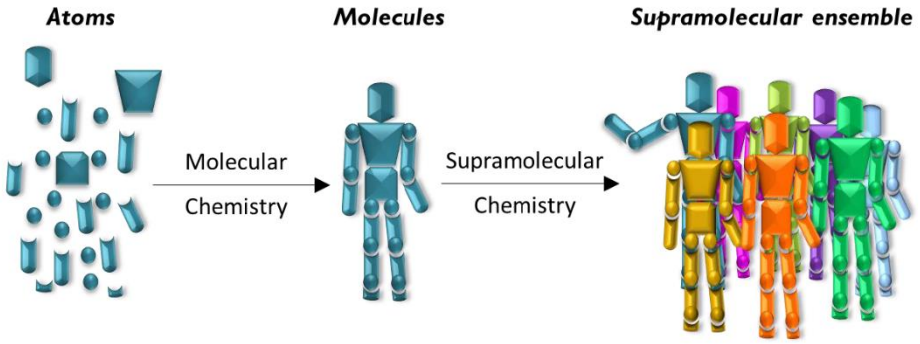

Figure 11. Schematic representation that illustrates the difference between molecular and supramolecular chemistry. *Adapted from A. Llopis-Lorente, Enzyme-functionalized hybrid mesoporous nanodevices for sensing, controlled release and molecular communication, PhD Dissertation, Universitat Politècnica de València, 2019.*

1.2.2. Mesoporous silica materials

According to IUPAC nomenclature, porous materials are classified into three categories depending on pore diameter: (i) microporous (pore size <2 nm), (ii) mesoporous (2-50 nm) and (iii) macroporous (>50 nm) as shown in Figure 12.[54]

Ordered porous materials are of great interest due to their many advantages such as large surface area combined with large and uniform pore size, well-defined pores, enhanced accessibility, and their ability to anchor diverse chemical compounds on their surface. These materials have been explored as promising candidates in various fields such as adsorption, catalysis, chemical separations, sensors, chromatography, gas storage and biotechnology devices applications.

[54] Faustini, M.; Nicole, L.; Ruiz-Hitzky, E.; Sanchez, C. *Adv Funct Mater*, **2018**, *28*, 1704158.

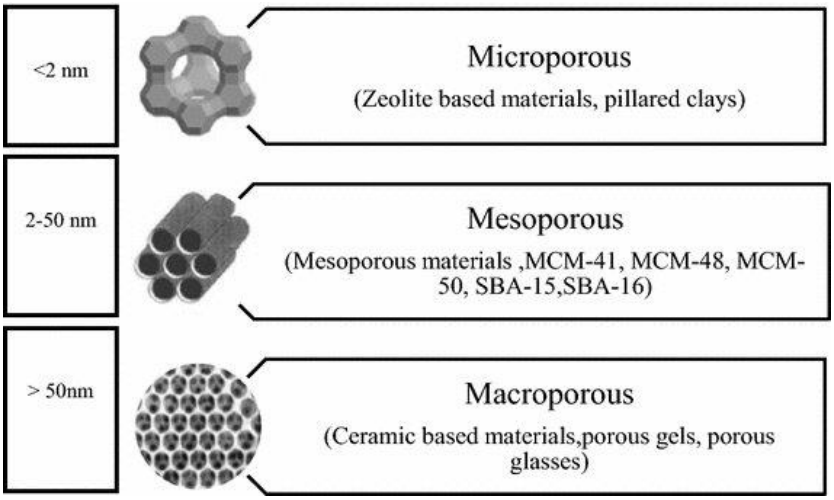

Figure 12. IUPAC classification of the ordered porous materials. *Reprinted by permission Springer Nature Customer Service Centre: J. Porous Mater* ***2017****, 24, 741-749. Copyright © 2017 Springer Nature.*

Zeolites and in general, microporous molecular sieves are the most recognized member from the family of microporous materials which have excellent properties by virtue of their narrow pore size distribution and possess good stability, high selectivity and activity due to their crystallinity. Crystalline zeolites have well-defined micropores with excellent shape selectivity due to which they have become exceptionally successful as catalysts for oil refining and petrochemistry and organic synthesis in the production of fine and specialty chemicals. In spite of large application of zeolites in the field of catalysis, pore size (0.4-1.2 nm) remains a strong limitation in conversion processes involving bulky molecules.[55]

In the same way, other type of porous materials that are not based on the silicate, are porous carbon, coordination solids or porous heteropolyanion salts. The non-silica mesoporous materials are very important to be used as catalysts due

[55] Bensebaa, F. *Chapter 1-Interface Science and Technology*, Bensebaa, F. *Elsevier*, **2013**, *19*, 1-84.

to their transition-state property. However, these kinds of mesoporous materials are not stable because of the mesopores of these materials can be collapsed during synthesis. Calcinations and synthesis techniques are also complicated. Due to above difficulties most of the researchers are focusing on silica mesoporous materials.

Mesoporous silica was first discovered in 1990 by researchers in Japan and later, in 1992 it was synthesized in Mobil Corporation Laboratories and named as molecular 41 sieves (M41S). These materials show some important characteristics such as:

- Chemical inertness, thermal stability, and easy handling.
- Tunable pore diameter (2-30 nm).
- Controllable morphology.
- High specific surface area (>800 m^2/g).
- Their synthesis requires inexpensive and non-hazardous chemicals and can be produced in large scales.
- Different structure of these materials such as rods, sheets and 3D structures can be obtained by using different surfactants.
- Easy possibility of organic functionalisation.
- Biocompatibility.

As a result of these features, mesoporous silica materials are useful for supports as adsorption, sensors, catalysis, chemical separations, and biotechnology devices applications. Among this group of materials, MCM-41, MCM-48 and MCM-50 (MCM for Mobil Crystalline Materials) are the most widely known in M41S family which have different methods of synthesis and applications based on instability and limitation of mesoporous structure. Especially for MCM-41 and MCM-48, the pore size can be controlled and both materials are widely used as adsorbents, catalysts and supports. MCM-41 is in hexagonal packed rod-shaped micelle structure,

whereas MCM-48 is in cubic, and MCM-50 is in lamellar structure form as shown in Figure 13. [56]

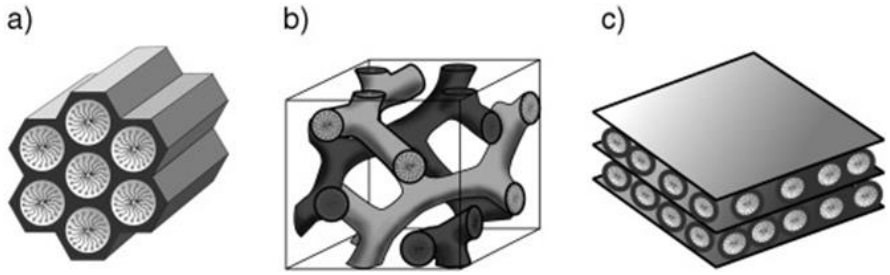

Figure 13. Structures of mesoporous M41S materials a) MCM-41 (2D hexagonal, space group p6mm), b) MCM-48 (cubic, space group Ia3d), and c) MCM-50 (lamellar, space group p2). *Adapted from Angew. Chem. Int. Ed.* ***2006****, 45, 3216-3251. Copyright © 2006 Wiley-VCH.*

Through this huge research, in 1995 new families of mesoporous silica material, such as SBA, MSU, and FSM, were developed with characteristic porosities and particle shapes. In 1998, Santa Barbara Amorphous No.15 (SBA-15) was prepared. SBA-15 have a hexagonal array of pores with larger pore size from 4.6-30 nm and was a research gambit in mesoporous material development.[57]

After the discovery of the above-mentioned materials, significant research efforts have been started to achieve control over the characteristics of mesoporous silica with special emphasis on pore size and morphology. These mesoporous silica materials are highly ordered, presented large specific surface areas, a hexagonal array of pores, and uniform mesoporous channels.

1.2.2.1. Synthesis of mesoporous silica materials

[56] Narayan, R.; Nayak, U. Y.; Raichur, A. M.; Garg, S. *Pharmaceutics*, **2018**, *10*.
[57] Chaudhary, V.; Sharma, S. *J Porous Mater*, **2017**, *24*, 741-749.

Mesoporous materials can be synthesized by different techniques such as: (1) Sol-Gel processing, (2) Template assisted techniques, (3) Microwave assisted techniques and (4) Chemical etching technique.[58]

Mesoporous silica materials are still generally synthesised using the process developed by Stöber in 1968 based on sol-gel chemistry. Generally, sol-gel process is a wet chemical technique which is widely used in the fields of materials science and ceramic engineering. In the sol-gel process, a starting a colloidal suspension (sol) is prepared for the growth of inorganic network and then, gelation process of the sol is carried out to form a network in a continuous liquid phase (gel). The precursors used for synthesizing these colloids usually consist of a metal or metalloid element surrounded by various reactive ligands. The starting material is processed to form a dispersible oxide yielding a sol in contact with water or dilute acid. Calcination of the gel produces the oxide. The reactions involved in the sol-gel chemistry are mainly based on the hydrolysis following by condensation of metal alkoxides wherein corresponding oxides and mixed oxides with different stoichiometry. Nowadays, this method is widely used to synthesize mesoporous materials with different morphologies. For the synthesis of mesoporous material by sol-gel process, different templates can be used as the structure directing agents such as cationic surfactants (in the case of MCM-41), triblock copolymers (in the case of SBA) and organic small molecules.

In this sense, the synthesis of mesoporous silica is based on the formation of liquid-crystalline mesophases of amphiphilic molecules (surfactants) that serve as templates for the *in-situ* polymerization of orthosilicic acid. The synthesis can be performed either in acidic or basic conditions, and the source of silica can be fumed silica, sodium silicate, or a tetra-alkyl oxide of silane. The first material reported by the Mobil researchers (designated as MCM-41) was micrometer-sized particles

[58] Kumar, S.; Malik, M. M.; Purohit, R. *Mater Today: Proc*, **2017**, *4*, 350-357.

with hexagonally ordered mesopores. The morphology of the particles was variable, with a very small amount of hexagonally shaped nanoparticles. Later works were performed to control the morphology of the particles by manipulation of the pH during synthesis or by the addition of cosolvents.[59]

Particularly, this process involves the hydrolysis and condensation of silanes ($Si(OX)_4$), where OX is typically OEt or OMe) or organosilanes ($[(XO)_3Si]_n$-R, where R is an organic group, n ≥ 1), and the kinetics of both processes can be regulated by acid and base (see Figure 14). The first hydrolysis step leads to the generation of reactive silanolates species (R_3-Si-O^-), which are capable of reacting with other silanes or organosilanes, forming covalent siloxane bonds (Si-O-Si) and consequently, a sol of silicate oligomers. As time goes by, such a hydrothermal process produces silica or silsesquioxane frameworks.[60]

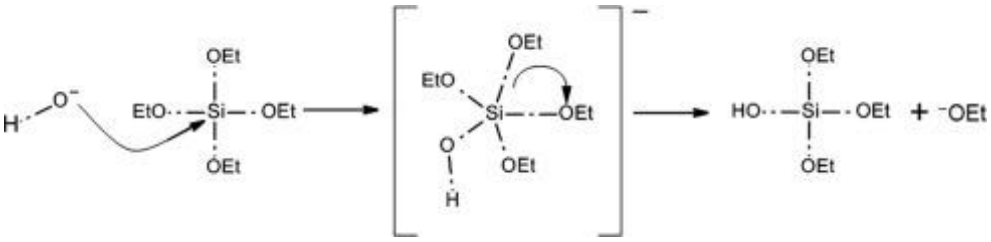

Figure 14. Mechanism of basic medium polymerization of tetraethylorthosilicate (TEOS) performed in the synthesis of mesoporous silica nanoparticles of the MCM-41 type. *Reprinted from Biomedical, Therapeutic and Clinical Applications of Bioactive Glasses, Chapter 3* ***2019****, 3, 69-123. Copyright 2019, with permission from Elsevier.*

To further obtain mesoporous structure, cationic surfactants such as cetyltrimethylammonium bromide (CTAB) are often utilized as structural-directing agents (SDAs) for guiding the aforementioned reaction process. The negatively charged reactive silanolates species (≡Si-O^-) can be electrostatically linked to

[59] Wu, S.-H.; Mou, C.-Y.; Lin, H.-P. *Chem Soc Rev*, **2013**, *42*, 3862-3875.
[60] Yang, B.; Chen, Y.; Shi, J. *Materials Science & Engineering R*, **2019**, *137*, 66-105.

positively charged CTAB ($-N^+(CH_3)_3$) micellar packings, thus favouring a templating effect. Consequently, the cooperative assembly and aggregation result in precipitation from a gel, during which microphase separation and continuous condensation of silicate oligomers occur. The process leads to the formation of mesoporous silicate-SDAs hybrid structure, which only takes 3-5 min in cationic surfactant solutions. Finally, mesoporous material is obtained after the removal of organic templates by either calcination (heating a high temperature material in absence or limited supply air) or extraction under or reflux in acid conditions or sonication. It is noted that when only a silica precursor, such as tetraethoxysilane (TEOS, $Si(OEt)_4$),[61] is used in the sol-gel reaction, the ultimate product will be mesoporous silica.

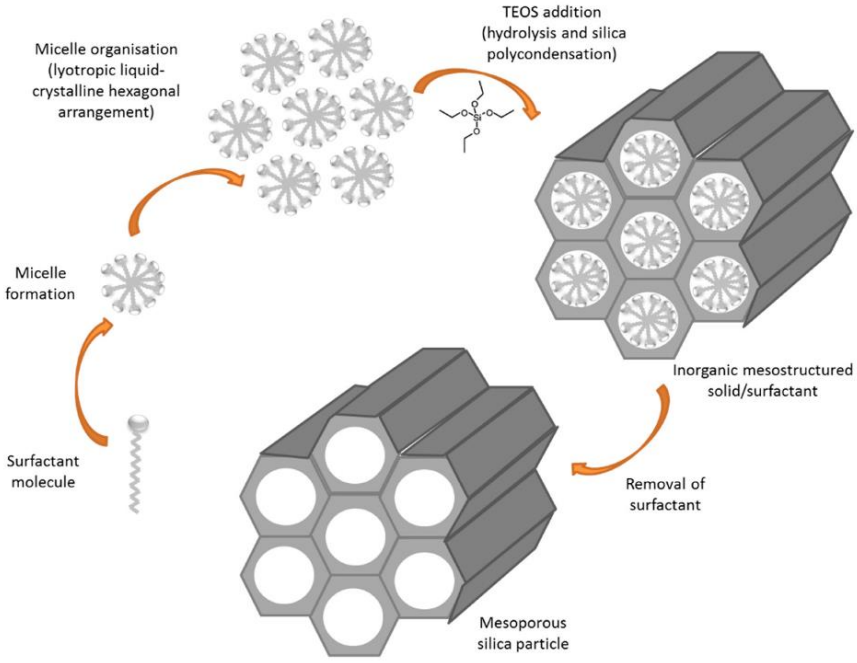

Figure 15. Typical synthesis of a mesoporous silica material, particularly of the MCM-41 type. *Materials* ***2018****, 11, 779. Copyright 2018, with permission from MDPI.*

[61] Bachar, A.; Catteaux, R.; Duée, C.; Désanglois, F.; Lebecq, I.; Mercier, C.; Follet-Houttemane, C. *Chapter 3-Biomedical, Therapeutic and Clinical Applications of Bioactive Glasses*, Kaur, G. Ed.; *Woodhead Publishing*, **2019**, 69-123.

Therefore, proper regulation of sol-gel chemistry by changing the reactants (silica sources and surfactant templates) or experimental conditions (pH, temperature, water content, etc.)[62] is of great significance in modulating the structural/compositional characteristics of the resulted nanomaterials.[63]

Regarding the particular material used during this PhD Thesis, 100 nm MCM-41 nanoparticles with a regular pore diameter of 2-3 nm, a solution of the structure directing agent, CTAB, in water basified with NaOH up to pH 11 is heated until reaching 80 °C. Under these conditions, self-organization of the surfactant molecules occurs, exceeding the critical micellar concentration, allowing the subsequent formation of a porous structure with hexagonal morphology. Then, tetraethylorthosilicate (TEOS), silica precursor, is added dropwise to the homogeneous surfactant solution to carry out condensation around the micelles giving rise to a turbid whitish solution that reacts for 2 hours. The solid is isolated by centrifugation and several times washed to neutralisation with distilled water and dried at 70 °C. The final mesoporous material is obtained after the removal of the surfactant by calcination at 550 °C in an oxidising atmosphere for 5 hours (see Figure 15).

1.2.2.2. Functionalization of mesoporous silica materials

Hybrid materials are composed by two constituents (within a size in the range of nanometers or even angstroms) in a synergetic way. These materials are often obtained by anchoring (organic) functional groups on nanoscopic inorganic materials as supporting platforms. In the words of Professor Clément Sanchez, "organic-inorganic hybrid materials are not simple physical mixtures. They can be broadly defined as nanocomposites with (bio)organic and inorganic components,

[62] Liberman, A.; Mendez, N.; Trogler, W. C.; Kummel, A. C. *Surf Sci Rep* **2014**, *69*, 132-158.
[63] Huang, R.; Shen, Y.-W.; Guan, Y.-Y.; Jiang, Y.-X.; Wu, Y.; Rahman, K.; Zhang, L.-J.; Liu, H.-J.; Luan, X. *Acta Biomater*, **2020**, *116*, 1-15.

intimately mixed in which at least one of the components domains from a few angstroms to several nanometres".[64] From materials scientist viewpoint, merging the properties of organic and inorganic building blocks within a single material is especially attractive because of the possibility of combining the enormous organic chemistry functional variation with the advantages provided by thermally stable and robust inorganic substrates. Thus, organic-inorganic hybrid materials combine the great variability of organic scaffolds. Therefore, the properties of hybrid materials are not merely the result of the sum of their components individual contributions, but also the strong synergy created by the presence of a very broad hybrid interface. Indeed, the organic-inorganic interface (nature of interactions, energy, and binding capacity) plays a major role in modulating numerous properties (optical, mechanical, separation, catalysis, chemical stability, and thermal stress).

Integration of organic moieties into solid inorganic supports provides a wide variety of advantages, such as:

- Receptors can be organized in a more or less compact monolayer (depending on the degree of the surface functionalization). Due to this, the movement of the different molecular units is reduced, and this generates new collective processes that improve the features of the recognition process, such as "surface chelate effect" with monodentate ligands or an increase on the "effective concentration" on the solids.
- It is possible to carry out subsequent anchoring processes to obtain a solid surface functionalized with different organic molecules and modulate their properties according to the nature of the anchored functional groups.
- Leaching processes involving the receptor are avoided.

[64] Sanchez, C.; Soler-Illia, G. J. d. A. A.; Ribot, F.; Lalot, T.; Mayer, C. R.; Cabuil, V. *Chem Mater*, **2001**, *13*, 3061-3083.

- If the solid support is functionalized with a receptor that could give reversible coordination processes, it can be reused several times without loss of their recognition features.

Traditionally, functionalisation is the process of introducing new functions, characteristics, capabilities, or properties by modifying the surface chemistry of the material in order to obtain organic-inorganic hybrid materials. It is a fundamental technique used in chemistry, materials science, biological engineering, textile engineering and nanotechnology. There are four main pathways for the porous hybrid materials synthesis based on organosilica units: 1) **physisorption**, 2) the subsequent modification of the pore surface of a purely inorganic silica material (**grafting**), 3) the simultaneous condensation of the corresponding silica and organosilica precursors (**co-condensation**), and 4) the incorporation of organic groups as bridging components directly and specifically into the pore walls by using organosilica precursors from a single bisylated source (**production of periodic mesoporous organosilicas**, PMOs).[65]

- **Physisorption**

One of the most straightforward methods for mesoporous silica materials surface functionalisation is physisorption. In this method, the mesoporous silica is suspended in the solution of the organic molecule, which diffuses into the pores where it is bound by weak intermolecular forces, such as Van der Waals forces and hydrogen bonds. Nevertheless, the organic molecules are usually weakly bound and can be easily extracted and therefore it is not a widely used method.

- **Post-synthetic Functionalization of Silicas (Grafting)**

[65] Hoffmann, F.; Cornelius, M.; Morell, J.; Fröba, M. *Angew Chem Int Ed,* **2006**, *45*, 3216-3251.

Another significant functionalisation method is grafting. In this method, the inorganic mesoporous silica material is first synthesized, and, in a posterior step, it is functionalized with the selected organic groups. This procedure involves mainly the reaction of free silanol groups (Si-OH) present on the MSNs post-synthesis surface with a commercially available range of organosilanes of the type $(R'O)_3SiR$ (where R is an organic group and R' = CH_3, C_2H_5…) or other less frequently used silazanes $HN(SiR_3)_2$ or chlorosilanes $ClSiR_3$ (see Figure 16). This synthesis is quite versatile because that it allows the introduction of a wide variety of organic groups in the materials by simply varying the residue R of the organosilanes.

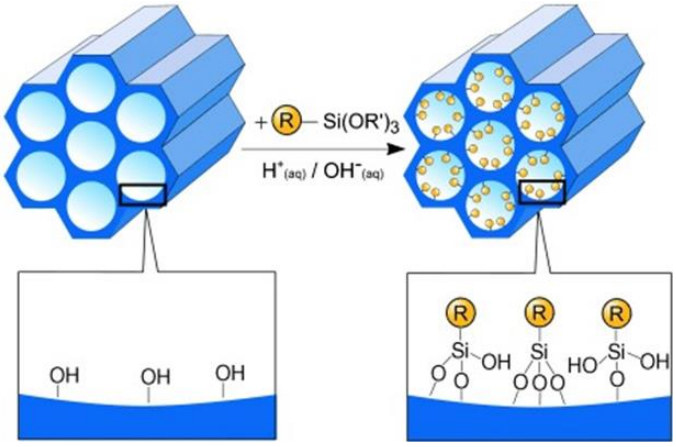

Figure 16. Depiction of the grafting method based on the internal surface modification of the mesoporous materials with organosilane moieties. *Adapted from Angew. Chem. Int. Ed.* ***2006****, 45, 3216. Copyright © 2006 Wiley-VCH.*

One of the main advantages of this route is the preservation of the meso-structure of the starting silica material, as well as their morphology, under the functionalization conditions used. These facts enable the well-known synthesis standard methods to be used and their scaling up. On the other hand, after template removal (by calcination or extraction), the mesoporous silica material external surface is more accessible than the inner counterpart. This avoids a decrease in pore size, a non-homogeneous distribution of the organosilanes

functional groups during grafting process, and a lower degree of occupation within the pores.

Additionally, it is possible to achieve regioselective functionalisation of the mesoporous materials by anchoring different groups on the outer and inner surface. For this, an attractive strategy is to use the mesoporous scaffold as synthesised (with the pores filled by the surfactant molecules) and treat it with an organosilane that will bind to the outer surface. The surfactant is then removed by extraction (with a solution of HCl in ethanol at reflux) and the resulting surfactant-free scaffold is further functionalised on its inner surface with a different organosilane.

- **Co-Condensation (Direct Synthesis)**

Other alternative method to synthesize organically functionalized mesoporous silica materials is the co-condensation procedure. This approach consists of a one-step reaction where the simultaneous tetraalkoxysilanes (TEOS or TMOS) and terminal trialkoxyorganosilanes of the type $(R'O)_3SiR$ hydrolysis and condensation (under acid or basic conditions) in the presence of the structure-directing agents is produced. The resulting silica matrix contains alkoxy silane groups anchored covalently to the pore walls and distributed homogenously both on the internal and external surfaces (see Figure 17).

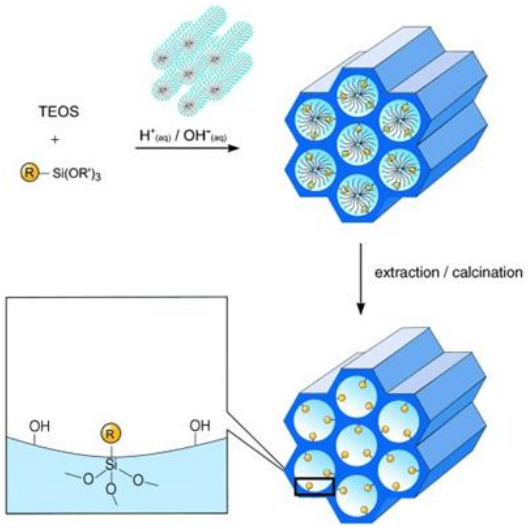

Figure 17. Schematization of mesoporous silica materials internal surface co-condensation procedure with TEOS and a non-bridged trialkoxyorganosilanes in the presence of structure-directing agent. *Adapted from Angew. Chem. Int. Ed.* ***2006****, 45, 3216. Copyright © 2006 Wiley-VCH.*

In this approach, the organic groups are distributed homogeneously over the entire surface of the mesoporous silica matrix, thus overcoming one of the main drawbacks of grafting. On the other hand, this method shows several disadvantages as the degree of mesoscopic order of the products decreases with increasing concentration of $(R'O)_3SiR$ in the reaction mixture due to the homocondensation reactions. Moreover, another disadvantage purely methodological is the destruction of the organic functionality during surfactant removal, so that normally only extractive methods can be used, and calcination is not suitable in most cases.

- **Periodic Mesoporous Organosilicas (PMOs)**

There is another possibility for the functionalization of mesoporous materials, that consists of the hydrolysis and condensation of silsesquioxane precursors of type $(R'O)_3Si\text{-}R\text{-}Si(OR')_3$ (see Figure 18). In this case, organic units are integrated into three-dimensional network of silica matrix leading homogeneous

distribution in the pore walls. The major features of this method are the large internal surface areas of up to 1800 m^2g^{-1}, as well as the high thermal stability although the pores are generally completely disordered. These materials were first synthesised in 1999 by three independent research groups and constituted a new class of hybrid mesoporous materials. However, the variety of silsesquioxanes available on the market is smaller compared to the wide variety of trialkoxysilanes and this strategy has been less employed.[66]

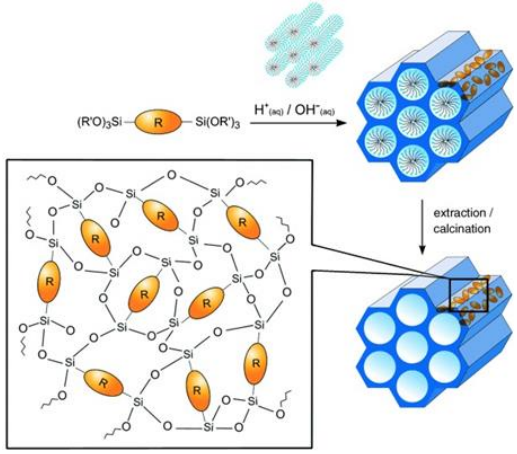

Figure 18. General synthetic route of PMOS. *Adapted from Angew. Chem. Int. Ed.* ***2006****, 45, 3216. Copyright © 2006 Wiley-VCH.*

1.2.2.3. Stimuli-responsive gated materials

In this appealing scenario, the anchoring of organic molecules, biomolecules or supramolecules on selected inorganic scaffolds with different chemical natures, sizes and shapes promotes the development of smart nanodevices that can be applied in certain scientific and technological fields.

An attractive concept in this prolific field is related to the design of stimuli-responsive gated materials. These materials consist in certain porous

[66] Hatton, B.; Landskron, K.; Whitnall, W.; Perovic, D.; Ozin, G. A. *Acc Chem Res*, **2005**, *38*, 305-312.

nanomaterials that allows the spatio-temporal controlled release of the confined cargo (a wide range of drugs or dyes/fluorophore) from the inorganic scaffold pores into solution mediated by the specific interaction of the molecular gate (molecular, supramolecular or biological assemblies grafted onto the external surface of the solid) with a selected external stimulus able to produce electrostatic or supramolecular interactions, the rupture/formation of covalent bonds, or changes in the physical properties of molecules or macromolecules. Specifically, stimuli responsive gated materials are constituted by two subunits: (i) a porous inorganic scaffold on which a selected cargo is entrapped and (ii) several molecular or supramolecular assemblies, usually anchored to the inner surface, which can control cargo release from the pores (see Figure 19).[67]

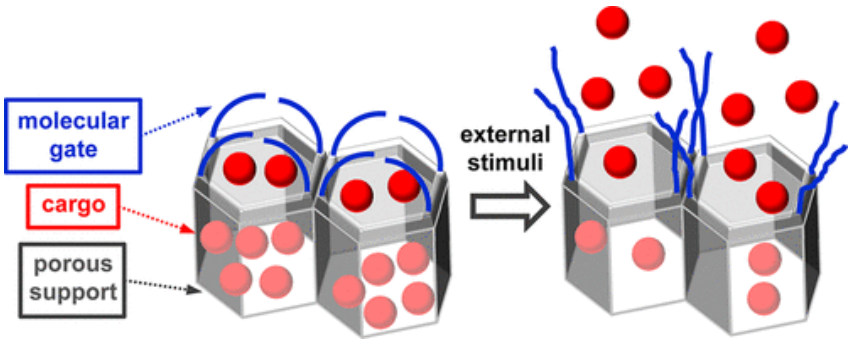

Figure 19. Schematic of the general behaviour mechanism of stimuli responsive gated nanomaterials. *Reprinted with permission from Chem. Rev.* ***2016****, 116, 561-718. Copyright 2016 American Chemical Society.*

Since the first reported example in 2003 by Fujiwara and co-workers,[68] gated materials have been widely explored. Therefore, different inorganic supports as silica, silicon, aluminium oxide or titanium oxide can be used for the manufacture

[67] Thananukul, K.; Kaewsaneha, C.; Opaprakasit, P.; Lebaz, N.; Errachid, A.; Elaissari, A. *Adv Drug Delivery Rev*, **2021**, *174*, 425-446.
[68] Mal, N. K.; Fujiwara, M.; Tanaka, Y. *Nature* **2003**, *421*, 350-353.

of smart nanodevices.[69] One of the most noteworthy materials are mesoporous silica nanoparticles (MSNs) due to biocompatibility, high loading capacity, high specific surface and versatility enabled by an easy functionalization via well-known chemistry methodologies. Extensive reviews about different kind of gatekeepers have been published to display the whole spectrum of options in the synthesis of the stimuli responsive gated materials. The main logic molecular gates reported respond to seven general types of stimuli, such as (i) light, (ii) temperature, (iii) alternating magnetic field (AMF) and ultrasound, (iv) redox potentials, (v) pH, (vi) molecules and biomolecules, and (vii) enzymes.[70,71]

In particular, in this PhD thesis, the functionalization of MSNs with biomolecules such as antibodies or proteins[72] (specific neurotransmitter transporters and receptors) that responds to selected drugs is reported. These gated materials provide remarkable recognition capability in sensing protocols.

- ***Molecules and biomolecules as molecular gates***

The design of gated systems triggered by specific small molecules and involving biomolecules as capping agents for sensing applications has been explored very recently. In these cases, the gating mechanism is based on supramolecular interactions, chemical reactions or displacement after coordination between the biomolecule assembly and the target molecule (anions, cations, neutral molecules and biomolecules).[73] Although a wide variety of such materials

[69] Hecht, M.; Climent, E.; Biyikal, M.; Sancenón, F.; Martínez-Máñez, R.; Rurack, K. *Coord Chem Rev*, **2013**, *257*, 2589-2606.
[70] Aznar, E.; Oroval, M.; Pascual, L.; Murguía, J. R.; Martínez-Máñez, R.; Sancenón, F. *Chem Rev*, **2016**, *116*, 561-718.
[71] Salve, R.; Kumar, P.; Ngamcherdtrakul, W.; Gajbhiye, V.; Yantasee, W. *Mater Sci Eng, C*, **2021**, *124*, 112084.
[72] Climent, E.; Bernardos, A.; Martínez-Máñez, R.; Maquieira, A.; Marcos, M. D.; Pastor-Navarro, N.; Puchades, R.; Sancenón, F.; Soto, J.; Amorós, P. *J Am Chem Soc*, **2009**, *131*, 14075-14080.
[73] Mu, J.; He, L.; Huang, P.; Chen, X. *Coord Chem Rev*, **2019**, *399*.

can be found in the literature, four main categories of gating assemblies have been generally reported: (i) oligonucleotides to recognize complementary chains or certain analytes (using aptamers and DNAzymes),[74] (ii) antibody-antigen interactions that respond to small molecules (mainly anions and cations),[75] (iii) peptide sequences or organic groups that are hydrolysed by certain enzymes,[76] (iv) proteins.[77]

Specifically, antibody-antigen interaction is a biomimetic strategy that promises high selectivity and sensitivity because of the high and specific affinity of binding between antibodies and their antigens in mixtures containing several different molecules. For instance, if the mesoporous scaffold is functionalized with the antigen on the external surface without close the pore, interaction with the correct antibody enables the complete blockage of the pores acting as a nanoscopic gatekeeper. Accordingly, the antibodies close the pores and delivery of the cargo can only be induced by the presence of the antigen in the sample. The possibility of selecting antibodies for a countless number of antigens, including low molecular weight targets, makes this approach highly appealing for a wide range of applications.[78] In this regard, the first example of such sensing material was reported by Martínez-Máñez and co-workers in 2009 (see Figure 20). In particular, MCM-41 pores were loaded with a fluorescent cargo, $[Ru(bipy)_3]Cl_2$, and then, the external surface was functionalized with a modified hapten (4-(4-aminobenzenesulfonylamino)benzoic acid). In a sub-sequent step, the pores were completely capped with an antibody, that shows good affinity and selectivity toward the anchored hapten via suitable interaction through its two

[74] Damase, T. R., Allen, P. B. *Bioconjug Chem,* **2019**, *30*, 2-12.
[75] Auría-Soro, C., Nesma, T., Juanes-Velasco, P., Landeira-Viñuela, A., Fidalgo-Gomez, H., Acebes-Fernandez, V., Gongora, R., Parra, M., Raúl Manzano-Roman, R., Fuentes, M. *Nanomaterials*, **2019**, *9*, 1365
[76] Hu, J., Xiao, D., Zhang, X. *Small*, **2016**, *12*, 3344-3359.
[77] Hong, S., Choi, D.,Kim, H., Park, C., Lee, W., Park, H. *Pharmaceutics*, **2020**, *12*, 604.
[78] Huang, P.; Lian, D.; Ma, H.; Gao, N.; Zhao, L.; Luan, P.; Zeng, X. *Chin Chem Lett*, **2021**.

immunoglobulin G binding regions. The presence in solution of sulfonamide antibiotic sulfathiazole induces the uncapping of the pores and the release of the entrapped dye. The opening mechanism consists in the displacement of the capping antibody due to a higher affinity for the antibiotic in solution than for the anchored hapten.[72]

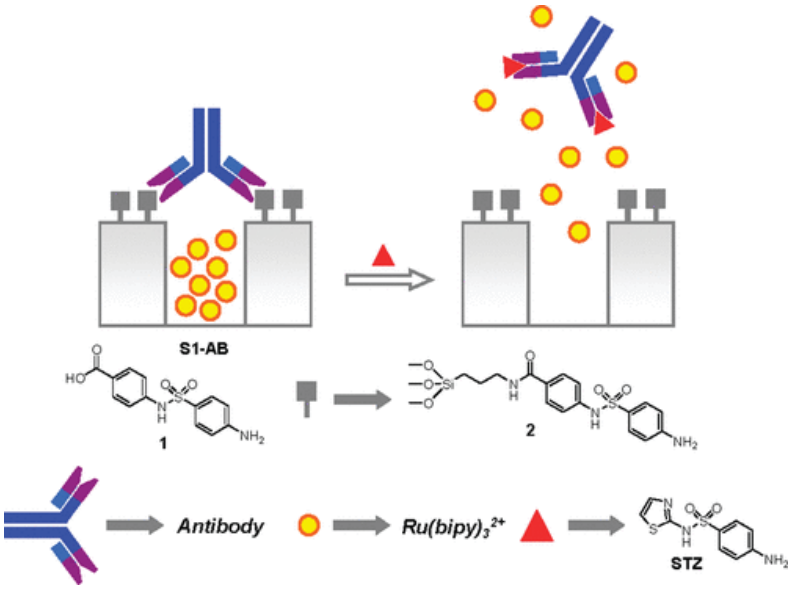

Figure 20. Schematic representation of a supramolecular complex as the gating ensemble for antibiotic recognition based on antibody-antigen interaction. *Reprinted with permission from J. Am. Chem. Soc.* ***2009****, 131, 39. Copyright 2009 American Chemical Society.*

Using enzyme-inhibitor interactions, Martínez-Mañez and co-workers reported in 2016 an innovative logic nanodevices based on MCM-41 scaffolds loaded with a fluorescent reporter, rhodamine B and functionalized with pyridostigmine derivative (P1) that interact preferentially with acetylcholinesterase (AChE) active site capping the pores. In the presence of diisopropyl

fluorophosphate (DFP), a well-known inhibitor of AChE, the enzyme was displaced of the external surface allowing the cargo release (see Figure 21).[79]

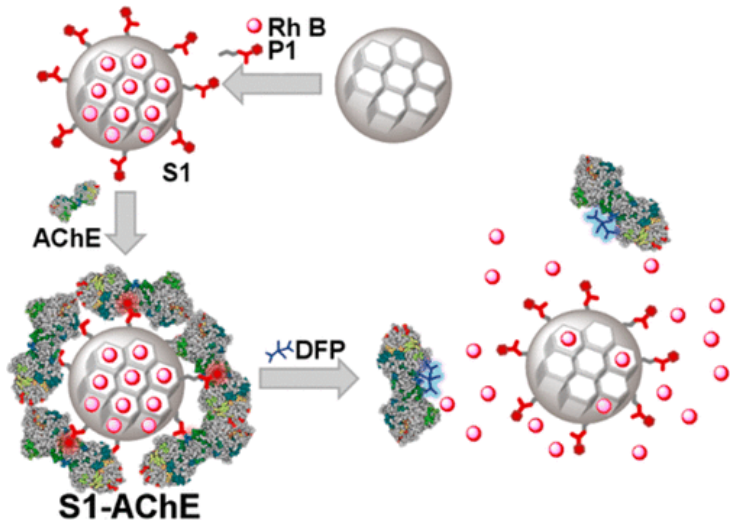

Figure 21. Action mechanism of AChE-P1 gated nanoparticles responding to DFP. *Reprinted (adapted) with permission Org. Lett.* ***2016****, 18, 5548−5551. Copyright 2016 American Chemical Society.*

The idea of designing nanodevices capable of sensing the environment due to the incorporation of numerous biomolecules such as neurotransmitter transporters and receptors, holds enormous potential towards future nanoprocessors of higher complexity.[80]

[79] Pascual, L.; Sayed, S. E.; Martínez-Máñez, R.; Costero, A. M.; Gil, S.; Gaviña, P.; Sancenón, F. *Org Lett* **2016**, *18*, 5548-5551.
[80] Luo, C.; He, L.; Chen, F.; Fu, T.; Zhang, P.; Xiao, Z.; Liu, Y.; Tan, W. *Cell Rep Phys Sci*, **2021**, *2*, 100350.

1.3. Chemosensors

The development of highly selective and sensitive methods for the detection of a broad variety of analytes with applications in multidisciplinary areas (such as environmental studies, medicine, biology, pharmacy) is still a challenge. Among methodologies developed in detection protocols, the use of molecular-based sensors has emerged as an attractive approach in the last decades. In spite of this interest, one of the main issues that need to be overcome in the design of these molecular sensors is the difficulty of establishing a preferential and selective recognition between the probe and the target molecule. Based on the above, the development of new chemical sensors with sensitive and selective responses for small molecules, ions, biological macromolecules, or certain organisms has become an emerging field in the last decades.[81,82,83]

According to the IUPAC definition, molecular sensor or chemosensor is a device that transforms chemical information into a detectable analytically useful signal (transducer).[84] Thus, chemosensors combine molecular recognition events

[81] Liu, R.; Li, Z.; Huang, Z.; Li, K.; Lv, Y. *TrAC, Trends Anal Chem*, **2019**, *118*, 123-137.
[82] He, Q.; Vargas-Zúñiga, G. I.; Kim, S. H.; Kim, S. K.; Sessler, J. L. *Chem Rev*, **2019**, *119*, 9753-9835.
[83] Li, Z.; Askim, J. R.; Suslick, K. S. *Chem Rev*, **2019**, *119*, 231-292.
[84] Hulanicki, A.; Glab, S.; Ingman, F. *Pure Appl Chem*, **1991**, *63*, 1247-1250.

with the generation of a macroscopic signal (by a reporter molecule) that revealed the presence of the guest. Specifically, in molecular recognition processes a guest molecule selectively recognizes its host partner through several molecular interactions forming a host-guest complex with a high complementarity and cooperativity between both components (see Figure 22).[85,86,87]

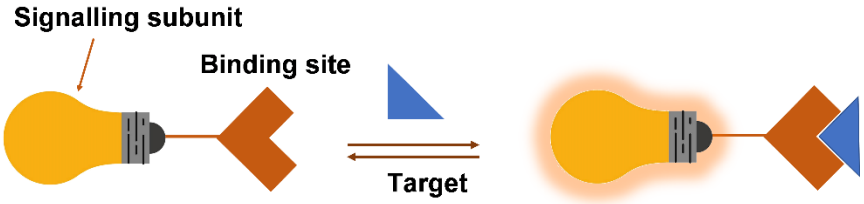

Figure 22. General scheme of the behaviour of a molecular sensor.

Generally, chemical sensors are constituted by two essentials components that can be connected through non-covalent interactions (hydrogen bonding, metal coordination, hydrophobic forces, Van der Waals forces and π-π interactions) or by a covalent bond: (i) receptor and (ii) signalling subunit.[88]

1. Receptor subunit is the unit responsible of the recognition of the analyte. The process of recognition depends on the host molecule characteristics. The binding subunit is designed in order to achieve a selective coordination via a suitable receptor-guest complementarity.

2. Signalling Subunit acts as a signal transducer and informs of the recognition process that occurs at molecular level through changes in a measurable macroscopic signal.

[85] Martínez-Máñez, R.; Sancenón, F. *Chem Rev*, **2003**, *103*, 4419-4476.
[86] Moragues, M. E.; Martínez-Máñez, R.; Sancenón, F. *Chem Soc Rev*, **2011**, *40*, 2593-2643.
[87] Roy, A.; Nandi, M.; Roy, P. *TrAC, Trends Anal Chem,* **2021**, *138*, 116204.
[88] Shakya, S.; Khan, I. M. *J Hazard Mater*, **2021**, *403*, 123537.

Dealing with the signalling unit, and despite the variety of detection channels, optical methods have perhaps been the most widely used in the development of chemosensors because they offer several advantages such as high sensitivity, low cost, the use of simple installations and fast response time as well as multiple responses to different analytes. The coupling of optical signalling units (dyes and/or fluorophores) with selected binding sites leads to the development of chromogenic and fluorogenic/luminescent molecular sensors. Chromogenic sensors undergo a colour change in the presence of a certain analyte whereas in luminescent probes, modifications in photophysical properties of the signalling unit (e.g. changes in the emission intensity, in the wavelength of the emission maximum, in the quantum yield or in the ratio of various luminescence emitters) are produced after binding with the selected target analyte. Additionally, one of the most important advantages of chromogenic and luminescent probes is that they can provide qualitative and semiquantitative information by the naked eye therefore excluding the use of any sophisticated instrumentation.[89]

Most luminescent chemosensors are based in common organic dyes, and hence, respond to the analyte interaction with a fluorescence signal. Nevertheless, there are other types of luminescence chemosensors that exhibit an optical response and are mainly based on metallic complexes.[90] In fact, metallic complexes have been extensively applied as signalling units, as alternative to common organic dyes, as they display distinctive photophysical properties including high quantum yields, large Stokes shifts or long emissive lifetimes compared to purely organic luminophores.

1.3.1. Approaches for optical chemical sensors design

[89] Salinas, Y.; Martínez-Máñez, R.; Marcos, M. D.; Sancenón, F.; Costero, A. M.; Parra, M.; Gil, S. *Chem Soc Rev*, **2012**, *41*, 1261-1296.
[90] Upadhyay, S.; Singh, A.; Sinha, R.; Omer, S.; Negi, K. *J Mol Struct* , **2019**, *1193*, 89-102.

Reported chromogenic and luminescent sensors can be classified in one of the three well known approaches for the design of optical probes; namely (i) the binding site-signalling unit approach, (ii) the displacement protocol, and (iii) the chemodosimeter paradigm (see Figure 23). The selection of one of the three approaches for the synthesis of an innovative optical chemosensor depends mainly on a number of parameters such as the affinity of the analyte, the selectivity of the binding and the medium in which the detection is performed.[91,92]

- **Binding site-signalling subunit approach**

In the binding site-signalling subunit approach, the binding and the signalling units are covalently linked in such way that the interaction of an analyte with the binding site induces visual changes in the signalling subunit. One of the most important properties of these probes is that they exhibit a high reversibility of the recognition process, due to the lability of the non-covalent receptor-analyte interactions. This approach is still today the most widely used for the design of chemical sensors. The relevance of this binding site-signalling subunit approach is highlighted by the broad range of transition metal-based probes such as Pt(II), Ru(II), Re(I), Ir(III), Cu(I), Au(I) and Os(II) that have been developed in recent decades.[93]

- **Displacement protocol**

An alternative design approach for chemosensors is the use of indicator displacement assays (IDA). In this approach, an analyte is reversibly recognised by the receptor causing displacement of the indicator from the host, resulting in an optical signal. In this paradigm, the binding and signalling subunits are not

[91] Martínez-Máñez, R.; Sancenón, F. *J Fluoresc*, **2005**, *15*, 267-285.
[92] Khan, S.; Chen, X.; Almahri, A.; Allehyani, E. S.; Alhumaydhi, F. A.; Ibrahim, M. M.; Ali, S. *J Environ Chem Eng*, **2021**, *9,* 106381.
[93] Yeung, M. C.-L.; Yam, V. W.-W. *Chem Soc Rev*, **2015**, *44*, 4192-4202.

covalently linked. This detection strategy can be classified as either colorimetric IDA, which uses colorimetric reporters, or fluorescent IDA, which uses fluorescent indicators. In addition, in a third type, called metal displacement approach (MDA), the metal contained in the sensor forms a complex with the analyte. In this case, changes in emission and/or absorption properties result from the displacement of the metal from the fluorophore or chromophore unit.[94]

Chemodosimeter paradigm

Chemodosimeters are usually based on an irreversible and selective chemical interaction with the target analyte that causes deep alterations in the chemical structure of the sensor and, consequently, changes in its optical properties. Consequently, chemodosimeter consist of the integration of a signalling unit and a reaction/recognition site on a detection molecule.[95]

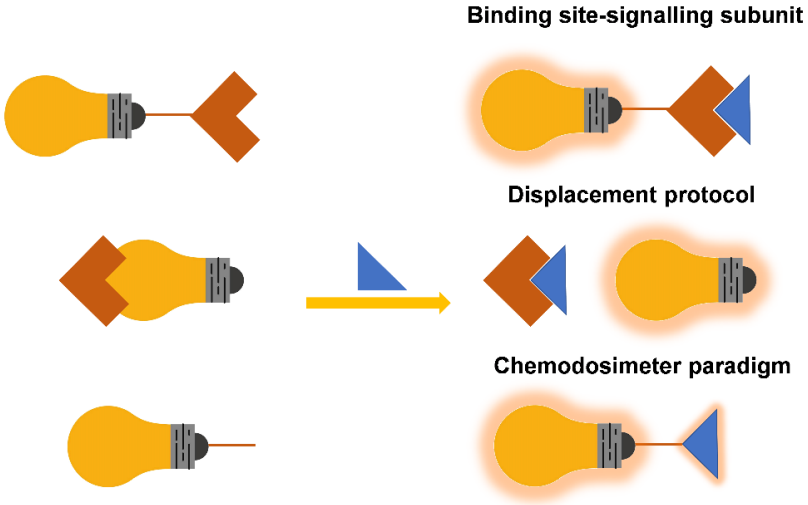

Figure 23. Representative scheme of the three main approaches used in the development of optical chemosensors.

[94] Descalzo, A. B.; Rurack, K.; Weisshoff, H.; Martínez-Máñez, R.; Marcos, M. D.; Amorós, P.; Hoffmann, K.; Soto, J. *J Am Chem Soc*, **2005**, *127*, 184-200.
[95] Martínez-Máñez, R.; Sancenón, F. *Coord Chem Rev*, **2006**, *250*, 3081-3093.

In this context, this PhD thesis has explored the development of different sensors based on smart organic-inorganic hybrid mesoporous silica nanomaterials capped with logic molecular gates based on biomolecules, as well as metal complexes-based chemical sensors for the *in-situ* detection of the main illicit substances of interest.

CHAPTER 2

OBJECTIVES

Considering the exponential growth in the consumption of psychoactive substances and the difficulty of a selective detection after ingestion, the development of chromo-fluorogenic sensors able to detect them *in situ* and in short time periods is a crucial challenge. Thus, taking advantage of the versatility of mesoporous silica materials as well as transition metal coordination complexes, this PhD thesis has contributed to the field of sensors with the development of certain smart systems based on mesoporous silica nanoparticles and coordination complexes for the selective and sensitive detection of illicit drugs in realistic environments.

In particular, we focused on the synthesis, characterization and evaluation of nanodevices based on mesoporous silica nanoparticles functionalized with antibodies and receptor-substrate supramolecular complexes as molecular gates for the fluorogenic detection of psychoactive drugs of interest. In addition, we carried out the preparation and studied the sensing behavior toward drugs of a coordination complex using transition metals.

The specific objectives have been

- To prepare a nanosensor for the fluorometric selective detection of 25I-NBOMe (25I-N-Methoxybenzyl) based on gated MSNs and evaluate its sensing behavior in sweets.
- To develop a fluorogenic nanosensor able to detect 3,4-methylenedioxypyrovalerone (MDPV) in competitive media such as saliva and blood plasma using gated MSNs.
- To design a user-friendly portable strip assay for the simultaneous *in situ* detection of scopolamine and MDPV in saliva using a dual-channel strip with smartphone readout.
- To synthesize a sensing ensemble based on a Cu^{2+} complex with a tetradentate ligand and the fluorescent dye coumarin 343, that can detect GHB through an indicator displacement assay (*IDA*) and check the performance integrated into a lateral flow assay with smartphone readout.

CHAPTER 3

NANOSENSOR FOR SENSITIVE DETECTION OF THE NEW PSYCHEDELIC DRUG 25I-NBOME

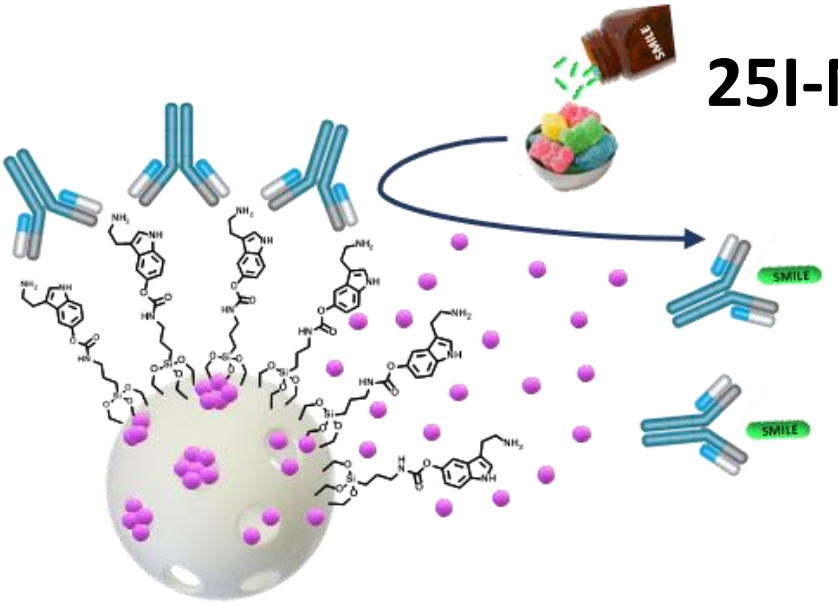

NANOSENSOR FOR SENSITIVE DETECTION OF THE NEW PSYCHEDELIC DRUG 25I-NBOME

Eva Garrido,[a],[b],[c],[d] María Alfonso,[a],[c],[d] Borja Díaz de Greñu,[a],[b],[c],[d] Beatriz Lozano-Torres,[a],[b],[c],[d] Margarita Parra,[a],[b],[e] Pablo Gaviña,[a],[b],[e] M. Dolores Marcos,[a],[b],[c],[d],[f] Ramón Martínez-Máñez,*[a],[b],[c],[d],[f] and Félix Sancenón*[a],[b],[c],[d],[f]

[a] Instituto Interuniversitario de Investigación de Reconocimiento Molecular y Desarrollo Tecnológico (IDM), Universitat Politècnica de València, Universitat Politécnica de València, Camino de Vera s/n, 46022, Valencia (Spain). E-mail: rmaez@qim.upv.es; fsanceno@upvnet.upv.es

[b] CIBER de Bioingeniería, Biomateriales y Nanomedicina (CIBER-BBN) (Spain)

[c] Unidad Mixta de Investigación en Nanomedicina y Sensores. Universitat Politècnica de València, Instituto de Investigación Sanitaria La Fe. Avenida Fernando Abril Martorell, Torre 106 A 7ª planta, 46026, Valencia (Spain)

[d] Unidad Mixta UPV-CIPF de Investigación en Mecanismos de Enfermedades y Nanomedicina. Universitat Politècnica de València, Centro de Investigación Príncipe Felipe Carrer d'Eduardo Primo Yúfera, 3, 46012, Valencia (Spain)

[e] Departamento de Química Orgánica, Universitat de València. Doctor Moliner 50, Burjassot, 46100, Valencia (Spain)

[f] Departamento de Química, Universitat Politècnica de València, Camino de Vera s/n, 46022, Valencia (Spain)

Published online: 14 January *2020*

(Reprinted with permission from ***Chem. Eur. J.*** **2020, *26*, 2813-2816**)

3.1. ABSTRACT

This work reports the synthesis, characterization, and sensing behavior of a hybrid nanodevice for the detection of the potent abuse drug 25I-NBOMe. The system is based on mesoporous silica nanoparticles, loaded with a fluorescent dye, functionalized with a serotonin derivative and capped with the 5-HT_{2A} receptor antibody. In the presence of 25I-NBOMe the capping antibody is displaced, leading to pore opening and rhodamine B release. This delivery was ascribed to 5-HT_{2A} receptor antibody detachment from the surface due to its stronger coordination with 25I-NBOMe present in the solution. The prepared nanodevice allowed the sensitive (limit of detection of 0.6 μM) and selective recognition of the 25I-NBOMe drug (cocaine, heroin, mescaline, lysergic acid diethylamide, MDMA, and morphine were unable to induce pore opening and rhodamine B release). This nanodevice acts as a highly sensitive and selective fluorometric probe for the 25I-NBOMe illicit drug in artificial saliva and in sweets.

KEYWORDS: *25I-NBOMe, agonist 5-HT_{2A}, serotonin receptor, hallucinogenic drugs, mesoporous silica nanoparticles, sensors.*

3.2. INTRODUCTION

In recent years, the appearance and availability of new psychoactive substances (NPS) in the illicit market has increased exponentially, becoming a serious worldwide problem causing concern for governments and international institutions. Indeed, according to the last reports published,[1] 275 million people, approximately 5.6% of the global population used drugs, at least once, in 2016. Among NPS, hallucinogenic drugs are proliferating and gaining popularity.

Recently, a new synthetic family of N-benzylphenethylamines (NBOMes) as hallucinogenic potent abuse drugs started to be available online. Normally, these drugs are consumed as a powder, in solution and in different supports such as

blotting paper administered sublingually (in doses around 750 mg).[2] Moreover, these drugs have also been detected in adulterated commercial sweets (gummy bears), which are normally distributed in pubs.[3]

One of the most remarkable members, among NBOMes derivatives, is 25I-NBOMe, well-known by its street names of “Smiles”, “Solaris”, “N-Bomb” or “Wizard”. Structurally, 25I-NBOMe is a phenethylamine derived from the 2C family of NBOMes in which the 2- and 5-positions of a benzene ring have been substituted by methoxy groups. 25I-NBOMe, as well as other members of the NBOMe family, act as extremely potent and highly selective agonists of the serotonin 5-HT_{2A} receptor.[4] This drug is considered a highly powerful hallucinogen in humans, and among its main effects can be found euphoria, anxiety, paranoia, memory suppression, or empathy enhancement. Furthermore, its consumption (common dosage between 0.2 and 1 mg)[5] is highly toxic and is associated with fatal cases published in recent years.[6] All these issues make the detection of this drug highly important.

25I-NBOMe can be detected by several instrumental techniques such as HPLC-MS,[7] GC-MS,[8] differential pulse voltammetry,[9] ATR-FTIR spectrometry,[10] and bioanalytical procedures.[11] However, for most of these methods, samples must be moved to qualified laboratories, require the use of complex techniques and the supervision of trained personnel, and cannot be applied to in situ or at-site analysis. In order to overcome these typical drawbacks of classical analytical techniques, the development of chemo-fluorogenic probes has become a matter of concern for the rapid and easy detection of analytes. However, as far as we know, there are no reported optical probes for the detection of the new drug 25I-NBOMe.

Among different approaches to develop optical probes, the use of hybrid organic–inorganic gated materials have been recently reported. These sensing hybrid probes are based on the use of a porous inorganic scaffold in which a

reporter unit (usually a dye or a fluorophore) is stored and a bulky (supra)-molecular ensemble is used as a cap, blocking the pores and inhibiting dye/fluorophore release. The capping ensemble is designed in such a way that interaction/coordination with a target analyte induces changes in its conformation/size/shape or is displaced, resulting in pore opening and dye/fluorophore release. One of the advantages of these sensing materials is the potential existence of amplification features. In particular, it has been demonstrated that the presence of a few analyte molecules may induce the release of a relatively high amount of entrapped dye/fluorophore molecules.[12] As support for the development of such sensing hybrid materials, mesoporous silica nanoparticles (MSNs) have been used. The main advantages provided by MSNs are their high specific surface area, homogeneous porosity, high load capacity, tunable pore size (2-10 nm), and easy functionalization using well-known chemistries.[13] Based on the above, we report herein the preparation of a selective and sensitive fluorogenic probe for the hallucinogen drug 25I-NBOMe.

The probe consists of MSNs loaded with rhodamine B, functionalized with a serotonin derivative (**3**) and capped with a polyclonal antibody of the 5-HT_{2A} receptor. The nanoparticles are designed to show “zero” release, yet open in the presence of the 25I-NBOMe drug. The base of the sensing mechanism arises from a competition between the grafted serotonin derivative and 25I-NBOMe for the coordination with the antibody of the 5-HT_{2A} receptor. The antibody is known to have more affinity for 25I-NBOMe than for the serotonin derivative and therefore the presence of 25I-NBOMe is expected to induce a displacement of the cap and selective dye delivery (Scheme 1).

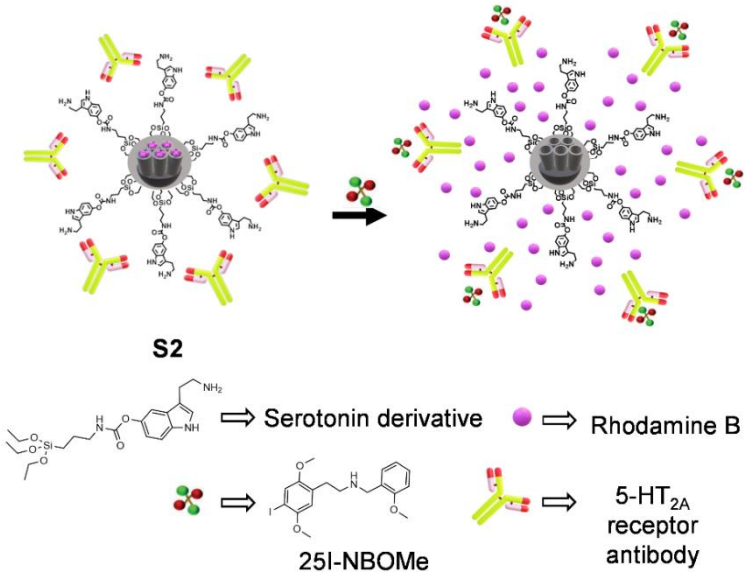

Scheme 1. Mechanism of release of solid **S2** in the presence of 25I-NBOMe.

3.3. RESULTS AND DISCUSSION

MSNs were synthesized by base-catalyzed sol-gel condensation of tetraethyl orthosilicate (TEOS) in the presence of hexadecyltrimethylammonium bromide (CTABr) as structure directing agent following well-known procedures.[14] The pores of the MSNs were loaded with rhodamine B (solid **S0**) and the external surface of the nanoparticles was functionalized with the serotonin derivative **3** (Scheme 2, **S1-Boc**). The Boc protecting group from **3** was then removed using trifluoroacetic acid (TFA), giving rise to the solid **S1**. The final probe (**S2**) was obtained after stirring a suspension of **S1** containing the antibody of the 5-HT_{2A} receptor (see experimental details in the Supporting Information (SI)). Moreover, compound **3** was synthesized by the protection of the amino group of serotonin (**1**) with ditert-butyl dicarbonate (Boc_2O) to obtain **2**[15] that was further reacted with (3-isocyanatopropyl)triethoxysilane (Scheme 2). Compound **3** was characterized by using magnetic resonance techniques such as ^{1}H NMR and ^{13}C NMR (Figures S1 and S2, SI). Furthermore, the nanoparticles were characterized by using standard

techniques as powder X-ray diffraction (PXRD), transmission electron microscopy (TEM), N_2 adsorption–desorption isotherms, and elemental and thermogravimetric analyses (Figures S3–S6, SI).

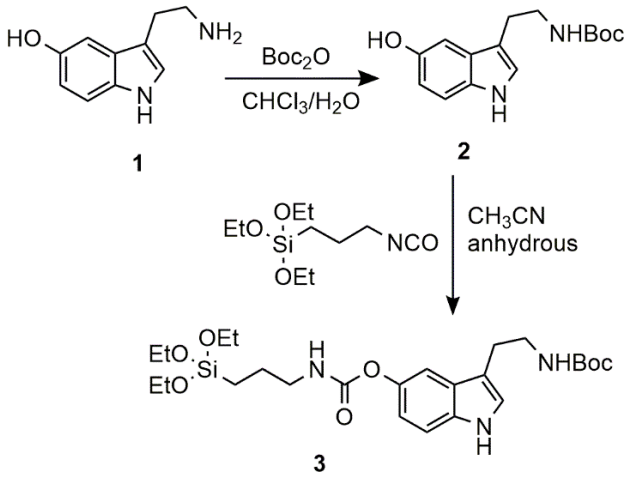

Scheme 2. Synthetic route used for the preparation of serotonin derivative **3**.

The response of the sensing material **S2** to the "Smiles" drug was evaluated. Figure 1 shows the dye release profile (TRIS saline Buffer at pH 7.3) from **S2** obtained in the absence and the presence of the drug. Dye delivery was followed measuring the fluorescence of the rhodamine B at 572 nm at scheduled times in the solution. As can be seen, a large signal (i.e., dye delivery) was observed in the presence of 25I-NBOMe when compared with the same material in the absence of the drug. This confirms the preferential interaction of the antibody for 25I-NBOMe that results in pore opening and cargo release.

To further confirm that the 5-HT_{2A} antibody plays a key role in the gating mechanism, we also studied the delivery profiles of the uncapped solid **S1** in the absence and presence of 25I NBOMe. In this case, a marked rhodamine B release was observed in both cases (Figure S7, SI).

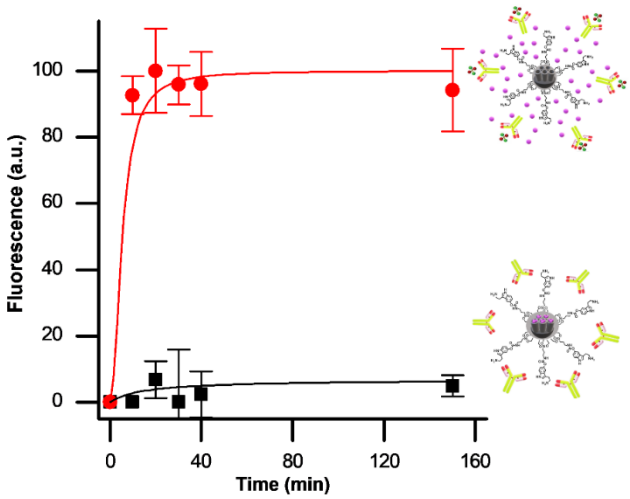

Figure 1. Release profile of rhodamine B from suspensions of solid **S2** in TRIS saline buffer at pH 7.3, in the absence (black line) and in the presence (red line) of 25I-NBOMe (300 µM). Error bars are expressed as 3σ.

The sensitivity of **S2** towards the "Smiles" drug was also tested. In this case, dye delivery from **S2** in TRIS saline buffer towards increasing concentrations of the drug was followed. Figure S8 shows the gradual rise in the fluorescent emission with increasing concentrations of "Smiles" (each point measured 30 min after addition). From the titration profile, a detection limit of 0.6 µM for 25I-NBOMe was obtained. This value is enough to detect a common dose (0.75 mg) even if diluted in 2 L of water.

The response of the antibody-capped solid **S2** was also studied against other selected drugs (Scheme 3). In particular, we selected lysergic acid diethylamide (LSD) because "Smiles" drug is used as a substitute for LSD due to its cheaper cost and comparable effects. Mescaline was selected because it also belongs to NBOMe family. Finally, the other common drugs such cocaine, heroin, MDMA, and morphine were included in the study since their consumption as psychoactive drugs is widespread. For this study, solid **S2** was suspended in TRIS saline buffer at pH 7.3 in the presence of a final concentration of 75 µM of the

drugs. As showed in Figure 2, after 20 min only 25I-NBOMe produces a remarkable enhancement in the emission fluorescence (at 572 nm) when compared with the blank (absence of drugs), whereas other drugs induce either no or poor delivery. In addition, solid **S2** can be stored dried at 4℃ for at least 1 month, without dropping selectivity and sensitivity.

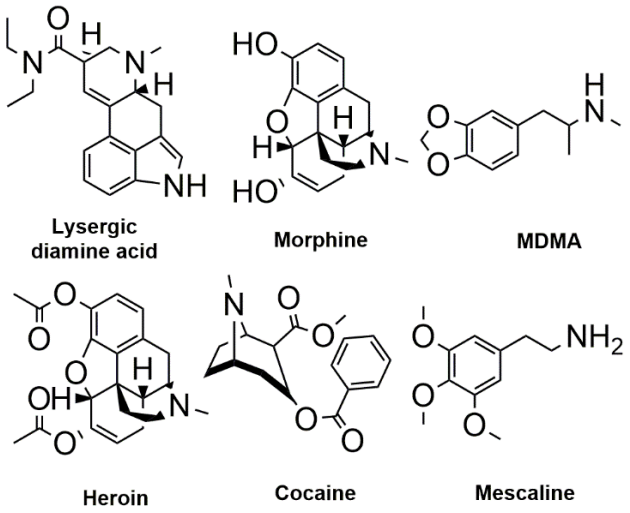

Scheme 3. Chemical structure of the drugs used as interferents for selectivity studies.

In order to test the potential applicability of the probe in competitive environments, we tested the ability of **S2** to detect 25I-NBOMe in artificial saliva and commercial sweets. For this purpose, we prepared artificial saliva and measured the controlled release of rhodamine B from **S2** nanoparticles in the absence and in the presence of the drug. The results obtained are depicted in Figure S9, which shows that even in this competitive medium 25I-NBOMe induced a remarkable uncapping of the **S2** probe. Additional studies indicated that in artificial saliva a detection limit of 0.9 µM for 25I-NBOMe was obtained (Figure S10), which is a value comparable with that found in TRIS buffer solution.

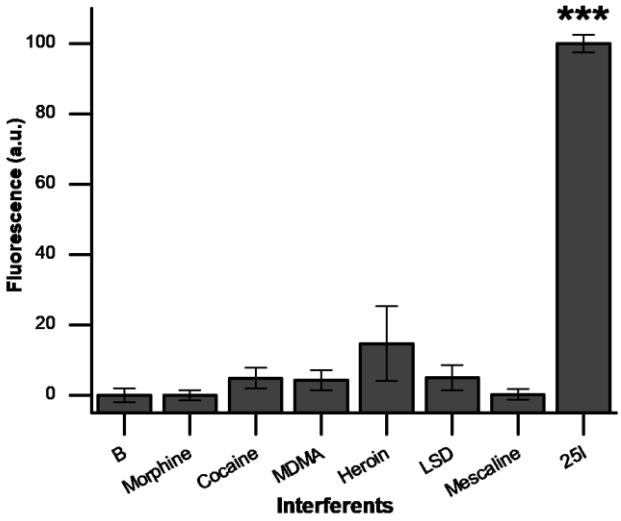

Figure 2. Released rhodamine B from solid **S2** (measured as fluorescence intensity at 572 nm) in the presence of 75 µM of the indicated drugs in TRIS saline buffer at pH 7.3 (after 20 min of addition). Error bars are expressed as 3σ for three independent experiments (***p<0.0001).

For the detection of "Smiles" in adulterated candies with probe **S2**, a commercial sweet was adulterated with 5 mg of the drug (Figure S11). The adulterated sweet was introduced in an Erlenmeyer flask with 10 mL of EtOH and shaken at room temperature for 30 minutes to extract 25I-NBOMe. As shown in Figure 3, rhodamine B release is significantly higher when the candies are adulterated. Additional studies demonstrated that the probe does not respond to typical components of sweet such as tartrazine, starch, glucose, saccharose, and jelly (Figure S12).

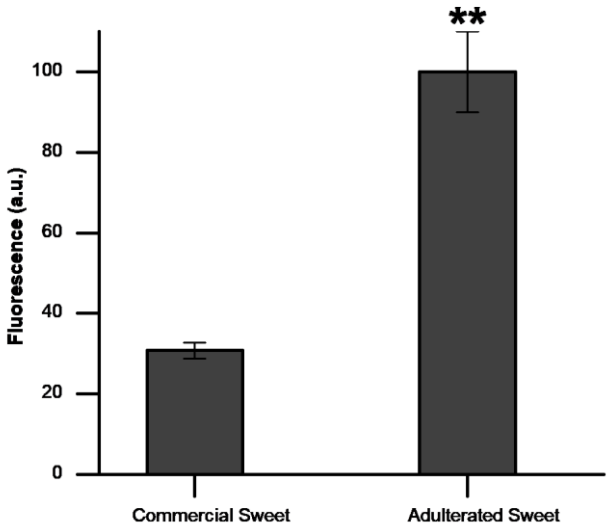

Figure 3. Fluorescence emission at 572 nm (λ_{exc} = 565 nm) associated with rhodamine B released from **S2** after 30 min of incubation with adulterated and non-adulterated sweet extract. Error bars are expressed as 3s for three independent experiments (**p≤0.001).

3.4. CONCLUSIONS

In summary, we have developed a first, rapid, highly selective and sensitive sensor for the fluorogenic detection of the synthetic drug 25I-NBOMe. The sensing material is synthesized using mesoporous silica nanoparticles loaded with rhodamine B (as a model fluorophore) and capped with 5-HT_{2A} receptor antibody through its interaction with the serotonin derivative **3** grafted onto the external surface of the material. Only in the presence of 25I-NBOMe, a remarkable release of rhodamine B from the nanodevice is observed due to the detachment of the 5-HT_{2A} receptor antibody from the nanoparticle surface due to its marked affinity toward the drug. Furthermore, solid **S2** shows a highly selective response against 25I-NBOMe with a detection limit as low as 0.6 µM in TRIS saline buffer. We also demonstrated that solid **S2** can be used for the reliable identification “in situ” and “at-site” of 25I-NBOMe in artificial saliva and adulterated sweets. We have taken advantage of the use of antibodies as promising biomolecules for the preparation of custom-made nanodevices for sensing applications. The possibility to select a

countless number of antibodies for a number of targets makes this approach highly appealing.

ACKNOWLEDGEMENTS

The authors thank the Spanish Government (projects RTI2018-100910-B-C41 (MCUI/AEI/FEDER, UE) and CTQ2017-87954-P) and the Generalitat Valencia (PROMETEO/2018/024) for support. E.G. is grateful to the Spanish MEC for her FPU grant. The authors also thank the Electron Microscopy Service at the UPV for support.

3.5. REFERENCES

[1] a) World drug report. United Nations Office on Drugs and Crime (UNODC). Inform **2018**; b) European drug report: Trends and Developments. European Monitoring Centre for Drugs and Drug Addition (EMCDDA). Inform **2018**.

[2] a) D. Zuba, K. Sekula, A. Buczek, *Forensic Sci. Int.* **2013**, *227*, 7–14; b) J. L. Poklis, S. A. Raso, K. N. Alford, A. Poklis, M. R. Peace, *J. Anal. Toxicol.* **2015**, *39*, 617–623; c) Agenda item 4.19. *Expert Committee on Drug Dependence. Thirty-sixth Meeting.* Geneva, 16–20, June **2014** (World Health Organization).

[3] A. Batisse, N. Taright, C. Chevallier, M. Marillier, S. Djezzar, *Eur. Psychiatry* **2016**, *33*, S72.

[4] A. Rickli, D. Luethi, J. Reinisch, D. Buchy, M. C. Hoener, M. E. Liechti, *Neuropharmacology* **2015**, *99*, 546–553.

[5] W. Lawn, M. Barratt, M. Williams, A. Horne, A. Winstock, *J. Psychopharmacol.* **2014**, *28*, 780–788.

[6] a) V. B. Kueppers, C. T. Cooke, *Forensic Sci. Int.* **2015**, *249*, e15–e18; b) L. K. Laskowski, F. Elbakoush, J. Calvo, G. Exantus-Bernard, J. Fong, J. L. Poklis, A. Poklis, L. S. Nelson, *J. Med. Toxicol.* **2015**, *11*, 237–241; c) K. G. Shanks, T. Sozio, G. S. Behonick, *J. Anal. Toxicol.* **2015**, *39*, 602 –606.

[7] K. Francisco da Cunha, M. N. Eberlin, J. L. Costa, *Forensic Toxicol*. **2018**, *36*, 113–121.

[8] A. T. Caspar, A. G. Helfer, J. A. Michely, V. Auwaerter, S. D. Brandt, M. R. Meyer, H. H. Maurer, *Anal. Bioanal. Chem.* **2015**, *407*, 6697–6719.

[9] a) A. F. B. Andrade, S. K. Mamo, J. Gonzalez-Rodriguez, *Anal. Chem.* **2017**, *89*, 1445–1452; b) A. F. Belchior de Andrade, J. Gonzalez-Rodriguez, *Analyst* **2019**, *144*, 2965–2972.

[10] J. Coelho Neto, *Forensic Sci. Int.* **2015**, *252*, 87–92.

[11] X. Wu, C. Eriksson, A. Wohlfarth, J. Wallgren, R. Kronstrand, M. Josefsson, J. Dahlen, P. Konradsson, *Tetrahedron* **2017**, *73*, 6393–6400.

[12] a) E. Aznar, M. Oroval, L. Pascual, J. R. Murguia, R. Martinez-Manez, F. Sancenon, *Chem. Rev.* **2016**, *116*, 561–718; b) I. I. Slowing, J. L. Vivero- Escoto, B. G. Trewyn, V. S. Y. Lin, *J. Mater. Chem.* **2010**, *20*, 7924–7937; c) E. Aznar, C. Coll, M. D. Marcos, R. Martínez-Mañez, F. Sancenón, J. Soto, P. Amorós, J. Cano, E. Ruiz, *Chem. Eur. J.* **2009**, *15*, 6877–6888; d) A. Ribes, E. Aznar, S. Santiago-Felipe, E. Pérez-Xifré, M. A. Tormo-Mas, J. Pemán, Ll. F. Marsal, R. Martínez-Máñez, *ACS Sens.* **2019**, *4*, 1291–1298.

[13] a) C. Coll, A. Bernardos, R. Martinez-Manez, F. Sancenon, *Acc. Chem. Res.* **2013**, *46*, 339–349; b) F. Sancenón, L. Pascual, M. Oroval, E. Aznar, R. Martínez-Máñez, *ChemistryOpen* **2015**, *4*, 418–437; c) E. Aznar, R. Villalonga, C. Giménez, F. Sancenón, M. D. Marcos, R. Martínez-Máñez, P. Díez, J. M. Pingarrón, P. Amorós, *Chem. Commun.* **2013**, *49*, 6391–6393; d) C. Giménez, C. de la Torre, M. Gorbe, E. Aznar, F. Sancenón, J. R. Murguía, R. Martínez-Máñez, M. D. Marcos, P. Amorós, *Langmuir* **2015**, *31*, 3753–3762.

[14] a) J. S. Beck, J. C. Vartuli, W. J. Roth, M. E. Leonowicz, C. T. Kresge, K. D. Schmitt, C. T. W. Chu, D. H. Olson, E. W. Sheppard, S. B. McCullen, J. B. Higgins, J. L. Schlenker, *J. Am. Chem. Soc.* **1992**, *114*, 10834–10843; b) W. Stöber, A. Fink, E. Bohn, *J. Colloid Interface Sci.* **1968**, *26*, 62–69.

[15] H. Meng, Y. Liu, Y. Zhai, L. Lai, *Eur. J. Med. Chem.* **2013**, *59*, 160–167.

3.6. SUPPORTING INFORMATION

MATERIALS AND METHOD

General techniques: Powder X-ray diffraction (PXRD), thermogravimetric analysis (TGA), elemental analysis, transmission electron microscopy (TEM) and N_2 adsorption-desorption isotherms were employed to characterize synthesized materials. PXRD measurements were taken on a D8 Advance diffractometer using Cu Kα radiation (Bruker, Massachusetts, United States). Thermogravimetric analyses were carried out on a TGA/SDTA 851e balance (Mettler Toledo, Columbus, OH, USA) in an oxidizing atmosphere (air, 80 mL min^{-1}) with a heating rate program between 393-1273 °C at 10 °C min^{-1}, followed by an isothermal heating step at 1273 °C for 30 min. TEM images were taken with a 100 kV CM10 microscope (Philips). N_2 adsorption-desorption isotherms were recorded with a Tristar II Plus automated analyser (Micromeritics, Norcross, GA, USA). The samples were degassed at 90 or 120 °C under vacuum overnight. Specific surface areas were calculated from the adsorption data within the low-pressure range using the Brunauer-Emmett-Teller (BET) model. Pore size was determined following the Barrett-Joyner-Halenda (BJH) method. Fluorescence spectroscopy measurements were taken on a JASCO FP-8300 spectrophotometer.

Solvents: All solvents were ACS reagent grade or better quality and were used without any further purification. Chloroform, anhydrous acetonitrile, anhydrous dichloromethane, anhydrous tetrahydrofuran (THF), ethanol (EtOH), diethyl ether (Et_2O), ethyl acetate, hexane, triethylamine (Et_3N), glacial acetic acid, trifluoracetic acid (TFA), and dimethyl sulfoxide (DMSO) were purchased from Scharlab S.L.

Chemicals reagents: Tetraethylorthosilicate (TEOS), *n*-cetyltrimethylammonium bromide (CTABr), sodium hydroxide, (3-isocyanatopropyl)triethoxysilane, serotonin hydrochloride, acetic anhydride, iodine monochloride (ICl), lithium aluminium hydride, trans-2,5-dimethoxy-β-nitrostyrene, ethyl trifluoroacetate, sodium borohydride, di-tertbutyl dicarbonate (Boc_2O) and rhodamine B were purchased from Sigma Aldrich química (Madrid, Spain). 5-HT_{2A} receptor polyclonal antibody (internal region) was purchased from AntibodyBcn S.L. Other drugs tested, morphine, cocaine, heroin, and MDMA were kindly provided by "Agencia Española de Medicamentos y Productos Sanitarios" (AEMPS). Mescaline and lysergic acid diethylamide (LSD) were purchased from Sigma Aldrich química (Madrid, Spain).

Synthesis of mesoporous silica nanoparticles: NaOH (2.00 mol L^{-1}, 3.5 mL) was added to a solution of CTABr (1.00 g, 2.74 mmol) in deionized H_2O (480 mL) at 40 °C. The solution temperature was adjusted to 80 °C and then TEOS (5.00 mL, 2.57 × 10^{-2} mol) was added dropwise. The mixture was stirred for 2 h to give a white precipitate. The solid was isolated by centrifugation and washed with deionized H_2O, and then dried at 70 °C for 12 h to give MCM-41. In order to remove the template phase, MCM-41 was calcined at 550 °C for 5 h in an oxidizing atmosphere.

Synthesis of S2

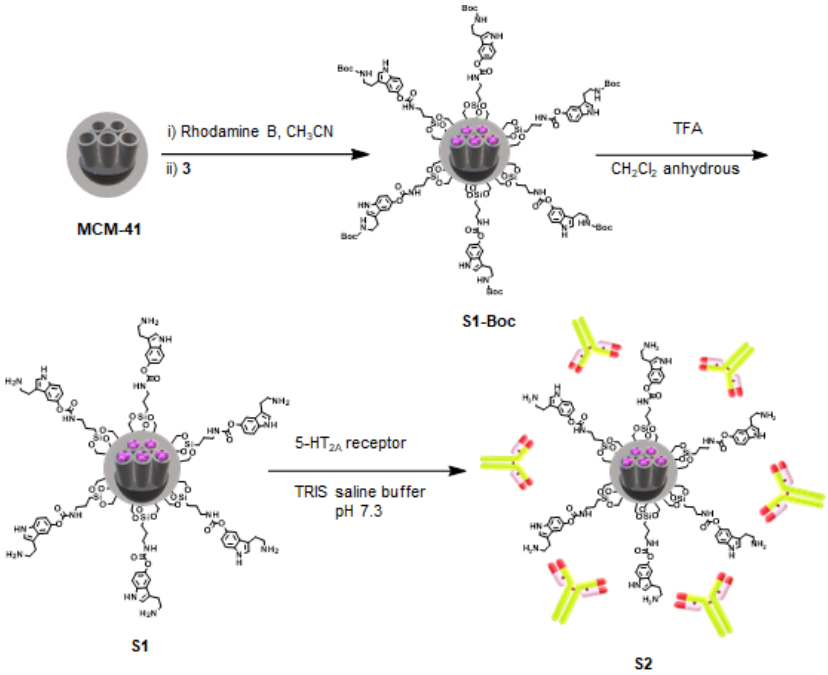

Scheme S1. Synthetic route for the synthesis of solid **S2**.

Synthesis of tert-butyl (2-(5-hydroxy-1H-indol-3-yl)ethyl)carbamate (2): Serotonin hydrochloride (**1**, 1.07 g, 5 mmol) was suspended in 10 mL of chloroform and then, sodium bicarbonate (0.42 g, 10 mmol) in 7 mL of H_2O, NaCl (1.00 g, 17 mmol) and ditert-butyl dicarbonate (1.1 g, 5 mmol) were successively added to the solution. The mixture was heated at 62 °C for 3 h. Afterward, the organic phase was washed with H_2O (40 mL), brine (20 mL), dried over $MgSO_4$, and filtered. Finally, the filtrate was concentrated under vacuum to obtain the product **2** as a grey oil (1.30 g, 4.71 mmol). Yield 94%.

Synthesis of tert-butyl(2-(5-(((3-(triethoxysilyl)propyl)carbamoyl)oxy)-1H-indol-3-ethyl)carbamate (3): To a solution of **2** (0.5 g, 1.81 mmol) in 20 mL of anhydrous CH_3CN, (3-isocyanatopropyl)triethoxysilane (0.5 mL, 1.81 mmol) was added and the reaction vessel was purged with Argon. The mixture was stirred at room temperature for 4 h. Finally, the solvent was removed under reduced

pressure to obtain the product **3** as an orange solid (940 mg, 1.81 mmol). Yield 99%. ^{1}H-NMR (400 MHz, $CDCl_3$) δ 8.18 (s, 1H), 7.29 (d, *J*=2.2 Hz, 1H), 7.28 (s, 1H), 6.98 (s, 1H), 6.94 (dd, *J1*=8.7, *J2*=2.2 Hz, 1H), 5.32 (dd, *J1*=12.3 Hz, *J2*=6.6 Hz, 2H), 4.60 (s, 1H), 3.84 (m, 9H), 3.32 (m, 6H), 2.88 (t, *J*=6.6 Hz, 2H), 1.72 (m, 2H), 1.43 (s, 9H), 1.23 (m, 6H) ppm. ^{13}C-NMR (101 MHz, $CDCl_3$) δ 155.96, 144.23, 133.87, 123.41, 116.75, 111.39, 111.12, 59.65, 58.51, 46.62, 41.33, 30.99, 28.42, 26.18, 23.22, 18.51, 18.30, 14.61, 7.72 ppm.

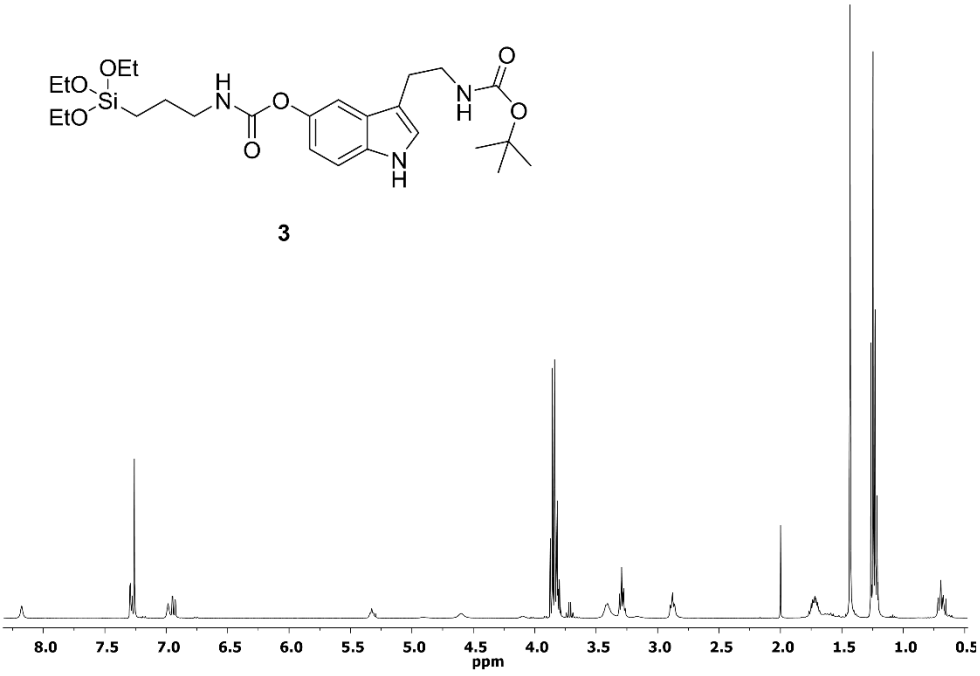

Figure S1. ^{1}H-NMR spectrum of **3** in $CDCl_3$.

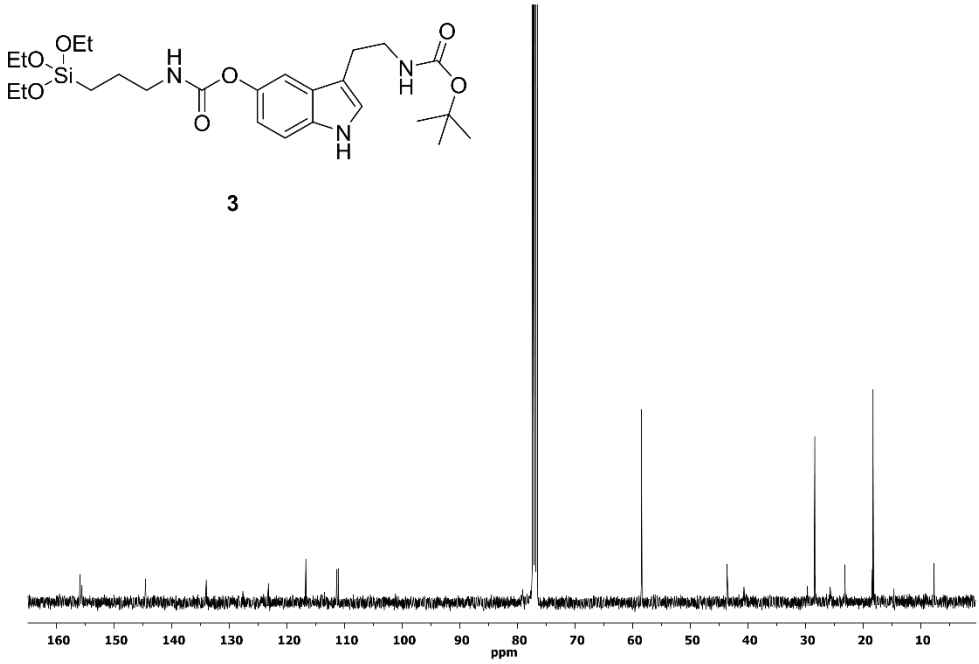

Figure S2. ^{13}C-NMR spectrum of **3** in $CDCl_3$.

Synthesis of S1-Boc: In a typical synthesis, a mixture of **c**alcined mesoporous silica nanoparticles (200 mg) and rhodamine B (76.64 mg, 0.16 mmol) were suspended in 7 mL of anhydrous CH_3CN. The system was purged with Argon. The suspension was stirred at room temperature for 24 h in order to load the MCM-41 pores. Then, compound **3** (107 mg, 0.2 mmol) was added and the final suspension was stirred at room temperature for further 5.5 h. Finally, the resulting pink solid was concentrated by rotary evaporation and then dried overnight at 37 °C, giving rise to **S1-Boc** (420 mg).

Synthesis of S1: S1-Boc (10 mg) was suspended in 2 mL of anhydrous CH_2Cl_2 and purged with Argon. Then the suspension was cooled to 0 ℃ and TFA (0.1 mL, 1.31 mmol) was added for the N-Boc deprotection reaction. The mixture was stirred at room temperature for 10 minutes and the solid was isolated by centrifugation and washed with deionized H_2O (2 × 8 mL) to reach pH 7.0. The final solid was dried

overnight at 37 °C. The proper functionalization of solid **S1** was assured by FTIR measurements (Figure S6).

Synthesis of S2: The solid **S1** (1.9 mg) was suspended in TRIS saline buffer (1.140 mL, 50 mM of TRIS and 150 mM of NaCl, pH 7.3) and then, 5-HT_{2A} receptor antibody (200 µL, 1.9 x 10^{-3} µM) was added. The mixture was stirred in a thermo-shaker at 25 ℃ for 5.5 h. After that, the suspension was centrifuged at 12,000 rpm for 5 min. **S2** was then washed with TRIS saline buffer (1 mL, 50 mM of TRIS and 150 mM of NaCl, pH 7.3) to eliminate the non-encapsulated dye and the unattached antibody.

Synthesis of 25I-NBOMe

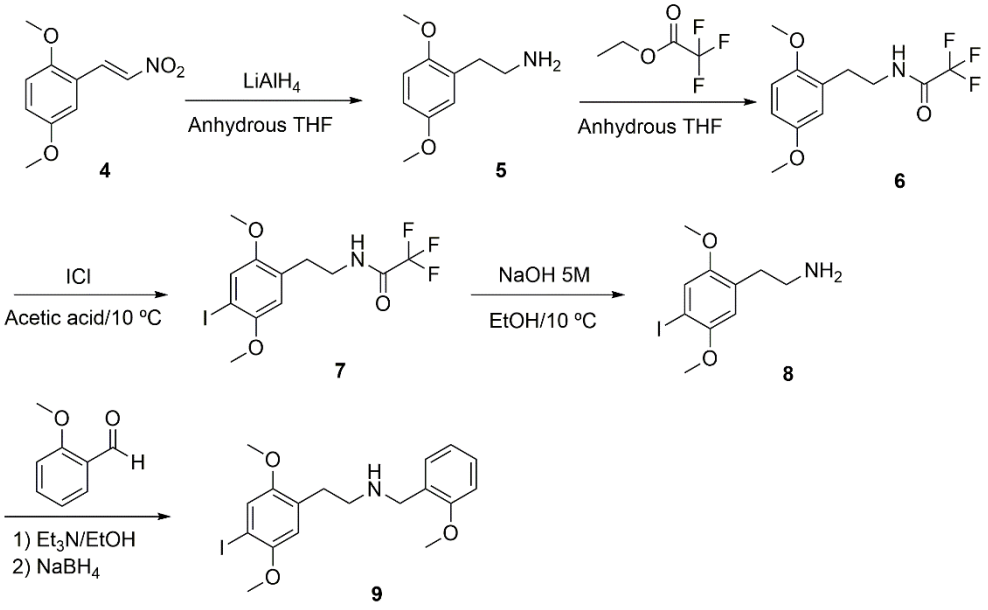

Scheme S2. Synthetic route of compound **9**, obtained according to the reported procedure[1].

Characterization of the prepared materials: The mesoporous silica nanoparticles and the mesoporous solid **S1** were characterized following standard techniques, including transmission electron microscopy (TEM), powder X-ray diffraction (PXRD) and N_2 adsorption/desorption analysis. The PXRD pattern of

siliceous MCM-41 nanoparticles as synthesized (Figure S3, curve a) shows four low-angle reflections typical of a hexagonal array, indexed as (100), (110), (200), and (210) Bragg peaks. Besides a cell parameter a_0 of 43.83 Å (distance between planes d_{100} = 38 Å) was determined. A significant displacement of 6-8 Å of the (100) peak in the PXRD pattern of the MCM-41 calcined nanoparticles is evident in curve b (see Figure S3), related to the further condensation of silanol groups in the calcination step. The displacement and widening of the (110) and (200) reflections are probably due to the condensation of the silanols on the surface of the material during the calcination process. Finally, curve c (also in Figure S3) corresponds to the **S1** PXRD pattern. The intensity decrease and the broadening of the (110) and (200) reflections is observed, related to a loss of contrast from filling pore voids with rhodamine B dye.

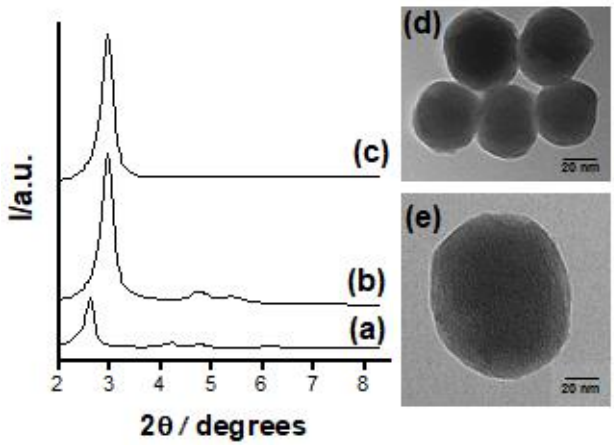

Figure S3. Powder X-ray diffraction (PXRD) patterns of solids (a) MCM-41 as synthesized, (b) calcined MSNs and (c) solid **S1**. TEM images of (d) calcined MCM-41 and (e) solid **S1**, showing both the typical porosity of the mesoporous silica matrix.

The presence of the mesoporous structure in the final functionalized solids was confirmed by TEM analyses, in which the mesopores, the morphology, and the typical hexagonal disordered porosity of the MCM-41 matrix are clearly visualized as alternate black and white stripes (see Figure S3). The figure also shows that

MCM-41 and solid **S1** are obtained as spherical particles with an average diameter of 100 ± 8 nm.

The N_2 adsorption–desorption isotherms of the calcined MCM-41 nanoparticles show a type 4 isotherm, typical from mesoporous materials, P/P_0 value (0.2–0.4) (curve a in Figure S4). This curve is ascribed to the condensation of nitrogen by capillarity inside the mesopores. The absence of hysteresis cycle in this interval and the shape of the curve suggest the existence of uniform and cylindrical mesopores with a pore diameter of 1.74 nm and a total pore volume of 0.26 cm^3 g^{-1} calculated by using the BJH model on the adsorption branch of the isotherm. The application of the Brunauer-Emmett-Teller (BET) model resulted in a value for the total specific surface of 1155 m^2 g^{-1}. The N_2 adsorption–desorption isotherm of **S1** (curve b in Figure S4) is typical of mesoporous systems with partially filled mesopores. A decrease in the pore volume (0.19 cm^3 g^{-1}) and surface area (79.24 m^2 g^{-1}) was observed.

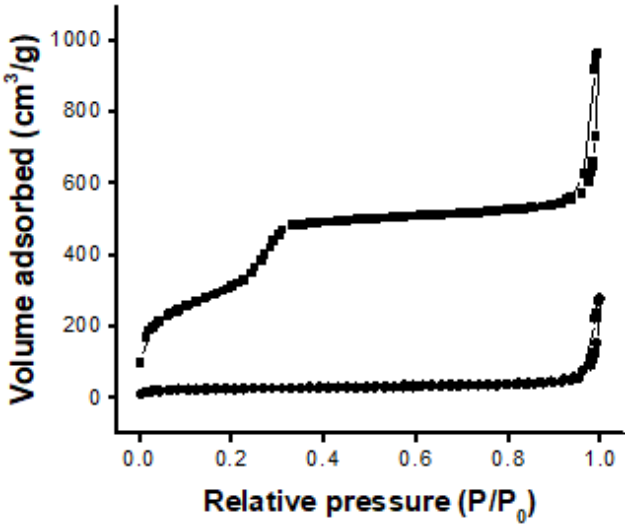

Figure S4. N_2 adsorption-desorption isotherms for (a) calcined MCM-41 nanoparticles and (b) **S1** material.

From thermogravimetric and elemental analysis studies (Figure S5), contents of 0.56 and 0.26 mmol g^{-1} of solid for rhodamine B and **3** respectively (in **S1**) were calculated, corresponding with 26 % of organic matter content in **S1** solid.

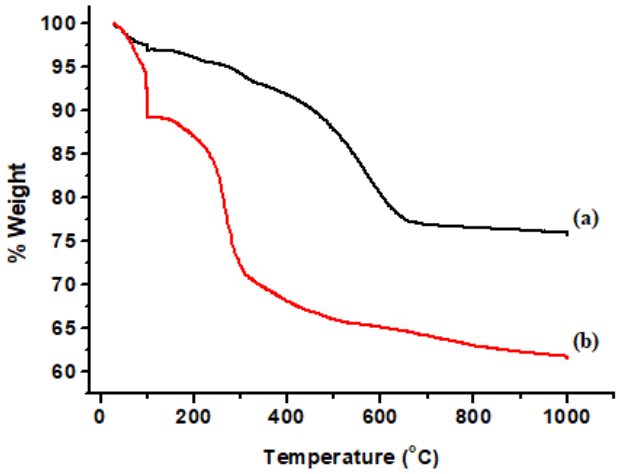

Figure S5. Thermogravimetric analysis for (a) calcined MCM-41 nanoparticles loaded with rhodamine B and (b) **S1** material.

FTIR spectrum of functionalized solid **S1** showed the typical absorption bands at ca. 1100 and 3400 cm^{-1} of the bond stretching vibrations of Si-O-Si and of O-H groups respectively (Figure S6). Moreover, the spectrum showed the stretching vibrations of amine groups at 3300 cm^{-1}.

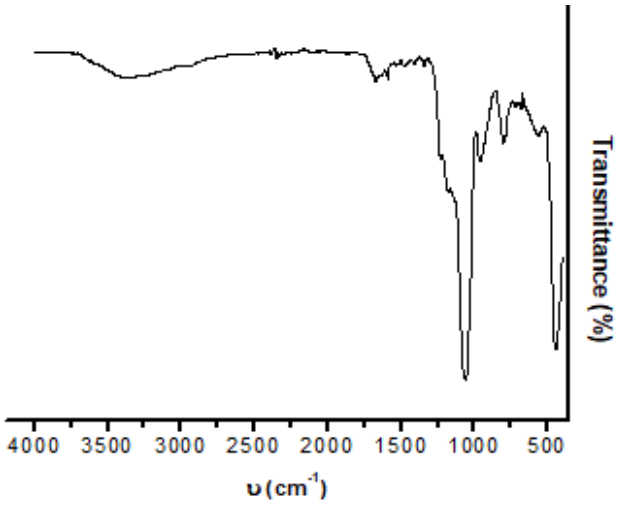

Figure S6. FTIR spectrum of solid **S1**.

Release experiments of solid S1 in the presence of 25I-NBOMe: To check the crucial role played by 5-HT_{2A} antibody, absent in **S1** but present in **S2**, 0.5 mg of solid **S1** were suspended in 400 µL of TRIS saline buffer (50 mM of TRIS and 150 mM of NaCl, pH 7.3) and this volume was separated into two aliquots of 200 µL. Both samples were centrifuged for 5 minutes at 12,000 rpm and the fluorescence (λ_{exc} = 565 nm, λ_{em} = 572 nm) of the supernatant (150 µL) was measured to obtain the initial point. This volume was returned to the corresponding aliquot. After that, 3 µL of a 20 mM solution of 25I-NBOMe in EtOH were added to one of the aliquots to obtain a final concentration of 300 µM, and simultaneously, 3 µL of EtOH were added to the blank aliquot. Both suspensions were stirred at 25 ̊C and, after certain time, 150 µL were separated, centrifuged (12,000 rpm for 5 min) and the fluorescence of the rhodamine B released (λ_{exc} = 565 nm, λ_{em} = 572 nm) was measured. Once measured, the 150 µL were returned to the initial suspension, stirred for another time interval and the emission of the dye released was measured over time (see Figure S7).

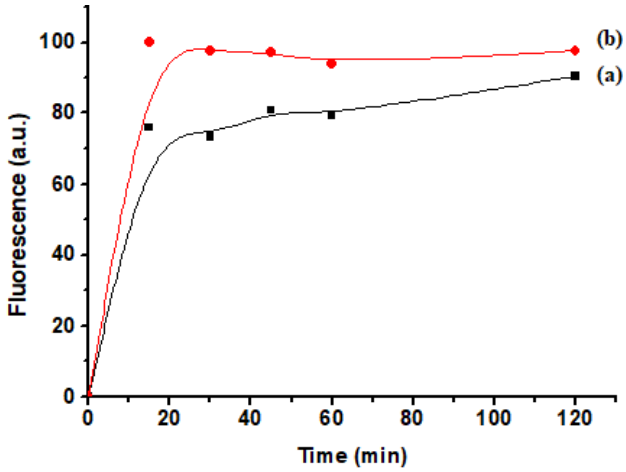

Figure S7. Release profiles of rhodamine B from TRIS saline buffer suspensions of solid **S1** at pH 7.3 (a) in the absence and (b) in the presence of 25I-NBOMe (300 µM).

Release experiments of solid S2 in the presence of 25I-NBOMe: The same procedure as in the previous experiment was followed using the solid **S2** (see Figure 1 in the manuscript).

Selectivity studies with S2: In order to test the selectivity of **S2** towards 25I-NBOMe, 0.5 mg of solid **S2** were suspended in 1.6 mL of TRIS saline Buffer (50 mM of TRIS and 150 mM of NaCl, pH 7.3) and this volume was separated into eight aliquots of 200 µL. Besides, several solutions in EtOH of different drugs (MDMA, morphine, lysergic acid diethylamide (LSD), heroin, cocaine, mescaline and 25I-NBOMe) at a concentration of 5 mM were prepared. All aliquots were centrifuged for 5 minutes at 12,000 rpm and the fluorescence (λ_{exc} = 565 nm, λ_{em} = 572 nm) of the supernatant (150 µL) was measured to obtain the initial point. This volume was returned to the corresponding aliquot. After that, 3 µL of each drug solution were added to the aliquots of **S2**, to reach a final concentration of 75 µM. Moreover, 3 µl of EtOH were added to the blank. The suspensions were stirred at 25 °C for 20 minutes and the fluorescence of the rhodamine B released was measured. (Figure 2 in the manuscript).

Determination of detection limit of S2 with 25I-NBOMe in TRIS Saline buffer: 0.5 mg of **S2** were suspended in 1.80 mL of TRIS saline buffer (50 mM of TRIS and 150 mM of NaCl, pH 7.3) and then divided into nine aliquots of 200 µL each one. Besides, several solutions of 25I-NBOMe in EtOH with concentrations within a range from 0.005 to 20 mM were prepared. All samples were centrifuged at 12,000 rpm for 5 minutes and the fluorescence (λ_{exc} = 565 nm, λ_{em} = 572 nm) of the supernatant (150 µL) was measured to obtain the initial point. This volume was returned to the corresponding aliquot. After that, 3 µL of each solution prepared were added to every aliquot (giving final concentrations ranging from 300 to 0.08 µM) and, simultaneously, 3 µL of EtOH were added to the blank aliquot. All suspensions were stirred at 25 ℃ for 30 minutes and the fluorescence of the rhodamine B released was measured over time (see Figure S8).

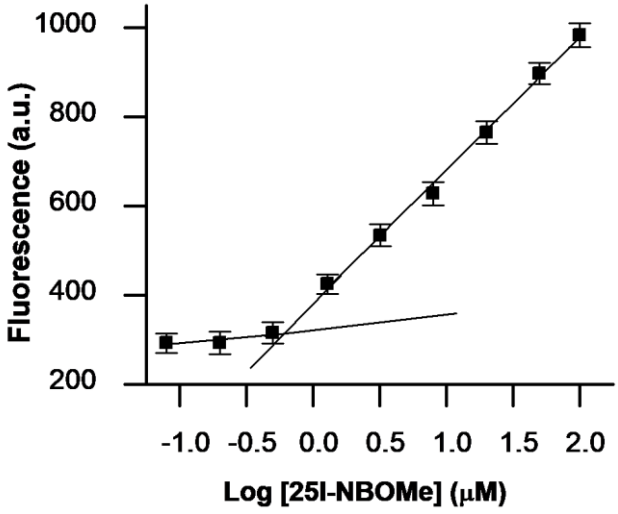

Figure S8. Fluorescence intensity of released rhodamine B from solid **S2** in the presence of different amounts of 25I-NBOMe in TRIS saline Buffer at pH 7.3 after 30 min of addition. Error bars are expressed as 3σ for three independent experiments.

Release experiments of solid S2 in the presence of 25I-NBOMe in artificial saliva: 0.5 mg of **S2** were suspended in 400 µL of artificial saliva[2] and this volume was separated into two aliquots of 200 µL each one. Both samples were centrifuged

for 5 minutes at 12,000 rpm and the fluorescence (λ_{exc} = 565 nm, λ_{em} = 572 nm) of the supernatant (150 µL) was measured to obtain the initial point. This volume was returned to the corresponding aliquot. After that, 3 µL of a 20 mM solution of 25I-NBOMe in EtOH were added to one of the aliquots to obtain a final concentration of 300 µM, and simultaneously, 3 µL of EtOH were added to the blank aliquot. Both suspensions were stirred at 25 ̊C and, after certain time, 150 µL were separated, centrifuged (12,000 rpm for 5 min) and the fluorescence of the rhodamine B released (λ_{exc} = 565 nm, λ_{em} = 572 nm) was measured. Once measured, the 150 µL were returned to the initial suspension, stirred for another time interval and the emission of the dye released was measured over time (Figure S9).

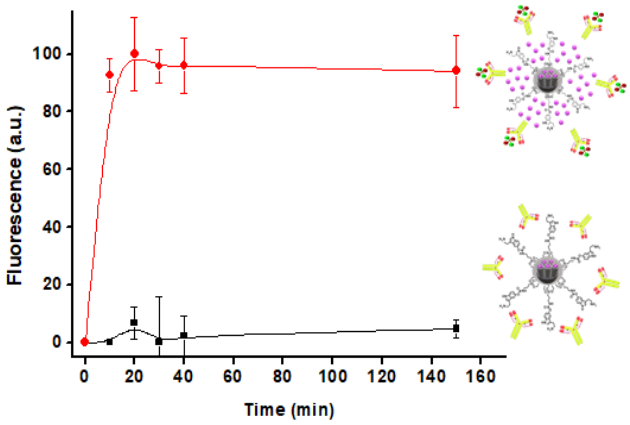

Figure S9. Release profiles of rhodamine B from artificial saliva suspensions of solid **S2** at pH 7.3 (a) in the absence and (b) in the presence of 25I-NBOMe (300 µM). Error bars are expressed as 3σ.

Determination of detection limit of S2 with 25I-NBOMe in artificial saliva: 0.5 mg of **S2** were suspended in 1.80 mL of 1% diluted artificial saliva and divided into nine aliquots of 200 µL each one. The experimental procedure is the same as the described in TRIS Saline buffer (see Figure S10).

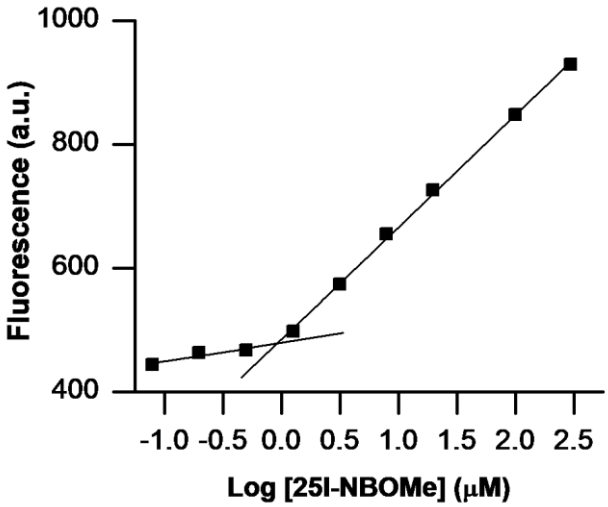

Figure S10. Release of rhodamine B from solid **S2** in the presence of different amounts of 25I-NBOMe in artificial saliva after 30 minutes of addition.

Release experiments of solid S2 in adulterated sweet: One commercial sweet was adulterated with 300 µL of a solution 0.039 M of 25I-NBOMe in EtOH, whereas another commercial sweet, used as blank extract, was sprinkled with 300 µL of EtOH. When the solvent of the spiked samples was evaporated, they were introduced in an Erlenmeyer flask with 10 mL of EtOH, and they were shaken at room temperature for 30 minutes to swell the sweet and extract 25I-NBOMe. Then, 100 µL were centrifuged at 12,000 rpm for 5 minutes and the supernatants were saved. At the same time, 0.5 mg of **S2** were suspended in 1.83 mL of TRIS saline Buffer (50 mM of TRIS and 150 mM of NaCl, pH 7.3) and this volume was separated into nine aliquots of 200 µL to evaluate the reproducibility. All samples were centrifuged for 5 minutes at 12,000 rpm and the fluorescence (λ_{exc} = 565 nm, λ_{em} = 572 nm) of the supernatant (150 µL) was measured to obtain the initial point. This volume was returned to the corresponding aliquot. After that, release experiments were carried out in triplicate. 3 µL of the adulterated sweet supernatant were added to three aliquots to obtain a final concentration of 1.17 mM. 3 µL of the blank extract supernatant were added to other three aliquots (blanks). Finally, other 3 µL

of ethanol were added to the last three aliquots (see Figure S11). Every suspension was stirred at 25℃ for 30 minutes and the fluorescence of the rhodamine B released was measured (see Figure 3 in the manuscript).

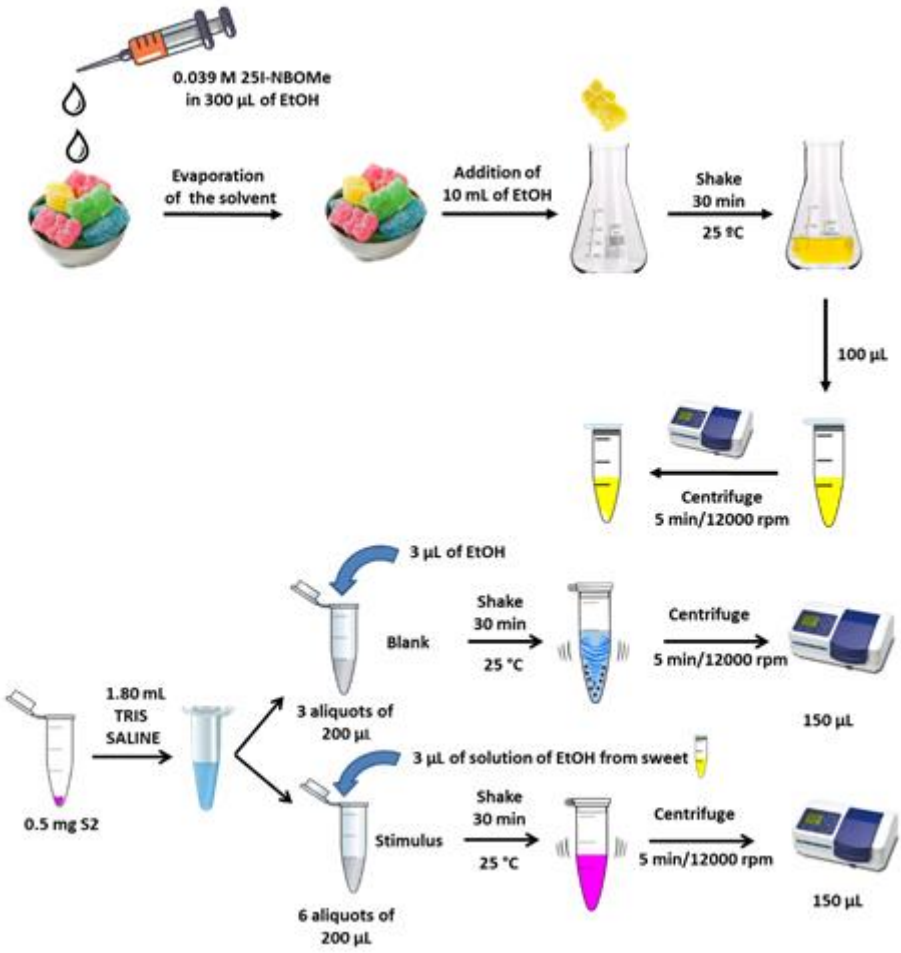

Figure S11. Drug detection procedure of 25I-NBOMe in adulterated sweets.

Selectivity studies with S2 in commercial sweet: According to literature, the composition of sweets is approximately 70-80 % of sucrose and glucose, 14 % of water, 5-6 % of jelly, 1 % of starch and dye (tartrazine).[3] For evaluation of the selectivity of the solid **S2** in sweet, 0.5 mg of **S2** were suspended in 1.4 mL of TRIS

saline Buffer (50 mM of TRIS and 150 mM of NaCl, pH 7.3) and were separated into seven aliquots of 200 µL each one. Besides, several solutions in EtOH of tartrazine, starch, glucose, sucrose, jelly, and 25I-NBOMe, at a concentration of 5 mM, were prepared. All aliquots were centrifuged for 5 minutes at 12,000 rpm and the fluorescence (λ_{exc} = 565 nm, λ_{em} = 572 nm) of the supernatant (150 µL) was measured to obtain the initial point. This volume was returned to the corresponding aliquot. After that, 3 µL of each interfering substance solution was added to six of the aliquots to obtain a final concentration of 75 µM, whereas 3 µl of EtOH were added to the blank. All suspensions were stirred at 25℃ for 20 minutes and the fluorescence of the rhodamine B released was measured. As showed in Figure S12, only 25I-NBOMe produces pore opening and subsequent rhodamine B release.

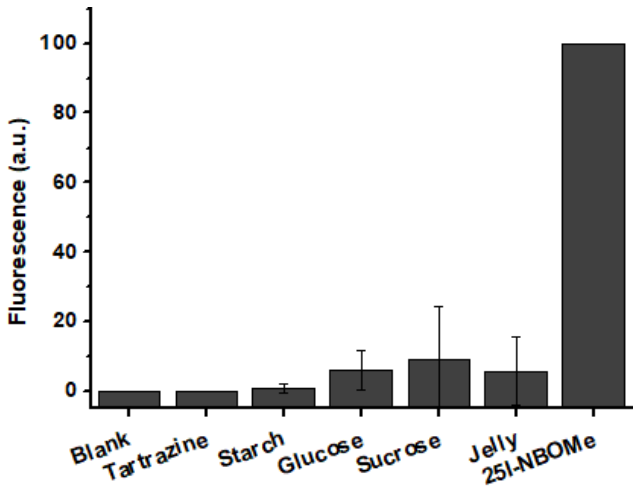

Figure S12. Release of rhodamine B from solid **S2** in the presence of 75 µM of tartrazine, starch, glucose, sucrose, jelly and 25I-NBOMe in TRIS saline buffer at pH 7.3 (after 20 minutes of addition). Error bars are expressed as 3σ for three independent experiments.

REFERENCES

[1] D. E. Nichols, S. P. Frescas, B. R. Chemel, K. S. Rehder, D. Zhong, A. H. Lewin, *Bioorgan. Med. Chem.* **2008,** *16 (11)*, 6116-6123.

[2] R. Saranya, R. Susai, *Der Pharma Chemica.* **2017,** *9*, 128-132.

[3] P. Burey, B. R. Bhandari, R. P. G. Rutgers, P. J. Halley, P. J. Torley, *Int. J. Food. Prop.* **2009,** *12*, 176-210.

CHAPTER 4

A SENSITIVE NANOSENSOR FOR THE *IN SITU* DETECTION OF THE CANNIBAL DRUG

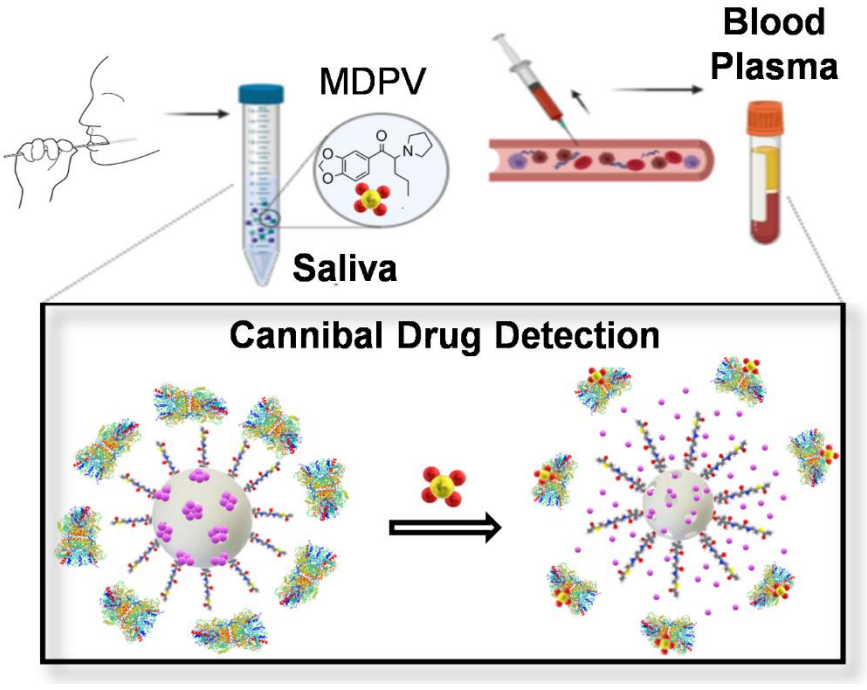

A SENSITIVE NANOSENSOR FOR THE *IN SITU* DETECTION OF THE CANNIBAL DRUG

Eva Garrido,[a],[b],[c],[d] María Alfonso,[a],[c],[d] Borja Díaz de Greñu,[a],[b],[c],[d] M. Dolores Marcos,[a],[b],[c],[d],[f] Ana M. Costero, [a],[b],[e] Salvador Gil, [a],[b],[e] Félix Sancenón*[a],[b],[c],[d],[f] and Ramón Martínez-Máñez,*[a],[b],[c],[d],[f]

[a] Instituto Interuniversitario de Investigación de Reconocimiento Molecular y Desarrollo Tecnológico (IDM), Universitat Politècnica de València, Universitat Politécnica de València, Camino de Vera s/n, 46022, Valencia (Spain). E-mail: rmaez@qim.upv.es; fsanceno@upvnet.upv.es

[b] CIBER de Bioingeniería, Biomateriales y Nanomedicina (CIBER-BBN) (Spain)

[c] Unidad Mixta de Investigación en Nanomedicina y Sensores. Universitat Politècnica de València, Instituto de Investigación Sanitaria La Fe. Avenida Fernando Abril Martorell, Torre 106 A 7ª planta, 46026, Valencia (Spain)

[d] Unidad Mixta UPV-CIPF de Investigación en Mecanismos de Enfermedades y Nanomedicina. Universitat Politècnica de València, Centro de Investigación Príncipe Felipe Carrer d'Eduardo Primo Yúfera, 3, 46012, Valencia (Spain)

[e] Departamento de Química Orgánica, Universitat de València. Doctor Moliner 50, Burjassot, 46100, Valencia (Spain)

[f] Departamento de Química, Universitat Politècnica de València, Camino de Vera s/n, 46022, Valencia (Spain)

Published online: 26 January *2020*

(Reprinted with permission from ***ACS Sens.*** **2020, *5*, 2966-2972**)

4.1. ABSTRACT

A bio-inspired nanodevice for the selective and sensitive fluorogenic detection of 3,4-methylenedioxypyrovalerone (MDPV), usually known as Cannibal drug, is reported. The sensing nanodevice is based on mesoporous silica nanoparticles (MSNs), loaded with a fluorescent reporter (rhodamine B), and functionalized on their external surface with a dopamine derivative (**3**), which specifically interacts with the recombinant human dopamine transporter (DAT), capping the pores. In the presence of MDPV, DAT detaches from the MSNs consequently, causing rhodamine B release and allowing drug detection. The nanosensor shows a detection limit of 5.2 µM, and it is able to detect the MDPV drug both in saliva and blood plasma samples.

KEYWORDS: *nanosensor, mesoporous silica nanoparticles, MDPV, cannibal drug, recombinant human dopamine transporter.*

4.2. INTRODUCTION

Over the last years, the unprecedented growth in the number of new psychoactive substances (NPS) globally available and the expansion of a more dynamic illegal market for these drugs is causing a great threat to public safety. Regarding last studies published, an estimated 271 million people worldwide had used psychoactive drugs at least once during 2019; roughly 5.5% of the global population.[1,2] Moreover, psychostimulants have reached popularity as potent abuse drugs.[3] Among NPS, synthetic cathinones have arisen as the most widespread class of designer drugs. This new group of recreational drugs, commonly known as bath salts, legal highs, plant food, or research chemicals, acts by improving the function of the three main monoamine neurotransmitters: i.e., dopamine, norepinephrine, and serotonin.[4,5] With regard to physical forms, cathinones are odorless, white or brownish solids, commonly presented in the illegal market as

powders or fine crystals and less frequently as tablets or capsules.[6,7] Main administration routes reported of cathinones are insufflation (snorting), oral ingestion (the substance is diluted in water or juice drink), and "bombing" (wrapping powders in a cigarette paper and next swallowed).[8]

Structurally, cathinones are β-ketone derivatives of psychoactive phenylalkylamine alkaloids, a naturally occurring stimulant in the khat plant (Catha edulis). One of the most remarkable constituents of the cathinone family is 3,4-methylenedioxypyrovalerone (MDPV). MDPV is popularly known as Cannibal drug, because, when taken in high doses, it spurs users into violent outbreaks of aggression, paranoia, and panic attacks.[9] MDPV differs from other synthetic cathinones in the fact that it contains a pyrrolidine ring, which gives the drug potent actions as an uptake blocker of dopamine and norepinephrine transporters. When consumed, MDPV links to the dopamine active transporter (DAT), blocking dopamine reuptake out of the synaptic cleft. In this way, MDPV leads to a rise in the extracellular dopamine levels, causing a powerful locomotive enhancement even 10 times more potent than that produced by cocaine.[10–12] Moreover, MDPV potentially produces some adverse effects derived from long-lasting psychostimulant-type toxidrome, including severe agitation, violent behavior, tachycardia, psychosis, profuse diaphoresis, paranoia, and anxiety, among others. Currently reported intoxications involving MDPV[13,14] established that the amount of synthetic cathinones consumed per dose ranged from 5 to 250 mg orally, which produced effects lasting from 1 to 3 h.[15]

MDPV is commonly detected by different techniques, such as HPLC–MS,[16–19] GC–MS,[20–22] high-performance ion mobility spectrometry (HPIMS),[23] and bioanalytical procedures.[24–26] Nevertheless, these methods are slow; the samples must be moved to qualified laboratories, and they usually require the supervision of trained personnel. An alternative promising approach to these techniques involves the development of chromo-fluorogenic sensors for the rapid,

selective, and in situ detection of MDPV.[27] However, as far as we know, no chromo-fluorogenic probes have been reported for the detection of MDPV so far. In this scenario, the development of new strategies to detect and quantify "drugs of abuse"-like MDPV in a fast, easy, and reliable way is timely and urgently required.

From another point of view, the development of hybrid organic–inorganic gated materials based on mesoporous silica nanoparticles (MSNs) with applications in drug delivery,[28,29] communication,[30,31] and detection protocols[32-34] has attracted great attention over the last decade. The main advantages provided by MSNs are a high specific surface area, homogeneous porosity, high load capacity, tunable pore size (2-10 nm), and easy functionalization. These sensing gated materials allow the controlled release of an entrapped cargo in the presence of a target molecule, usually triggering the displacement of the gating ensemble.[35] Moreover, these capped sensing materials also show inherent chemical amplification as only few molecules of the analyte can induce the delivery of a large amount of the entrapped cargo (usually a fluorophore).[36]

Based on the statement above, we report herein a gated nanodevice for the selective, sensitive fluorogenic sensing of MDPV (Scheme 1). The sensor selectively detects MDPV at concentrations as low as 5.2 μM and is able to determine the presence of MDPV both in saliva and blood plasma.

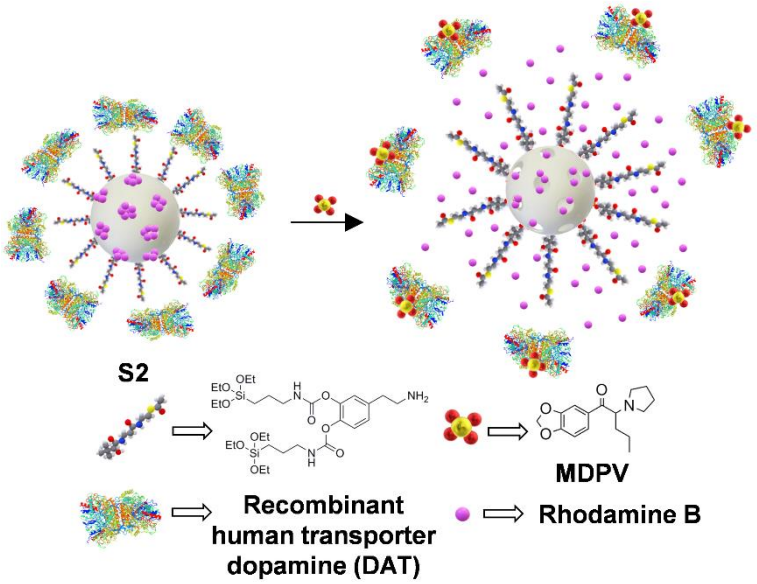

Scheme 1. Sensing Behavior of Solid **S2** in the Presence of MDPV.

4.3. EXPERIMENTAL SECTION

Synthesis of Mesoporous Silica Nanoparticles. NaOH (2.00 M, 3.5 mL) was added to a solution of CTABr (1.00 g, 2.74 mmol) in deionized H_2O (480 mL) at 40 °C. The solution temperature was adjusted to 80 °C and then TEOS (5.00 mL, 2.57×10^{-2} mol) was added dropwise. The mixture was stirred for 2 h to give a white precipitate. The solid was isolated by centrifugation and washed with deionized water and then dried at 70 °C for 12 h. In order to remove the template phase, the mesoporous nanoparticles were calcined at 550 °C for 5 h in an oxidizing atmosphere.

Synthesis of tert-Butyl(3,4-dihydroxyphenethyl)carbamate (2).[37] Dopamine hydrochloride (**1**, 1.00 g, 6.53 mmol) was suspended in 13 mL of chloroform, and then sodium bicarbonate (0.55 g, 6.53 mmol) in 9 mL of H_2O, NaCl (1.31 g, 22 mmol), and di-tert-butyl dicarbonate (1.49 g, 6.83 mmol) were successively added. The mixture was heated at 62 °C for 3 h. Afterward, the organic

phase was washed with H_2O (40 mL), brine (40 mL), dried over $MgSO_4$, and filtered. Finally, the filtrate was concentrated by rotary evaporation, and the residue was purified by silica gel column chromatography using ethyl acetate−hexane as eluent (1:1 v/v) to obtain product **2** as a pale pink solid (921 mg, 3.64 mmol, 56% yield) (Scheme 2a).

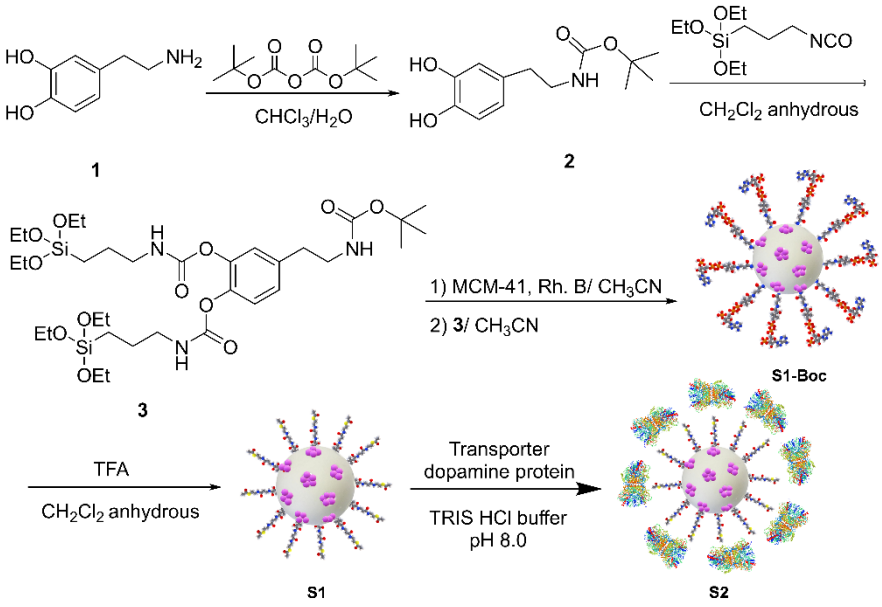

Scheme 2. (a) Synthesis of Dopamine Derivative **3**. (b) Synthetic Route for the Preparation of Solid **S2**.

Synthesis of 4-(2-((tert-Butoxycarbonyl)amino)ethyl)-1,2-phenylene bis((3-(triethoxysilyl)propyl)carbamate) (3). In a reaction vessel purged with Argon, a solution of **2** (0.3 g, 1.18 mmol) in 15 mL of anhydrous CH_3CN was prepared, and then (3-isocyanatopropyl)-triethoxysilane (0.6 mL, 2.36 mmol) was added. The mixture was stirred at room temperature for 4 h. Finally, the solvent was removed under reduced pressure to obtain product **3** as a pale yellow solid (882.6 mg, 1.18 mmol). ^{1}H NMR (400 MHz, $CDCl_3$, δ): 7.09 (d, *J* = 8.2 Hz, 1H), 6.99 (d, *J* = 7.3 Hz, 2H), 5.47 (s, 2H), 4.58 (s, 1H), 3.83 (qdd, *J1* = 7.0, *J2* = 5.0, J3 = 2.0 Hz, 15H), 3.36 (d, *J* = 5.7 Hz, 2H), 2.77 (t, *J* = 6.7, 2H), 1.43 (s, 11H), 1.23 (m, 25H) ppm.

^{13}C NMR (101 MHz, $CDCl_3$, δ): 157.05, 154.67, 152.89, 141.79, 140.38, 136.03, 125.16, 122.5, 77.99, 57.25, 42.47, 41.75, 40.27, 34.31, 27.18, 22.39, 21.94, 17.07, 6.41 ppm (Figures S1 and S2).

Synthesis of S1-Boc. In a typical synthesis, a mixture of calcined mesoporous silica nanoparticles (100 mg) and rhodamine B (38.3 mg, 0.08 mmol) were suspended in 5 mL of anhydrous CH_3CN and purged with Argon. The suspension was stirred at room temperature for 24 h in order to load the mesopores. Then, compound **3** (191.5 mg, 0.26 mmol) was added, and the final suspension was stirred at room temperature for 5.5 h. Finally, the resulting pink solid was filtered and then dried under vacuum overnight, giving rise to **S1-Boc** (195 mg).

Synthesis of S1. Solid **S1-Boc** (10 mg) was suspended in 2 mL of anhydrous CH_2Cl_2 and purged with Argon. The suspension was then cooled to 0 °C, and TFA (0.1 mL, 1.31 mmol) was added for N-Boc deprotection. The mixture was stirred at room temperature for 10 min, and the solid was isolated by centrifugation, washed with CH_2Cl_2 (2 × 8 mL), and dried overnight at 37 °C.

Synthesis of S2. Solid **S1** (1 mg) was suspended in TRIS-HCl buffer (300 µL, 20 mM of TRIS and $MgCl_2{\cdot}6H_2O$, pH 8.0), and then the recombinant human transporter dopamine protein (150 µL, 0.017 µg/µL) was added. The mixture was stirred in a thermo-shaker at 4 °C overnight. Then, the suspension was centrifuged at 12,000 rpm for 5 min. **S2** was then washed with TRIS−HCl buffer (300 µL) to eliminate the non-encapsulated dye and the unattached protein.

Release experiments of Solid S1 in the presence of MDPV. To check the crucial role played by transporter dopamine protein (DAT), absent in **S1** but present in **S2**, 1 mg of solid **S1** was suspended in 800 µL of TRIS-HCl buffer and this volume was divided into two aliquots of 400 µL. After that, 9 µL of a 20 mM solution of

MDPV in TRIS-HCl buffer was added to one of the aliquots (final concentration of 860 µM), and simultaneously, 9 µL of TRIS-HCl buffer was added to the blank aliquot. Both suspensions were stirred at 25 °C and, after certain time, aliquots were centrifuged (12,000 rpm for 5 min), and the fluorescence of the rhodamine B released in the supernatant (λ_{exc} = 565 nm, λ_{em} = 572 nm) was measured. Once measured, the 150 µL aliquot was returned to the initial suspension (Figure S9).

Release experiments of Solid S2 in the presence of MDPV. The same procedure described in the section above was carried out with **S2** (Figure 1).

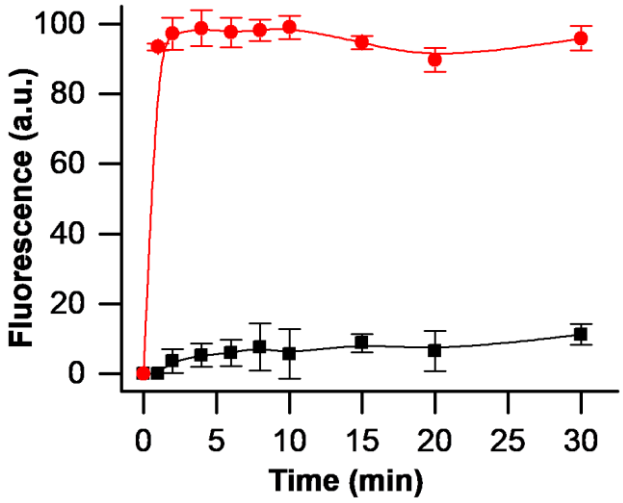

Figure 1. Kinetics of dye release from solid **S2** in TRIS-HCl Buffer at pH 8.0 in the absence (black line) and in the presence (red line) of MDPV (860 µM). Error bars are expressed as 3σ for three independent experiments.

Selectivity Studies with S2 in TRIS Buffer. S2 (1 mg) was suspended in 1.4 mL of TRIS-HCl buffer (20 mM of TRIS and $MgCl_2 \cdot 6H_2O$, pH 8.0), and this volume was separated into seven aliquots of 200 µL. In addition, several solutions in TRIS-HCl buffer of different drugs (MDMA, morphine, heroin, cocaine, MDPV, and dopamine) at a concentration of 1 mM were prepared. Then, 9 µL of each drug solution was added to the aliquots of **S2** to reach a final concentration of 43 µM.

Simultaneously, 9 µL of TRIS-HCl buffer was added to the blank. The suspensions were stirred at 25 °C for 2 min. After that, the aliquots were centrifuged, and the fluorescence of the rhodamine B released in the supernatant was measured (Figure 2).

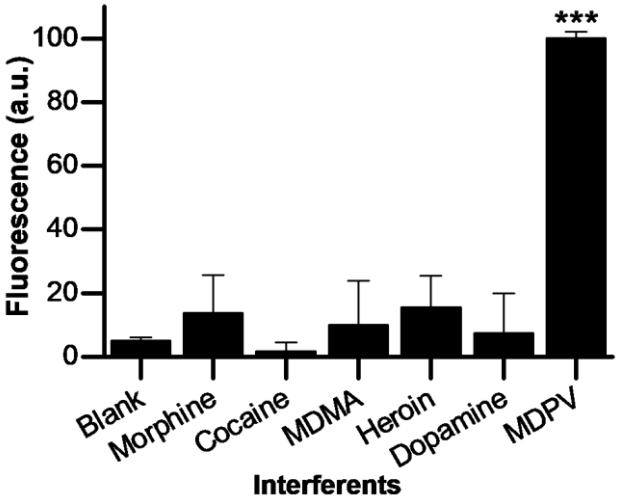

Figure 2. Effect of the indicated drugs (43 µM) on the relative rhodamine B release from solid **S2** in TRIS-HCl buffer at pH 8.0 20 min after addition. Error bars are expressed as 3σ for three independent experiments (***$p < 0.0003$).

Determination of the Detection Limit of S2 for MDPV. S2 (1 mg) was suspended in 2.4 mL of TRIS-HCl buffer (20 mM of TRIS and $MgCl_2 \cdot 6H_2O$, pH 8.0) and then divided into 12 aliquots of 200 µL. Then, different concentrations of MDPV were added to the aliquots. The suspensions were stirred at 25 °C for 2 min and then centrifuged (12,000 rpm for 5 min), and the fluorescence of the rhodamine B released in the supernatant (λ_{exc} = 565 nm, λ_{em} = 572 nm) was measured (Figure S10).

Determination of the Detection Limit of S2 with MDPV in Saliva. S2 (1 mg) was suspended in 2.4 mL of 30% saliva and divided into 12 aliquots of 200 µL each one. The experimental procedure followed was the same as described above (Figure S14).

Determination of the Detection Limit of S2 with MDPV in Blood Plasma. **S2** (1 mg) was suspended in 2.4 mL of 30% diluted blood plasma extracted and divided into 12 aliquots of 200 µL. The experimental procedure is the same as described above (Figure S15).

Detection of MDPV in Spiked Saliva and Plasma Blood Samples. Solid **S2** (0.1 mg) was added to 200 µL of 30% saliva or plasma sample spike with MDPV. All suspensions were stirred at 25 °C for 2 min. The aliquots were centrifuged (12,000 rpm for 5 min), and the fluorescence of the rhodamine B released in the supernatant (150 µL) was measured (Figures S11−S13).

4.4. RESULTS AND DISCUSSION

Design, Synthesis and Characterization of the Nanodevice. For the preparation of the sensing nanoparticles, MSNs was first synthesized by base-catalyzed sol−gel condensation of tetraethylorthosilicate (TEOS) in the presence of sodium hydroxide and hexadecyltrimethylammonium bromide (CTABr) as a micellar template, following previously reported procedures.[38,39] The as-made MSNs were calcined at 550 °C to obtain the starting nanoparticles. In a second step, the pores of the MSNs were loaded with rhodamine B by stirring a suspension of nanoparticles in a concentrated acetonitrile solution of the fluorophore (**S0**). Furthermore, dopamine derivative **3** was anchored onto the external surface of the loaded nanoparticles, yielding the solid **S1-Boc**. Synthesis of **3** was carried out by protecting the amino group of dopamine with di-tert-butyl dicarbonate following with the reaction with (3-isocyanatopropyl)triethoxysilane. The Boc protecting groups from **S1-Boc** were removed using trifluoroacetic acid (TFA), giving rise to solid S1 (Scheme 2b). The final sensing nanodevice (**S2**) was obtained after stirring a suspension of **S1** in TRIS−HCl buffer at pH 8.0 and the DAT protein overnight.

All the prepared solids were characterized using standard techniques such as powder X-ray diffraction (PXRD), transmission electron microscopy (TEM), N_2 adsorption−desorption isotherms, elemental and thermogravimetric analyses, dynamic light scattering (DLS), and FTIR (Figures S3−S8). In particular, the PXRD pattern of the MSNs as synthesized (Figure S3, curve a) shows four low-angle reflections typical of a hexagonal array, indexed as (1 0 0), (1 1 0), (2 0 0), and (2 1 0) Bragg peaks. In Addition, a cell parameter a_0 of 39.75 Å (distance between planes d_{100} = 34 Å) was determined. A significant displacement of 6−8 Å of the (1 0 0) peak in the PXRD pattern of the MCM-41 calcined nanoparticles is evident in curve b (Figure S3), related to the condensation of silanol groups in the calcination step. In **S1**, a broadening of the (1 1 0) and (2 0 0) reflections is observed, related to the loss of contrast due to the filling of the pore with rhodamine B. The presence of the mesoporous structure in the final functionalized solids was also confirmed by TEM analyses, in which the typical hexagonal porosity of a MCM-41-like matrix was clearly visualized (Figure S4). The figure also shows that the materials are spherical particles with an average diameter of 100 ± 4 nm (for **S2**, n = 100 particles). The N_2 adsorption−desorption isotherms of the calcined nanoparticles show a type IV isotherm, typical of mesoporous materials (Figure S5). The curve increment at the P/P_0 value (0.2−0.4) is ascribed to the condensation of nitrogen by capillarity inside the mesopores. A pore diameter of 2.54 nm and a total pore volume of 0.90 $cm^3\ g^{-1}$ were calculated using the BJH model on the adsorption branch of the isotherm. The application of the Brunauer−Emmett−Teller (BET) model resulted in a value for the total specific surface of 1129 $m^2\ g^{-1}$. The N_2 adsorption−desorption isotherm of **S1-Boc** (Figure S5) is typical of mesoporous systems with partially filled mesopores. A decrease in the pore volume (0.20 $cm^3\ g^{-1}$) and surface area (318.48 $m^2\ g^{-1}$) was observed. From thermogravimetric (Figure S6) and elemental analyses and delivery studies, contents of 0.3 and 0.19 mmol of rhodamine B and 3, respectively, per gram of **S1-Boc** solid were calculated. Moreover, contents of 0.07 and 0.16 mmol of rhodamine B and **3**, respectively, per gram of **S1** solid were determined.

Meanwhile, the zeta potential of −29.5 mV, in the starting MSNs, changed to 22.4 mV for **S1-Boc** due to the attachment of the dopamine derivative, **3**. In addition, solid **S1** presents a potential z value of 29.1 mV because of the deprotection of the amino group, whereas a value of −38.0 mV was found for solid **S2** on account of the DAT attachment. Additionally, the hydrodynamic diameter of the starting MSNs was 159 ± 1 nm. **S1-Boc** presented a hydrodynamic diameter of 238 ± 9 nm, which changed to 197 ± 2 nm for **S1** (Figure S7). This decrease in size is in agreement with the removal of the protective Boc groups from **S1-Boc** to give **S1**. Finally, the hydrodynamic diameter for **S2** increased to 501 ± 13 nm due to the attachment of the DAT protein. The FTIR spectrum of functionalized solid **S1** showed the typical absorption bands at ca. 1100 and 3400 cm^{-1}, related to the bond stretching vibrations of Si−O−Si and of O−H groups, respectively. In addition, the spectrum showed the stretching N−H vibrations of amine groups at 3300 cm^{-1}, which were not present in the FTIR spectrum of solid **S1-Boc** (Figure S8). **S2** showed absorption bands at ca. 3300, 1760, and 1500 cm^{-1}, related to the vibrations of N−H, C=O, and NH_3^+, respectively.

Controlled Delivery Studies. To assess the feasibility of the proposed sensing paradigm, controlled release experiments from **S2** in the presence of MDPV were carried out. For this purpose, **S2** was suspended in TRIS-HCl buffer at pH 8.0, and this volume was divided into two aliquots. Then, a solution of MDPV in TRIS-HCl buffer were added to one of the aliquots (an MDPV final concentration of 860 μM), and simultaneously, TRIS buffer was added to the blank aliquot. Both suspensions were stirred at 25 °C; after predefined times, aliquots were taken and centrifuged to eliminate the solid, and the fluorescence of the rhodamine B released in the supernatant (λ_{exc} = 565 nm, λ_{em} = 572 nm) was measured. The obtained release profiles are shown in Figure 1. As can be seen, in the absence of MDPV, a low cargo delivery (ca. 7% of the total rhodamine B released after 20 min) was observed, indicating that **S2** was effectively capped by the interaction of the

grafted dopamine derivative with DAT. However, in the presence of MDPV, a remarkable enhancement in the fluorescence emission at 572 nm was detected, as a consequence of the selective coordination of the drug with DAT, which resulted in DAT displacement from the solid, pore opening, and rhodamine B release. These results are consistent with the fact that MDPV shows a high affinity for DAT in the low nanomolar range (10 ± 2 nM) compared to the low affinity presented for other transporters such as serotonin (2.86 ± 0.1 μM).[40] Likewise, MDPV produces a highly potent DAT inhibition with an IC_{50} value of 4.1 ± 0.5 nM in contrast to the weak effect produced by serotonin and norepinephrine transporters (IC_{50} = 3349 ± 305 and 26 ± 8 nM, respectively).[41,42] In addition, in order to demonstrate that DAT plays a key role in the gating mechanism, we measured the delivery profiles of the uncapped solid **S1** in the absence and presence of MDPV (Figure S9). In both cases, the marked rhodamine B release was observed.

To study the sensitivity of **S2** towards MDPV, the fluorogenic response of TRIS−HCl buffer suspensions of the nanodevices upon the addition of increasing amounts of the drug was studied (Figure S10). The results showed an increase in the rhodamine B emission at 572 nm after 2 min upon the addition of increasing concentrations of MDPV. From the titration profile, a detection limit for MDPV of 5.2 μM was determined from the intersection between two linear sections of the calibration curve. The detection limit achieved enables a commonly occurring dose of MDPV (5 mg) to be detected in volumes as high as 3.5 L.

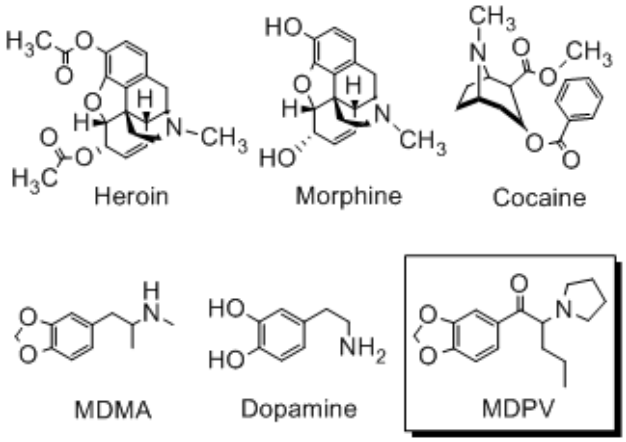

Scheme 3. Chemical Structure of the Drugs Used as Interferents for Selectivity Studies.

In a further step, the fluorogenic response of **S2** was also evaluated in the presence of other common drugs, such as cocaine, heroin, dopamine, MDMA, and morphine (Scheme 3). Figure 2 shows the emission of the released rhodamine B at 572 nm after 2 min from suspensions of **S2** in TRIS-HCl buffer at pH 8.0 upon the addition of the selected drugs (43 μM). As can be seen, a remarkable enhancement in the fluorescence intensity is only produced by MDPV, while other drugs were unable to induce such a remarkable change. The observed selectivity of **S2** toward MDPV is in agreement with its higher IC_{50} inhibition value (4.1 ± 0.5 nM) to DAT compared to other tested drugs, such as cocaine or MDMA (IC_{50} = 211 ± 19 and 93 ± 17, respectively).[41] Therefore, none of the other interferents tested presented remarkable affinities with DAT and, as a consequence, negligible rhodamine B release was observed in these cases. This suggested that **S2** could be used for the selective detection of MDPV.

Validation Studies in Realistic Samples. In order to evaluate the applicability of the nanosensor in realistic competitive environments, we tested the ability of **S2** to detect MDPV in real samples of both saliva and blood plasma. In this way, we prepared a solution of 30% saliva, and then the release of rhodamine B from **S2** nanoparticles in the presence (860 μM) and absence of the drug was

measured. The results obtained (Figure S11) showed that while in the absence of MDPV, a moderate dye release was found (15% of the total dye released after 30 min); in the presence of the illicit drug, a marked rhodamine B release was produced (98% after ca. 30 min). Moreover, the sensitivity of **S2** in saliva was measured, showing a detection limit for MDPV of 6.9 µM (Figure S14). In addition, we tested the ability of **S2** to detect MDPV in a solution of 30% blood plasma previously spiked with MDPV (860 µM) (Figure S12). As shown in Figure S13, rhodamine B release was observed when the drug was present in the blood plasma solution (98% of dye released after 20 min), while the nanoparticles remained closed when no MDPV was present, and the fluorescence emission was significantly lower (20% after ca. 20 min). The detection limit of MDPV in blood plasma for **S2** was as low as 12.1 µM (Figure S15). Detection limit values obtained in saliva and in plasma are slightly higher than that measured in TRIS−HCl solution (*vide ante*), most probably due to the presence of a higher competitive environment. Finally, the nanosensor was tested for MDPV detection in saliva and blood plasma samples (200 µL) spiked with 17.9 and 215 µM of the cannibal drug, respectively. Solid **S2** (0.1 mg) was added to the corresponding solution, and the samples were shaken for 2 min at room temperature. From the interpolation in calibration curves of the rhodamine B released from **S2** in these media, concentrations of MDPV of 17.6 and 200 µM were determined for the saliva and plasma samples, respectively (recovery values of 98 and 93%).

4.5. CONCLUSIONS

In summary, we report herein the design, synthesis, characterization, and sensing behavior of a probe for the fast and highly selective detection of cathinone MDPV (cannibal drug). The nanosensor consists of MSNs loaded with rhodamine B and capped with DAT. In the presence of the MDPV drug, DAT is detached from the nanosensor, inducing cargo release. This behavior is observed in the presence of MDPV but not with other common drugs like cocaine, morphine, heroin, or MDMA.

The probe shows high sensitivity in TRIS-HCl buffer (detection limit of 5.2 µM) and in realistic competitive media like saliva (6.9 µM) and blood plasma (12.1 µM). Finally, the probe is able to detect MDPV in spiked saliva and serum samples. Considering the sensitivity and selectivity of **S2** and its easy synthesis and handling, this material could be used as a reliable system for the accurate in situ and on site MDPV identification.

ACKNOWLEDGMENTS

The authors thank the Spanish Government (projects RTI2018-100910-B-C41 (MCUI/AEI/FEDER, UE) and CTQ2017-87954-P) and the Generalitat Valencia (PROMETEO/2018/024) for support. E.G. is grateful to the Spanish MEC for her FPU grant. M.A. thanks her postdoctoral fellowship (PAID-10-17). The authors also thank the Electron Microscopy Service at the UPV for support.

4.6. REFERENCES

(1) World drug report *United Nations Office on Drugs and Crime (UNODC). Inform*; **2019**.

(2) European drug report *Trends and Developments. European Monitoring Centre for Drugs and Drug Addition (EMCDDA). Inform*; **2019**.

(3) Maurer, H. H.; Brandt, S. D. *New Psychoactive Substances: Pharmacology, Clinical, Forensics and Analytical Toxicology. Handbook of Experimental Pharmacology;* Springer: **2004**, *252*.

(4) Zawilska, J. B.; Wojcieszak, J. Designer cathinones-An emerging class of novel recreational drugs*. Forensic Sci. Int.* **2013**, *231*, 42−53.

(5) Coppola, M.; Mondola, R. 3,4-Methylenedioxypyrovalerone (MDPV): Chemistry, pharmacology and toxicology of a new designer drug of abuse marketed online. *Toxicol. Lett.* **2012**, *208*, 12−15.

(6) Coppola, M.; Mondola, R. Synthetic cathinones: Chemistry, pharmacology and toxicology of a new class of designer drugs of abuse marketed as bath salts or plant food. *Toxicol. Lett.* **2012**, *211*, 144−149.

(7) Oliver, C. F.; Palamar, J. J.; Salomone, A.; Simmons, S. J.; Philogene-Khalid, H. L.; Stokes-McCloskey, N.; Rawls, S. M. Synthetic cathinone adulteration of illegal drugs. *Psychopharmacology* **2019**, *236*, 869−879.

(8) Riley, A. L.; Nelson, K. H.; To, P.; López-Arnau, R.; Xu, P.; Wang, D.; Wang, Y.; Shen, H.-W.; Kuhn, D. M.; Angoa-Perez, M.; Anneken, J. H.; Muskiewicz, D.; Hall, F. S. Abuse potential and toxicity of the synthetic cathinones (i.e., ”Bath salts”). *Neurosci. Biobehav. Rev.* **2020**, *110*, 150−173.

(9) Ibáñez, M.; Pozo, Ó. J.; Sancho, J. V.; Orengo, T.; Haro, G.; Hernández, F. Analytical strategy to investigate 3,4-methylenedioxypyrovalerone (MDPV) metabolites in consumers’ urine by highresolution mass spectrometry. *Anal. Bioanal. Chem.* **2016**, *408*, 151−164.

(10) Colon-Perez, L. M.; Pino, J. A.; Saha, K.; Pompilus, M.; Kaplitz, S.; Choudhury, N.; Jagnarine, D. A.; Geste, J. R.; Levin, B. A.; Wilks, I.; Setlow, B.; Bruijnzeel, A. W.; Khoshbouei, H.; Torres, G. E.; Febo, M. Functional connectivity, behavioral and dopaminergic alterations 24 hours following acute exposure to synthetic bath salt drug methylenedioxypyrovalerone. *Neuropharmacology* **2018**, *137*, 178−193.

(11) Eshleman, A. J.; Nagarajan, S.; Wolfrum, K. M.; Reed, J. F.; Swanson, T. L.; Nilsen, A.; Janowsky, A. Structure-activity relationships of bath salt components: substituted cathinones and benzofurans at biogenic amine transporters. *Psychopharmacology* **2019**, *236*, 939−952.

(12) Glennon, R. A.; Young, R. Neurobiology of 3,4-methylenedioxypyrovalerone (MDPV) and α-pyrrolidinovalerophenone (α-PVP). *Brain Res. Bull.* **2016**, *126*, 111−126.

(13) Kraemer, M.; Boehmer, A.; Madea, B.; Maas, A. Death cases involving certain new psychoactive substances: A review of the literature. *Forensic Sci. Int.* **2019**, *298*, 186−267.

(14) Liveri, K.; Constantinou, M. A.; Afxentiou, M.; Kanari, P. A fatal intoxication related to MDPV and pentedrone combined with antipsychotic and antidepressant substances in Cyprus. *Forensic Sci. Int.* **2016**, *265*, 160−165.

(15) Marinetti, L. J.; Antonides, H. M. Analysis of synthetic cathinones commonly found in bath salts in human performance and postmortem toxicology: method development, drug distribution and interpretation of results. *J. Anal. Toxicol.* **2013**, *37*, 135−146.

(16) Freni, F.; Bianco, S.; Vignali, C.; Groppi, A.; Moretti, M.; Osculati, A. M. M.; Morini, L. A multi-analyte LC−MS/MS method for screening and quantification of 16 synthetic cathinones in hair: Application to postmortem cases. *Forensic Sci. Int.* **2019**, *298*, 115−120.

(17) Peiró, M. D. L. N.; Armenta, S.; Garrigues, S.; de la Guardia, M. Determination of 3,4-methylenedioxypyrovalerone (MDPV) in oral and nasal fluids by ion mobility spectrometry. *Anal. Bioanal. Chem.* **2016**, *408*, 3265−3273.

(18) Cheng, S.-Y.; Ng-A-Qui, T.; Eng, B.; Ho, J. Detection of cathinone and mephedrone in plasma by LC-MS/MS using standard addition quantification technique. *J. Anal. Sci. Technol.* **2017**, *8*, 19.

(19) Glicksberg, L.; Bryand, K.; Kerrigan, S. Identification and quantification of synthetic cathinones in blood and urine using liquid chromatography-quadrupole/time of flight (LC-Q/TOF) mass spectrometry. *J. Chromatogr., B* **2016**, *1035*, 91−103.

(20) Mercieca, G.; Odoardi, S.; Cassar, M.; Strano Rossi, S. Rapid and simple procedure for the determination of cathinones, amphetamine- like stimulants and other new psychoactive substances in blood and urine by GC−MS. *J. Pharm. Biomed. Anal.* **2018**, *149*, 494−501.

(21) Gerace, E.; Caneparo, D.; Borio, F.; Salomone, A.; Vincenti, M. Determination of several synthetic cathinones and an amphetamine-like compound in urine by gas chromatography with mass spectrometry. Method validation and application to real cases. *J. Sep. Sci.* **2019**, *42*, 1577−1584.

(22) Woźniak, M. K.; Banaszkiewicz, L.; Wiergowski, M.; Tomczak, E.; Kata, M.; Szpiech, B.; Namieśnik, J.; Biziuk, M. Development and validation of a GC−MS/MS method for the determination of 11 amphetamines and 34 synthetic cathinones in whole blood. *Forensic Toxicol.* **2020**, *38*, 42−58.

(23) Joshi, M.; Cetroni, B.; Camacho, A.; Krueger, C.; Midey, A. J. Analysis of synthetic cathinones and associated psychoactive substances by ion mobility spectrometry. *Forensic Sci. Int.* **2014**, *244*, 196−206.

(24) Peters, J. R.; Keasling, R.; Brown, S. D.; Pond, B. B. Quantification of Synthetic Cathinones in Rat Brain Using HILICESI-MS/MS. *J. Anal. Toxicol.* **2016**, *40*, 718−725.

(25) Williams, M.; Martin, J.; Galettis, P. A Validated Method for the Detection of 32 Bath Salts in Oral Fluid. *J. Anal. Toxicol.* **2017**, *41*, 659−669.

(26) Diestelmann, M.; Zangl, A.; Herrle, I.; Koch, E.; Graw, M.; Paul, L. D. MDPV in forensic routine cases: Psychotic and aggressive behavior in relation to plasma concentrations. *Forensic. Sci. Int.* **2018**, *283*, 72−84.

(27) Garrido, E.; Pla, L.; Lozano-Torres, B.; El Sayed, S.; Martínez- Máñez, R.; Sancenón, F. Chromogenic and fluorogenic probes for the detection of illicit drugs. *ChemistryOpen* **2018**, *7*, 401−428.

(28) García-Fernández, A.; Aznar, E.; Martínez-Máñez, R.; Sancenón, F. New Advances in In Vivo Applications of Gated Mesoporous Silica as Drug Delivery Nanocarriers. *Small* **2020**, *16*, 1902242.

(29) Llopis-Lorente, A.; Lozano-Torres, B.; Bernardos, A.; Martínez- Máñez, R.; Sancenón, F. Mesoporous silica materials for controlled delivery based on enzymes. *J. Mater. Chem. B* **2017**, *5*, 3069−3083.

(30) Giménez, C.; Climent, E.; Aznar, E.; Martínez-Máñez, R.; Sancenón, F.; Marcos, M. D.; Amorós, P.; Rurack, K. Towards chemical communication between gated nanoparticles. *Angew. Chem., Int. Ed.* **2014**, *53*, 12629−12633.

(31) de Luis, B.; Llopis-Lorente, A.; Rincón, P.; Gadea, J.; Sancenón, F.; Aznar, E.; Villalonga, R.; Murguía, J. R.; Martínez-Máñez, R. An Interactive Model of

Communication between Abiotic Nanodevices and Microorganisms. *Angew. Chem.* **2019**, *58*, 14986−14990.

(32) Garrido, E.; Alfonso, M.; Díaz de Greñu, B.; Lozano-Torres, B.; Parra, M.; Gaviña, P.; Marcos, M. D.; Martínez Mañez, R.; Sancenón, F. Nanosensor for Sensitive Detection of the New Psychedelic Drug 25I-NBOMe. *Chem. − Eur. J.* **2020**, *26*, 2813−2816.

(33) Ribes, À.; Aznar, E.; Santiago-Felipe, S.; Xifre-Perez, E.; Tormo-Mas, M. Á.; Pemán, J.; Marsal, L. F.; Martínez-Máñez, R. Selective and Sensitive Probe Based in Oligonucleotide-Capped Nanoporous Alumina for the Rapid Screening of Infection Produced by Candida albicans. *ACS Sens.* **2019**, *4*, 1291−1298.

(34) Oroval, M.; Coll, C.; Bernardos, A.; Marcos, M. D.; Martínez-Máñez, R.; Shchukin, D. G.; Sancenón, F. Selective Fluorogenic Sensing of As(III) Using Aptamer-Capped Nanomaterials. *ACS Appl. Mater. Interfaces* **2017**, *9*, 11332−11336.

(35) Aznar, E.; Villalonga, R.; Gimenéz, C.; Sancenón, F.; Marcos, M. D.; Martínez-Máñez, R.; Díez, P.; Pingarrón, J. M.; Amorós, P. Glucose-triggered release using enzyme-gated mesoporous silica nanoparticles. *Chem. Commun.* **2013**, *49*, 6391−6393.

(36) Giménez, C.; Climent, E.; Aznar, E.; Martínez-Máñez, R.; Sancenón, F.; Marcos, M. D.; Amorós, P.; Rurack, K. Towards chemical communication between gated nanoparticles. *Angew. Chem., Int. Ed.* **2014**, *53*, 12629−12633.

(37) Maerten, C.; Garnier, T.; Lupattelli, P.; Chau, N. T. T.; Schaaf, P.; Jierry, L.; Boulmedais, F. Morphogen Electrochemically Triggered Self-Construction of Polymeric Films Based on Mussel-Inspired Chemistry. *Langmuir* **2015**, *31*, 13385−13393.

(38) Beck, J. S.; Vartuli, J. C.; Roth, W. J.; Leonowicz, M. E.; Kresge, C. T.; Schmitt, K. D.; Chu, C. T. W.; Olson, D. H.; Sheppard, E. W.; McCullen, S. B.; Higgins, J. B.; Schlenker, J. L. A new family of mesoporous molecular sieves prepared with liquid crystal templates. *J. Am. Chem. Soc.* **1992**, *114*, 10834.

(39) Cai, Q.; Luo, Z.-S.; Pang, W.-Q.; Fan, Y.-W.; Chen, X.-H.; Cui, F.-Z. Dilute solution routes to various controllable morphologies of MCM-41 silica with a basic medium. *Chem. Mater.* **2001**, *13*, 258−263.

(40) Paillet-Loilier, M.; Cesbron, A.; Le Boisselier, R.; Bourgine, J.; Debruyne, D. Emerging drugs of abuse: current perspectives on substituted cathinones. *Subst. Abuse Rehabil.* **2014**, *5*, 37−52.

(41) Marusich, J. A.; Antonazzo, K. R.; Wiley, J. L.; Blough, B. E.; Partilla, J. S.; Baumann, M. H. Pharmacology of novel synthetic stimulants structurally related to the "bath salts" constituent 3,4-methylenedioxypyrovalerone (MDPV). *Neuropharmacology* **2014**, *87*, 206−213.

(42) Baumann, M. H.; Partilla, J. S.; Lehner, K. R.; Thorndike, E. B.; Hoffman, A. F.; Holy, M.; Rothman, R. B.; Goldberg, S. R.; Lupica, C. R.; Sitte, H. H.; Brandt, S. D.; Tella, S. R.; Cozzi, N. V.; Schindler, C. W. Powerful Cocaine-Like Actions of 3,4-Methylenedioxypyrovalerone (MDPV), a Principal Constituent of Psychoactive 'Bath Salts' Products. *Neuropsychopharmacology* **2013**, *38*, 552−562.

4.7. SUPPORTING INFORMATION

MATERIALS AND METHODS

General techniques: Powder X-ray diffraction (PXRD), thermogravimetric analysis (TGA), elemental analysis, transmission electron microscopy (TEM), Fourier transform infrared (FTIR) and N_2 adsorption-desorption isotherms were employed to characterize synthesized materials. PXRD measurements were taken on a D8 Advance diffractometer using Cu Kα radiation (Bruker, Massachusetts, United States). Thermogravimetric analyses were carried out on a TGA/SDTA 851e balance (Mettler Toledo, Columbus, OH, USA) in an oxidizing atmosphere (air, 80 mL min^{-1}) with a heating rate program between 393-1273 °C at 10 °C min^{-1}, followed by an isothermal heating step at 1273 °C for 30 min. TEM images were taken with a 100 kV CM10 microscope (Philips). FTIR measurements were taken on a Tensor 27 (Bruker, Massachusetts, United States). N_2 adsorption-desorption isotherms were recorded with a Tristar II Plus automated analyser (Micromeritics, Norcross, GA, USA). The samples were degassed at 90 or 120 °C under vacuum overnight. Specific surface areas were calculated from the adsorption data within the low-pressure range using the Brunauer-Emmett-Teller (BET) model. Pore size was determined following the Barrett-Joyner-Halenda (BJH) method. DLS experiments were performed with a ZetaSizer Nano ZS (Malvern). Fluorescence spectroscopy measurements were taken on a JASCO FP-8300 spectrophotometer.

Solvents: All solvents were ACS reagent grade or better quality and were used without any further purification. Chloroform, anhydrous acetonitrile, anhydrous dichloromethane, ethyl acetate, hexane, triethylamine (Et_3N) and trifluoracetic acid (TFA) were purchased from Scharlab S.L.

Chemicals reagents: Tetraethylorthosilicate (TEOS), *n*-cetyltrimethylammonium bromide (CTABr), sodium hydroxide, (3-isocyanatopropyl) triethoxysilane, dopamine hydrochloride, ditert-butyl dicarbonate (Boc_2O), rhodamine B and 3,4-methylenedioxypyrovalerone hydrochloride (MDPV) were purchased from Sigma Aldrich química (Madrid, Spain). Sodium chloride (NaCl), sodium hydrogen carbonate and anhydrous magnesium sulfate ($MgSO_4$) were purchased from Scharlab S.L. Magnesium chloride hexahydrate ($MgCl_2 \cdot 6H_2O$) was purchased from Acros Organics. Recombinant human dopamine transporter (DAT) protein was purchased from Abcam PLC. Other drugs tested, morphine, cocaine, heroin, and MDMA were kindly provided by "Agencia Española de Medicamentos y Productos Sanitarios" (AEMPS).

Characterization of 3:

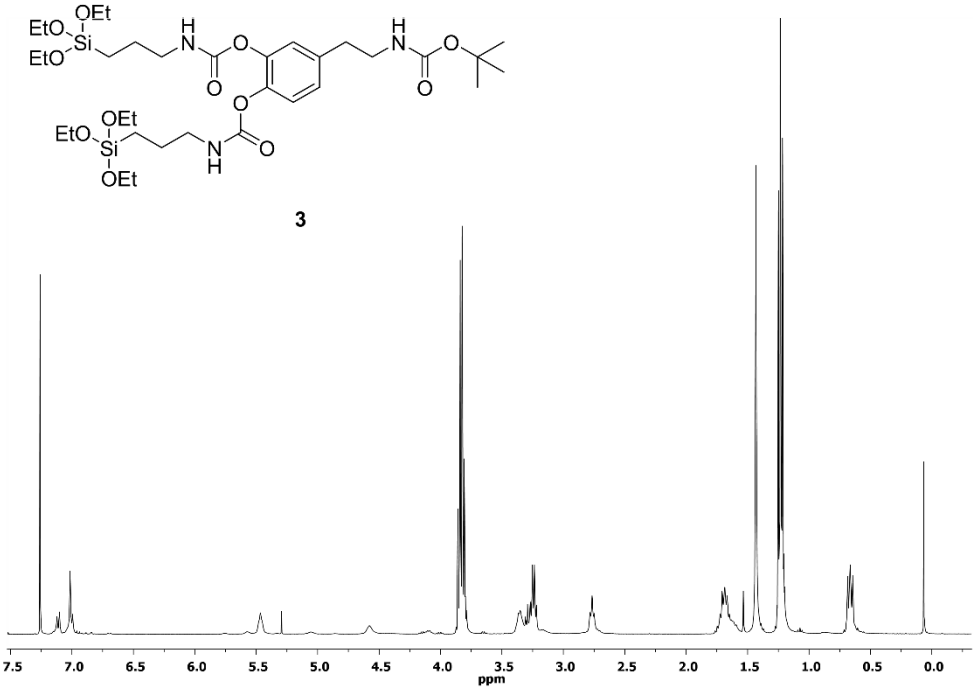

Figure S1. ^{1}H-NMR spectrum of **3** in $CDCl_3$.

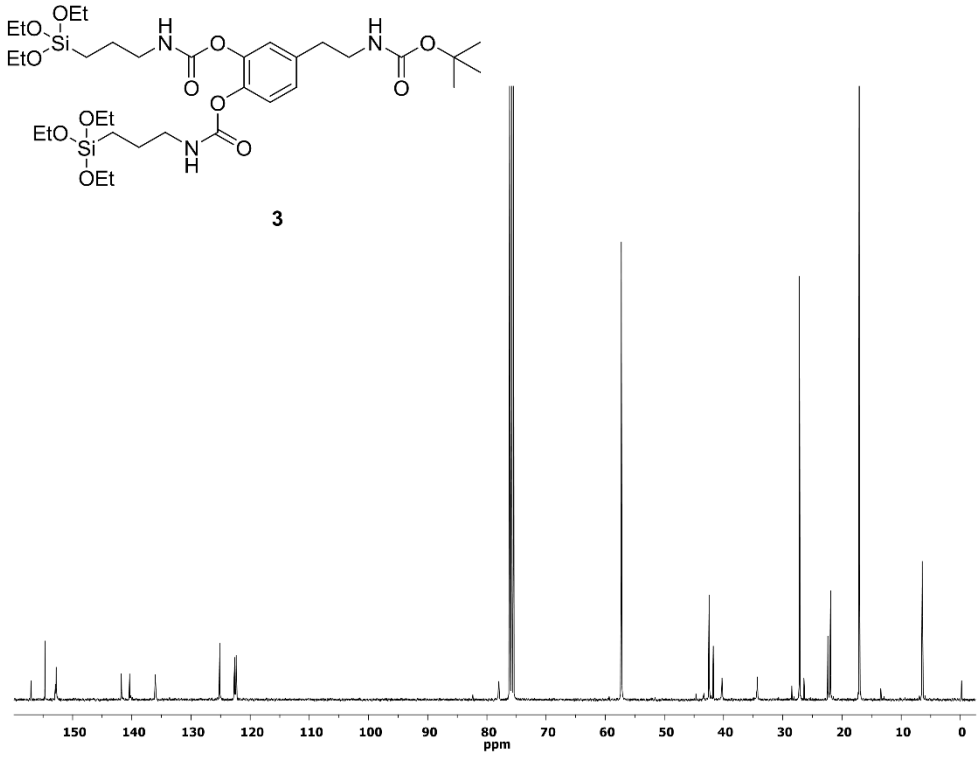

Figure S2. ^{13}C-NMR spectrum of **3** in $CDCl_3$.

Characterization of the prepared materials: The MCM-41 scaffold and mesoporous solid **S1** were characterized following standard techniques, including transmission electron microscopy (TEM), powder X-ray diffraction (PXRD) and N_2 adsorption/desorption analysis.

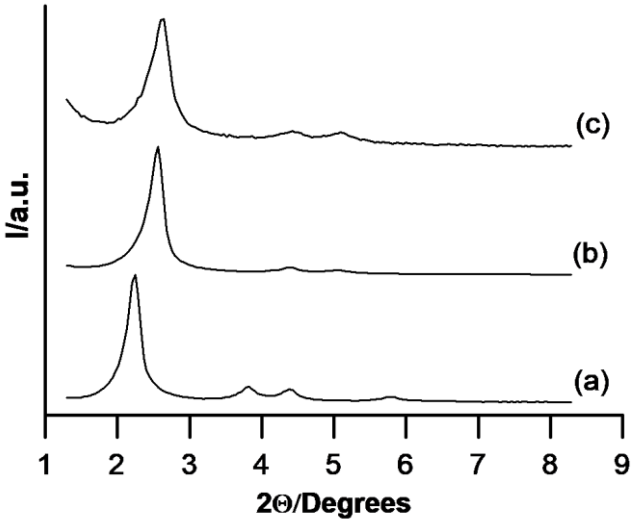

Figure S3. Powder X-ray diffraction (PXRD) patterns of solids (a) as-synthesized MCM-41, (b) calcined MSNs and (c) solid **S1**. Diffractograms are y-shifted for clarity.

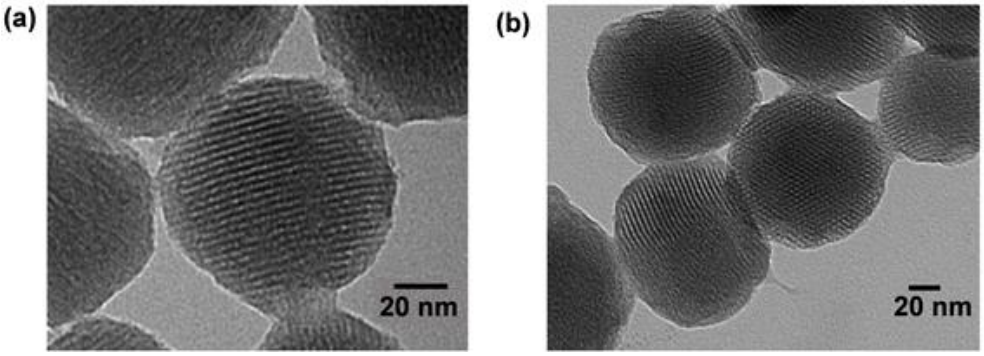

Figure S4. TEM images of (a) calcined MCM-41 and (b) solid **S1**, showing both the typical porosity of the mesoporous silica matrix.

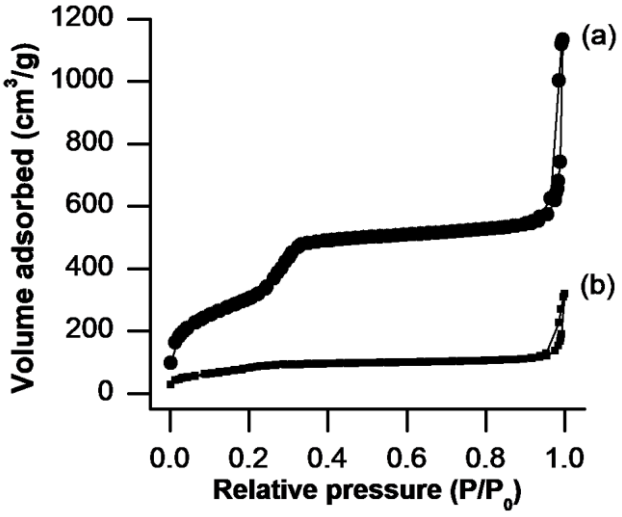

Figure S5. N_2 adsorption-desorption isotherms for (a) calcined MCM-41 nanoparticles and (b) **S1-Boc** material.

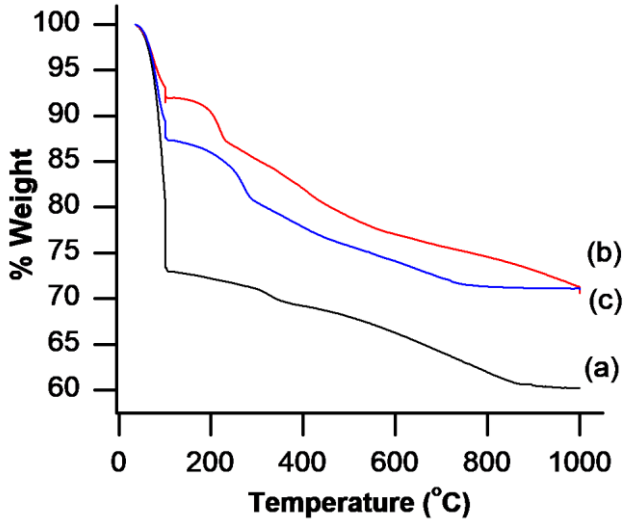

Figure S6. Thermogravimetric analysis for (a) calcined MCM-41 nanoparticles loaded with rhodamine B, (b) **S1-Boc** material and (c) **S1** material.

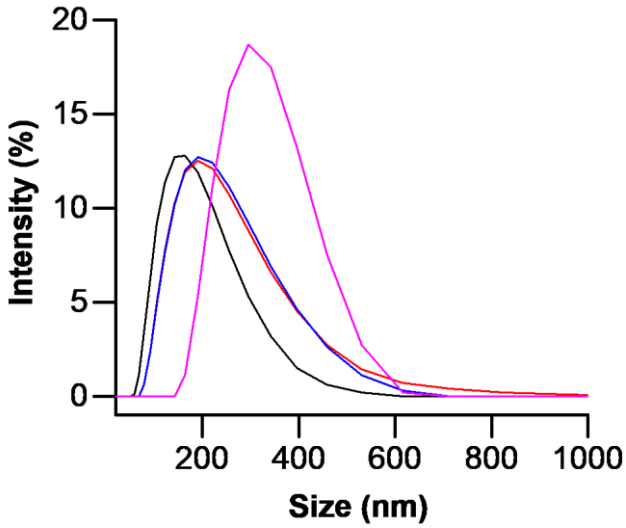

Figure S7. Hydrodynamic diameter distribution of calcined MCM-41 nanoparticles (black line), solid **S1-BOC** (blue line), the sensing nanodevice **S1** (red line) and final solid **S2** (pink line) determined by DLS.

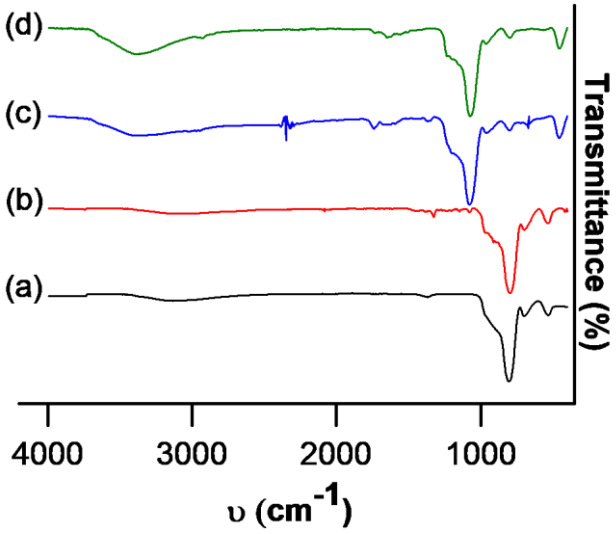

Figure S8. FTIR spectrum of (a) calcined MCM-41 nanoparticles, (b) **S1-Boc** material, (c) **S1** material and (d) **S2** material. Spectra are y-shifted for clarity.

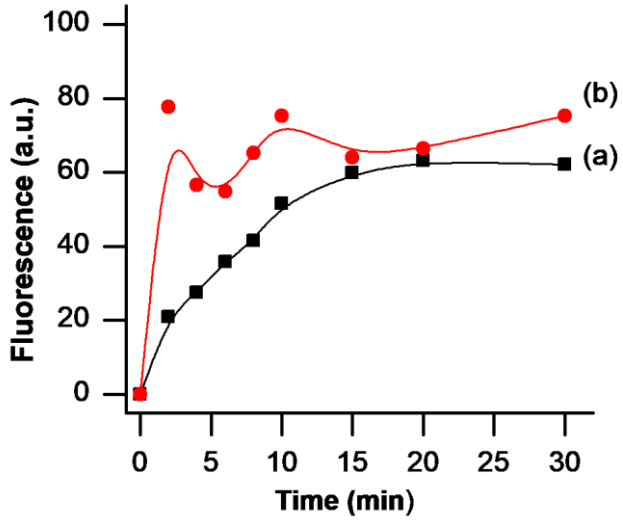

Figure S9. Release profiles of rhodamine B from TRIS HCl buffer suspensions of solid **S1** at pH 8.0 (a) in absence and (b) in the presence of MDPV (860 μM).

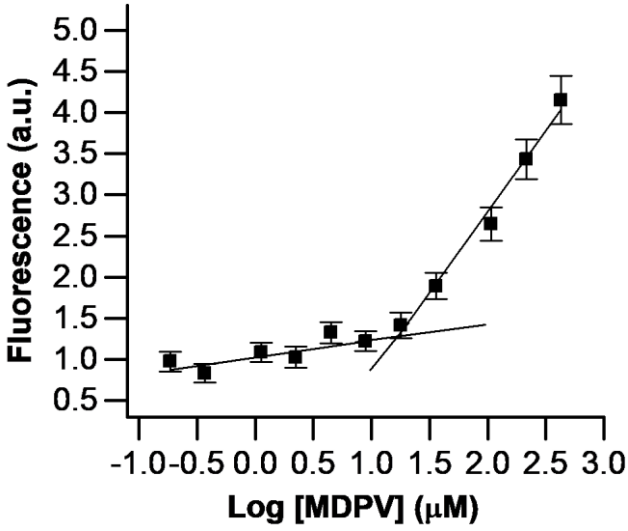

Figure S10. Fluorescence intensity of rhodamine B released from solid **S2** in the presence of different amounts of MDPV in TRIS HCl Buffer at pH 8.0 after 2 min of addition. Error bars are expressed as 3σ for three independent experiments.

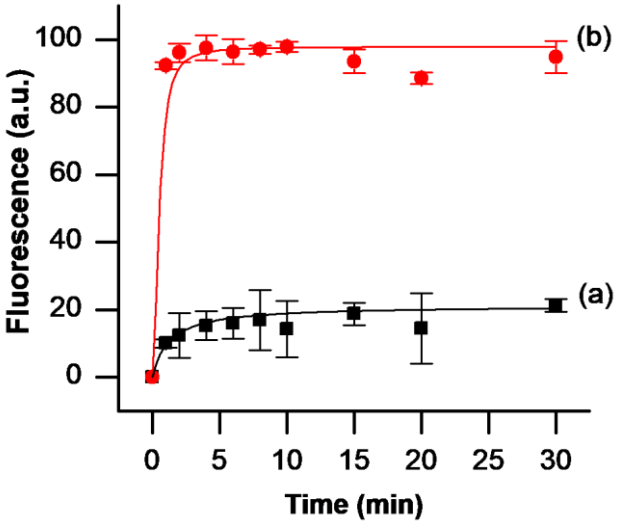

Figure S11. Release profiles of rhodamine B from 30% extracted saliva suspensions of solid **S2** at pH 8.0 (a) in the absence and (b) in the presence of MDPV (860 µM). Error bars are expressed as 3σ.

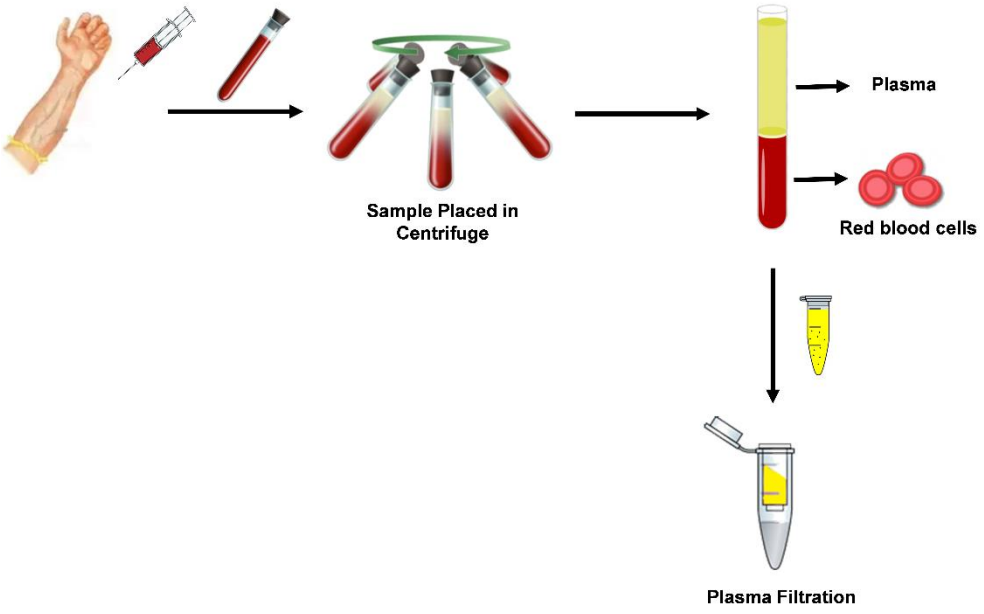

Figure S12. Plasma extraction procedure.

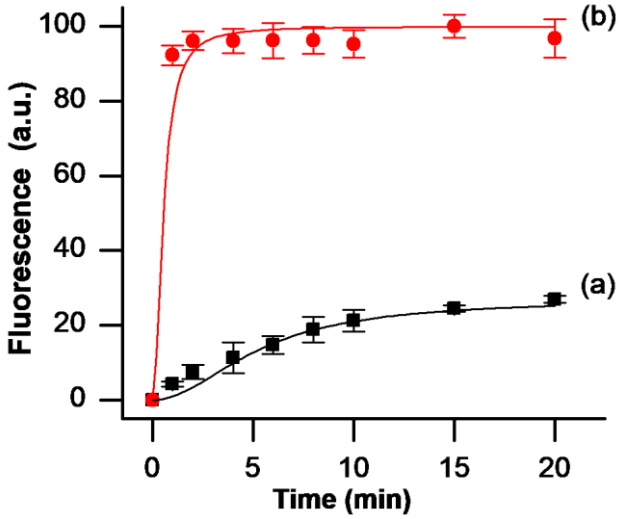

Figure S13. Release profiles of rhodamine B from 30% extracted blood plasma suspensions of solid **S2** at pH 8.0 (a) in absence and (b) in the presence of MDPV (860 µM). Error bars are expressed as 3σ.

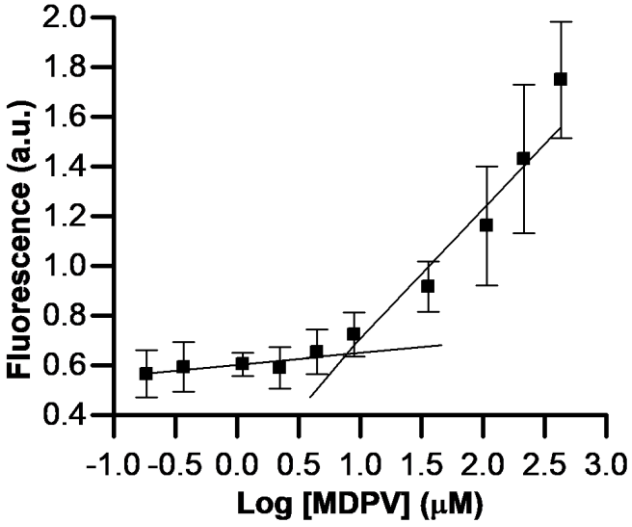

Figure S14. Release of rhodamine B from solid **S2** in the presence of different amounts of MDPV in 30% extracted saliva after 2 min of addition. Error bars are expressed as 3σ.

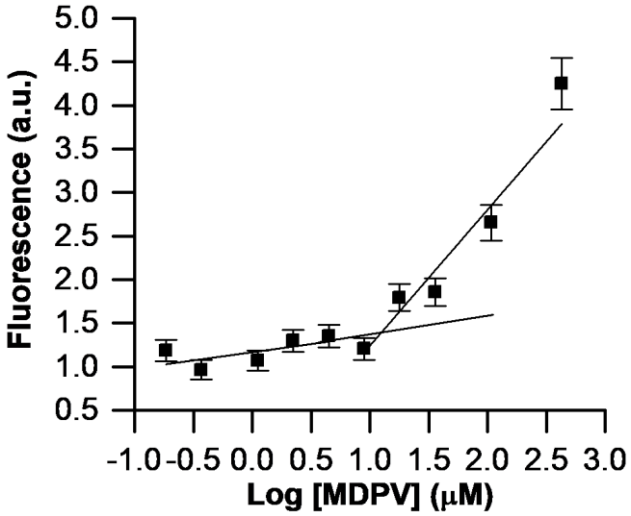

Figure S15. Release of rhodamine B from solid **S2** in the presence of different amounts of MDPV in 30% extracted blood plasma after 2 min of addition. Error bars are expressed as 3σ.

CHAPTER 5

SELECTIVE DUALPLEX LATERAL FLOW ASSAY FOR SIMULTANEOUS SCOPOLAMINE AND CANNIBAL DRUG DETECTION BASED ON RECEPTOR-GATED MESOPOROUS NANOPARTICLES

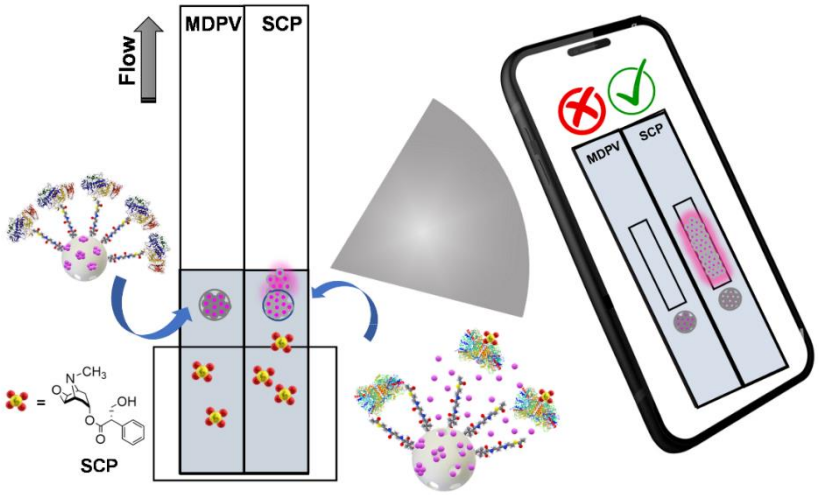

SELECTIVE DUALPLEX LATERAL FLOW ASSAY FOR SIMULTANEOUS SCOPOLAMINE AND CANNIBAL DRUG DETECTION BASED ON RECEPTOR-GATED MESOPOROUS NANOPARTICLES

Eva Garrido,[a],[b],[c],[d] Estela Climent,[f] M. Dolores Marcos,[a],[b],[c],[d] Félix Sancenón,[a],[b],[c],[d] Knut Rurack[f] and Ramón Martínez-Máñez*[a],[b],[c],[d]

[a] Instituto Interuniversitario de Investigación de Reconocimiento Molecular y Desarrollo Tecnológico (IDM), Universitat Politècnica de València, Universitat de València, Spain.

[b] CIBER de Bioingeniería, Biomateriales y Nanomedicina (CIBER-BBN).

[c] Unidad Mixta de Investigación en Nanomedicina y Sensores. Universitat Politècnica de València, Instituto de Investigación Sanitaria La Fe, Valencia, Spain.

[d] Unidad Mixta UPV-CIPF de Investigación en Mecanismos de Enfermedades y Nanomedicina, Universitat Politècnica de València, Centro de Investigación Príncipe Felipe, Valencia, Spain.

[f] Bundesanstalt für Materialforschung und-prüfung (BAM) Richard-Willstätter-Str. 11, 12489, Berlin, Germany.

Submitted

5.1. ABSTRACT

We report herein the design of a straightforward portable strip in combination with bio-inspired hybrid nanomaterials for scopolamine (SCP) drug *in situ* and *at site* detection using a smartphone for readout, allowing SCP identification in diluted saliva down to 40 nM in less than 15 min. For this purpose, we prepared a nanosensor based on mesoporous silica nanoparticles loaded with a fluorescent reporter (rhodamine B) and functionalized with bethanechol, a potent agonist of recombinant human muscarinic acetylcholine receptor M_2 (M_2-AChR). M_2-AChR interaction with the anchored bethanechol derivative leads to capping of the pores. The sensing mechanism relies on binding of SCP to M_2-AChR resulting in pore opening and delivery of the entrapped rhodamine B reporter. Moreover, the material was incorporated into strips for lateral-flow assays coupled to smartphone readout, giving fast response time, good selectivity, and exceptional sensitivity. Besides, a dualplex lateral flow assay capable of detecting SCP and cannibal drug is also developed.

KEYWORDS: *Scopolamine, lateral flow assay, mesoporous silica nanoparticles, M_2-AChR, MDPV.*

5.2. INTRODUCTION

Drug-facilitated sexual assault (DFSA) is a term used to define sexual assault without consent of the victim that is incapacitated and/or unable to provide approval to the sexual act as a result of administration of a psychoactive substance or drug cocktails usually without the permission of the victim.[1,2] In recent years, this phenomenon has acquired greater relevance worldwide and social impact fueled by the significantly increase in cases that already account for roughly 20.9% of sexually assaulted victims.[3] The psychoactive substance most commonly associated with DFSA is alcohol, yet the use of recreational drug is rising as the drug

market is expanding, providing faster and cheaper ways to disable the victim. Among psychoactive substances used in DFSA, γ-hydroxybutyric acid (GHB), 3,4-methylenedioxypyrovalerone (MDPV or cannibal drug), ketamine, flunitrazepam or scopolamine (SCP) are among the most noteworthy.

SCP, also known with the street name of burundanga, has emerged as a perfect psychotropic substance for aggressors, as it induces automatism in the brain of the victim causing a state of submission. Chemically, SCP is an extremely toxic tropane alkaloid found as a secondary metabolite in certain plants of *Solanaceae* family and for centuries it has been widely used for ritual and medical purposes.[4] Structurally, SCP is optically and biologically active, characterized by its unique bicyclic tropane ring system and its consumption produces potent psychotropic effects, including delirium-like states with hallucinations, altered mood, and cognitive deficits.[5] Pharmacological effects of SCP and their duration depend mainly on the format in which the drug is consumed, appearing within minutes for solutions, or elixirs (peaking at 15-60 min and lasting for 4 h) and within 20-30 min for capsules (peaking at 40-90 min and lasting for 12 h).[5] As a result of their powerful sedative-hypnotic effects, SCP has currently become well-known for being employed to commit crimes such as robbery, kidnapping and sexual assaults.[6,7] Biologically, SCP is a non-selective muscarinic acetylcholine receptor (M_1~M_5-AChR) non-competitive antagonist with rapid and robust antidepressant effects in humans and other species.[8,9,10] Particularly, SCP is able to block or dampen the biological response of the acetylcholine receptor due to binds to an allosteric M_2-AChR site that is separate from the active recognition site of acetylcholine, inducing free acetylcholine levels to increase.

Owing to the increasing use of SCP in rape-assaults as well as the broad diversification of new substances available on the underground market, an acute need has arisen to develop innovative and efficient analytical methods for the identification of DFSA substances. For SCP, a wide variety of techniques have been

used for its reliable identification in different adulterated samples, such as gas chromatography,[11,12] high-performance liquid chromatography[13,14] and capillary zone electrophoresis.[15] Most of these studies have been focused on the determination of SCP in serum, plasma, and other biological samples, such as urine or hair.[16] However, most of these analytical techniques are highly specialized and cannot be used *in situ* or *at site*. In this scenario, lateral flow assays (LFAs) have recently attracted special interest due to their friendly formats, short assay times, little interferences, low costs, and being easy operated by non-specialized personnel. Moreover, LFAs can be designed to detect several compounds simultaneously by obtaining results in a short time showing high selectivity and sensitivity in the ppb range.[17,18]

From another viewpoint, gated mesoporous silica nanoparticles (MSNs) has raised considerable interest owing to the properties of the silica support such as high stability, rigid framework, high specific surface area, homogeneous porosity, high load capacity, well-defined pore structure (2-10 nm), easily controllable morphology and tuneable surface chemistry.[19] Although gated MSNs have been widely used in drug delivery,[20,21] recently examples use gated MSNs in sensing[22,23] and communication applications.[24] Sensing gated MSNs are composed of MSNs loaded with selected fluorophores and functionalized with different supramolecular or biological assemblies (such as proteins,[25] enzymes,[26,27,28] antibodies,[29,30,31] among others) acting as 'molecular gates' (also known as gatekeepers or nanovalves). Gated MSNs show ideally "zero" release, yet the presence of a target analyte induces, usually, a displacement of the caping ensemble resulting in cargo delivery which is proportional to the analyte concentration. In addition, gated materials show inherent amplification features as just few analyte molecules can induce release of a large number of entrapped cargo molecules.[32] Besides, gated MSNs materials with fluorogenic response have been integrated in lateral flow assays achieving high sensitivity and selectivity for target

analytes, demonstrating to be simple powerful dipstick tests for different applications.[33]

Based on the above, we report herein the design, preparation, and characterization of a nanosensor based on gated MSNs for SCP detection. The SCP nanosensor consists of caped MSNs loaded with rhodamine that is selectively uncapped with SPC, resulting in the release of the entrapped reporter. The probe shows a highly sensitivity in buffer solution and in a competitive environment such as saliva and is selective for SCP versus other common drugs. The SCP sensor is incorporated into strips for lateral-flow assays coupled to smartphone readout achieving a fast response and good selectivity and sensitivity. Taking into account the versatility of the gated material and the modularity of the assay, a dualplex lateral flow assay capable of detecting *in situ* and *at site* both, SCP and cannibal drug is also developed.

5.3. EXPERIMENTAL SECTION

Synthesis of MCM-41 mesoporous nanoparticles[34]: NaOH (2.00 mol L^{-1}, 3.5 mL) was added to a solution of CTABr (1.00 g, 2.74 mmol) in deionized H_2O (480 mL) at 40 °C. The solution temperature was adjusted to 80 °C and then TEOS (5.00 mL, 2.57×10^{-2} mol) was added dropwise. The mixture was stirred for 2 h to give a white precipitate. The solid was isolated by centrifugation and washed with deionized H_2O, and then dried at 70 °C for 12 h to give MCM-41. To remove the template phase, MCM-41 was calcined at 550 °C for 5 h in an oxidizing atmosphere.

Synthesis of 4-oxo-4-((3-(triethoxysilyl)propyl)amino)butanoic acid (2)[35]: Succinic anhydride (**1**, 1.5 g, 15 mmol) was dissolved in 1,4-dioxane (10 mL) and then, (3-aminopropyl) triethoxysilane (3.3 g, 15 mmol) in 1,4-dioxane (10 mL), were added dropwise to the solution. The mixture was heated at 80 °C for 30 minutes.

Afterwards, the solvent was removed under reduced pressure to obtain the product **2** as a pale-yellow oil (4.82 g, 15 mmol).

Synthesis of S1: In a typical synthesis, a mixture of calcined MCM-41 (100 mg) and rhodamine B (38.32 mg, 0.8 mmol) were suspended in ethanol (3.5 mL). The suspension was stirred at room temperature for 24 h to load the MCM-41 pores. Then, compound **2** (1.52 g, 4.73 mmol) was added and the final suspension was stirred at room temperature for 5.5 h. Finally, the resulting pink solid was filtered and dried under vacuum overnight, giving rise to **S1** (164 mg).

Synthesis of S2[36]**: S1** (164 mg) was suspended in ethanol (40 mL). Benzoic anhydride (1.07 g, 4.73 mmol) and $ZnCl_2$ (26.86 mg, 4.73 mmol) were successively added to the solution. The mixture was stirred at room temperature for 10 minutes and then, bethanechol chloride (930 mg, 4.73 mmol) was added. The reaction was left at room temperature for 2.5 h. Afterwards, the solid was isolated by centrifugation (12,000 rpm for 5 minutes). The final solid was dried overnight at 37 °C. The proper functionalization of solid **S2** was assured by FTIR measurements (Figure S4).

Synthesis of S3: Solid **S2** (1 mg) was suspended in TRIS HCl buffer (300 µL, 20 mM of TRIS and $MgCl_2 \cdot 6H_2O$, pH 8.0) and then, recombinant human muscarinic acetylcholine receptor M2/CM2 protein, M_2-AChR, (71.43 µL, 0.07 µg/µL) was added. The mixture was stirred in a thermo-shaker at 4 °C overnight. After that, the suspension was centrifuged at 12,000 rpm for 5 min. **S3** was then washed with TRIS HCl buffer (300 µL, 20 mM of TRIS and $MgCl_2 \cdot 6H_2O$, pH 8.0) to eliminate non-encapsulated dye and unattached protein. The proper recognition between the receptor and the bethanechol derivative was estimated by means of a BCA protein assay.

Release experiments of solid S2 in the presence of SCP: To check the crucial role played by muscarinic acetylcholine receptor M_2-AChR, absent in **S2** but present in **S3**, 1 mg of solid **S2** was suspended in 800 µL of TRIS HCl buffer (20 mM of TRIS and $MgCl_2 \cdot 6H_2O$, pH 8.0) and this volume was divided into two aliquots of 400 µL. Both samples were centrifuged for 5 minutes at 12,000 rpm and the fluorescence (λ_{exc} = 565 nm, λ_{em} = 572 nm) of the supernatant (150 µL) was measured to obtain the initial point. This volume was returned to the corresponding aliquot. After that, 54 µL of a 20 mM solution of SCP in TRIS HCl buffer were added to one of the aliquots (final concentration of 2.7 mM), and simultaneously, 54 µL of TRIS HCl buffer were added to the blank aliquot. Both suspensions were stirred at 25 ^{o}C and, after certain time, both aliquots were centrifuged (12,000 rpm for 5 min) and the fluorescence of the rhodamine B released in the supernatant (λ_{exc} = 565 nm, λ_{em} = 572 nm) was measured. Once measured, the 150 µL were returned to the initial suspension, stirred for another time interval and the emission of the dye released was measured over time (see Figure S5).

Release experiments of solid S3 in the presence of SCP: The same procedure described in previous experiment was used with solid **S3** (see Figure 2a).

Concentration-dependence studies of S3 with SCP in TRIS HCL buffer: 1 mg of **S3** was suspended in 2.4 mL of TRIS HCl buffer (20 mM of TRIS and $MgCl_2 \cdot 6H_2O$, pH 8.0) and then divided into twelve aliquots of 200 µL. All samples were centrifuged at 12,000 rpm for 5 minutes and the fluorescence (λ_{exc} = 565 nm, λ_{em} = 572 nm) of the supernatant (150 µL) was measured to obtain the initial point. This volume was returned to the corresponding aliquot. On the other hand, several solutions of SCP in TRIS HCl buffer with concentrations within a range from 0.052 to 70 mM were prepared. Then, 9 µL of each MDPV solution prepared were added to every aliquot (giving final concentrations ranging from 2.24 to 3150 µM respectively). Simultaneously, 9 µL of TRIS HCl buffer were added to the blank

aliquot. All suspensions were stirred at 25 °C for 10 minutes. After that, all aliquots were centrifuged, and the fluorescence of the rhodamine B released in the supernatant was measured (see Figure 2b).

Determination of Limit of detection (LOD): Limits of detection (LODs), which describe the smallest concentration of analyte that can be reliably detected, were derived calculating in a first instance the Limits of Blank (LOBs; describing the smallest concentration of analyte that can be observed) and calculating the corresponding concentration of the signal as follows[37]:

$LOB = \text{mean blank} + 1.645(\sigma_{blank})$

$LOD = LOB + 1.645(\sigma_{\text{low concentration sample}})$

Selectivity studies with S3: To test the selectivity of **S3** towards SCP, 1 mg of solid **S3** was suspended in 1.4 mL of TRIS HCl Buffer (20 mM of TRIS and $MgCl_2 \cdot 6H_2O$, pH 8.0) and this volume was separated into seven aliquots of 200 µL. Besides, several solutions in TRIS HCl buffer of different drugs (MDMA, morphine, heroin, cocaine, MDPV, and SCP) at a concentration of 8 mM were prepared. All aliquots were centrifuged for 5 minutes at 12,000 rpm and the fluorescence of the supernatant (150 µL) was measured (λ_{exc} = 565 nm, λ_{em} = 572 nm) to obtain the initial point. This volume was returned to the corresponding aliquot. After that, 9 µL of each drug solution were added to the aliquots of **S3**, to reach a final concentration of 345 µM. Simultaneously, 9 µl of TRIS HCl buffer were added to the blank. The suspensions were stirred at 25 °C for 2 minutes. After that, the aliquots were centrifuged, and the fluorescence of the rhodamine B released in the supernatant was measured (Figure 3).

Release experiments of solid S3 in the presence of SCP in saliva: 1 mg of **S3** was suspended in 400 µL of 30% extracted saliva and this volume was divided into two aliquots of 200 µL. Both samples were centrifuged for 5 minutes at 12,000 rpm and the fluorescence (λ_{exc} = 565 nm, λ_{em} = 572 nm) of the supernatant (150 µL)

was measured to obtain the initial point. This volume was returned to the corresponding aliquot. After that, 54 µL of a 20 mM solution of SCP in TRIS HCl buffer were added to one aliquot (final concentration of 2.7 mM), and simultaneously, 54 µL of TRIS HCl buffer were added to the blank aliquot. Both suspensions were stirred at 25 °C and, after certain time, both aliquots were separated, centrifuged (12,000 rpm for 5 min) and the fluorescence of the rhodamine B released (λ_{exc} = 565 nm, λ_{em} = 572 nm) in the supernatant was measured. Once measured, the supernatant was returned to the initial suspension, stirred for another time interval, and the emission of the dye released was measured over time (Figure S6).

Concentration-dependence studies of S3 with SCP in saliva: 1 mg of **S3** was suspended in 2.4 mL of 30% extracted saliva and divided into twelve aliquots of 200 µL each one. The experimental procedure followed was the same as that described for TRIS HCl buffer (Figure S7).

Preparation of wax-patterned, glass fibre paper (WAX-GF): First, a wax pattern of approximately 13 x 13 cm presenting wax free spots of 5 mm diameter was printed on an aluminium foil using a commercially available wax printer (Xerox Color Qube 8580). In a second step, the wax pattern was transferred to glass fiber (GF) strips by lamination. Finally, the strips were cured at 110 °C during 30 min. This step melts the wax and creates hydrophobic barriers across the thickness of the paper. The as-prepared **WAX-GF** were cut in individual 0.5 x 4 cm strips and were stored at room temperature until the next step.

Concentration-dependence studies of S3-WAX-GF strips with SCP in TRIS HCl buffer: Wax-patterned glass fibre (**WAX-GF**) strips of 0.5 x 2.5 cm using absorbent pad were prepared, 2 µL of a suspension (1 mg/mL) of **S3** were deposited at ca. 1 cm from one end of the strip (zone A), obtaining as result of **S3-WAX-GF**. **S3-WAX-GF** were dipped into 75 µL of a TRIS HCl solution at pH 8.0 containing

different concentrations of SCP from 9.99 mM to 8.6 µM in a microwell plate for 10 minutes. Afterwards, the strips were dried for 2 minutes at room temperature and the fluorescence of the released dye was measured with a smartphone setup using one LED at 522 as excitation sources powered by the smartphone via a USB-OTG link and filtered by a short-pass filter (532 nm) while collecting the emission through a long-pass filter (550 nm) after inserting the developed strip in a 3D-printed, customized holder previously described.[38] The amount of dye released for each concentration was calculated according to the fluorescence intensity of zone B using ImageJ program (Figure S8).

Concentration-dependence studies of S3-WAX-GF strips with SCP in saliva: WAX-GF strips of 0.5 × 2.5 cm using absorbent pad were prepared, and 2 µL of a suspension (1 mg/mL) of solid **S3** in 30% extracted saliva were deposited at ca. 1 cm from one end of the strip (zone A). The experimental procedure followed was the same as described above (Figure 4a).

Selectivity studies with S3-WAX-GF strips: S3-WAX-GF strips of 0.5 × 2.5 cm using absorbent pad were prepared, and 2 µL of a suspension (1 mg/mL) of solid **S3** in 30% extracted saliva were deposited at ca. 1 cm from one end of the strip (zone A). The strips containing solid **S3** were then dipped into 75 µL of the saliva 30% diluted sample solutions containing 200 µM of different drugs (MDMA, morphine, heroin, cocaine, MDPV and scopolamine) in a microwell plate for 10 min and then, the strip was dried for 2 minutes at room temperature. Afterwards, the strips fluorescence was measured using a smartphone readout at 550 nm (λ_{exc} = 522 nm). The amount of dye released for each concentration was calculated according to the fluorescence intensity of zone B using ImageJ program (Figure S9).

Concentration-dependence studies with S6-WAX-GF strips with MDPV in saliva: WAX-GF strips of 0.5 x 2.5 cm using absorbent pad were prepared as detailed above. Then 2 µL of a suspension (1 mg/mL) of **S6** in 30% extracted saliva

were deposited at ca. 1 cm from one end of the strip (zone A). Therefore, the materials containing the nanosensor **S6** (**S6-WAX-GF**) were dipped into 75 µL of a 30% extracted saliva containing different concentrations of MDPV from 9.99 mM to 2.1 µM in a microwell plate for 10 minutes. Afterwards, the strips were dried for 2 minutes at room temperature and the fluorescence of the released dye was measured smartphone setup using one LED at 522 nm as excitation sources powered by the smartphone via a USB-OTG link and filtered by a short-pass filter (532 nm) while collecting the emission through a long-pass filter (550 nm) after inserting the developed strip in a 3D-printed, customized holder. The amount of dye released for each concentration was calculated according to the fluorescence intensity of zone B using ImageJ program (Figure 4b).

Selectivity studies with S6-WAX-GF strips: S6-WAX-GF strips of 0.5 × 2.5 cm using absorbent pad were prepared, and 2 µL of a suspension (1 mg/mL) of solid **S6** in 30% extracted saliva were deposited at ca. 1 cm from one end of the strip (zone A). **S6-WAX-GF** membranes were then dipped into 75 µL of the saliva 30% diluted sample solutions containing 200 µM of different drugs (MDMA, morphine, heroin, cocaine, MDPV and scopolamine) in a microwell plate for 10 min and then, the strip was dried for 2 minutes at room temperature. Afterwards, the strips fluorescence was measured using a smartphone readout at 550 nm (λ_{exc} = 522 nm). The amount of dye released for each concentration was calculated according to the fluorescence intensity of zone B and the fluorescence of the entire strip (Figure S10).

Dualplex lateral flow assay for SCP and MDPV detection with S6@S3-WAX-GF in saliva: On a dual-channel strip, 2 µL of a 1mg/mL dilution of solid **S3** and 2 µL of a 1mg/mL dilution of solid **S6** were deposited on one strip and on the other strip (**S6@S3-WAX-GF**). Both strips were immersed in a microplate with extracted saliva solutions (300 µL) containing different concentrations of both SCP and MDPV for 10 minutes (Figure S11). Then, the strips were left to dry for 5 minutes at room

temperature, and the fluorescence of rhodamine released from each strip was measured using a smartphone readout at 550 nm (λ_{exc} = 522 nm). The amount of dye released for each concentration was calculated according to the ratio of the fluorescence of zone B and the fluorescence of the entire strip (Figure 5).

5.4. RESULTS AND DISCUSSON

The nanosensor design is depicted in Scheme 1. It consists of MSNs loaded with a fluorescent reporter (rhodamine B), and functionalised on the external surface with a bethanechol derivative (carbamyl-β-methylcholine chloride, also known as bethanechol) which is a non-selective muscarinic receptor agonist that increases the M_2-AChR activity.[39] In addition, the loaded system is finally capped by interaction between the grafted bethanechol derivative and M_2-AChR (**S3** in Scheme 1). For the M_2-AChR receptor, the reported dissociation constants of agonist binding (K_D) to bethanechol is 171 µM (for comparison it is 15.8 ± 3.8 µM for acetylcholine)[40] which explain the rationale behind the use of M_2-AChR for pore blocking.

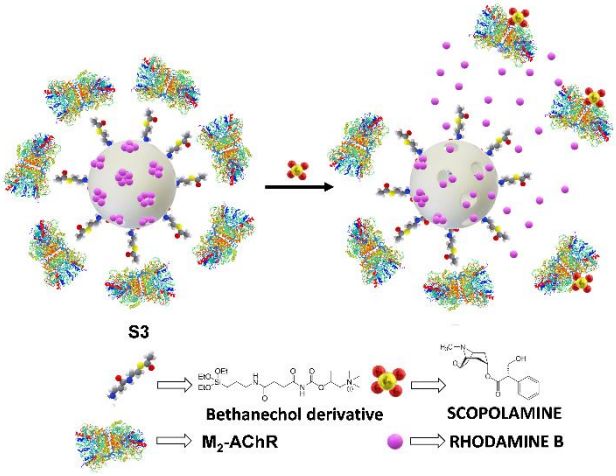

Scheme 1. Schematic of the behaviour mechanism of solid **S3** in the presence of SCP.

MSNs is prepared following reported procedures based on the condensation of tetraethyl orthosilicate (TEOS) in the presence of cetyltrimethylammonium bromide (CTAB) as micellar template. The as-made MSNs were calcinated at 550 °C for surfactant removal[41] and the empty pores are loaded with rhodamine B by soaking MSNs into an ethanolic solution of the fluorophore. Subsequently, the external surface of MSNs is functionalized with compound **2** yielding a pink solid (**S1**). Compound **2** is synthetized through the reaction between succinic anhydride and 3-(aminopropyl)triethoxysilane (**1**) using a previously described procedure (Scheme 2a).[42] In a next step, bethanechol chloride is grafted covalently to **2** on solid **S1** in the presence of benzoic anhydride and $ZnCl_2$,[43] giving solid **S2**. The final sensing nanomaterial (**S3**) is obtained by stirring overnight a suspension of **S2** in TRIS HCl buffer at pH 8.0 containing M_2-AChR (Scheme 2b).

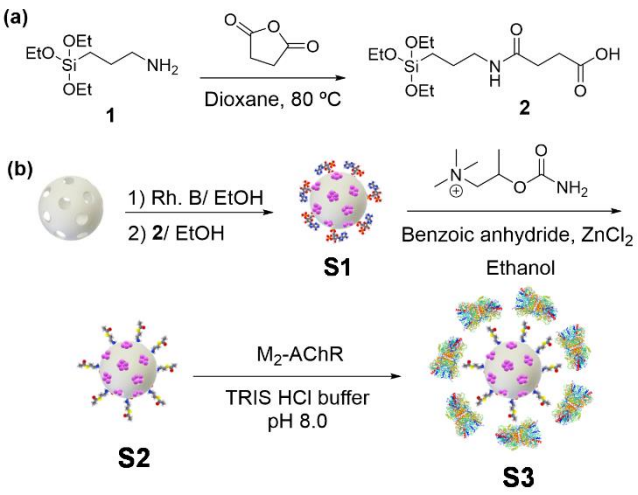

Scheme 2. Synthetic route for the synthesis of solid **S3**.

To confirm the successful synthesis of nanomaterials, the MCM-41 scaffold and solids **S1**, **S2** and **S3** were characterized following standard techniques (see Section 2 and Figures S1-S4 in the Supporting Information). X-ray diffraction (PXRD) of MCM-41 nanoparticles as-synthesized (Figure S1, curve a) shows four low-angle reflections typical of a hexagonal array, indexed as (100), (110), (200), and (210)

Bragg peaks. Besides, a cell parameter a_0 of 44.16 Å (distance between planes d_{100} = 38 Å) is determined. A significant displacement of 6-8 Å of the (100) peak in the PXRD pattern of the MCM-41 calcined nanoparticles is observed (Figure S1, curve b), related to condensation of silanol groups in the calcination step. Curve c in Figure S1 shows the **S2** PXRD pattern. Peaks intensity decrease and the broadening of the (110) and (200) reflections is found and related to a loss of contrast due to the filling of the pore voids with rhodamine B dye and surface functionalization. N_2 adsorption-desorption studies of the calcined MCM-41 nanoparticles show a type IV isotherm, typical of mesoporous materials (curve (a) in Figure S2). The absence of hysteresis cycle in this interval and the shape of the curve suggests the existence of uniform and cylindrical mesopores, with a pore diameter of 1.95 ± 0.05 nm and a total pore volume of 1.18 $cm^3\ g^{-1}$, both calculated by using the BJH model on the adsorption branch of the isotherm. Furthermore, the application of the Brunauer-Emmett-Teller (BET) model results in a value for the total specific surface of 946.89 $m^2\ g^{-1}$ for starting MSNs. The N_2 adsorption-desorption isotherm of **S2** (curve (b) in Figure S2) is typical of mesoporous systems with partially filled mesopores, for which BET and BJH models indicated a reduction of the specific surface (16.31 $m^2\ g^{-1}$) and a decrease of pore volume (0.21 $cm^3\ g^{-1}$). From thermogravimetric and elemental analysis studies (Figure S3), contents of 0.25 ± 0.01 and 0.65 ± 0.01 mmol of rhodamine B and bethanechol respectively per gram of **S2** solid were calculated (27.9% of organic matter content in **S2**). Moreover, the M_2-AChR content in solid **S3** was determined by BCA Protein assay. An amount of 0.0246 µg of M_2-AChR per milligram of solid was anchored to the **S3** outer surface.

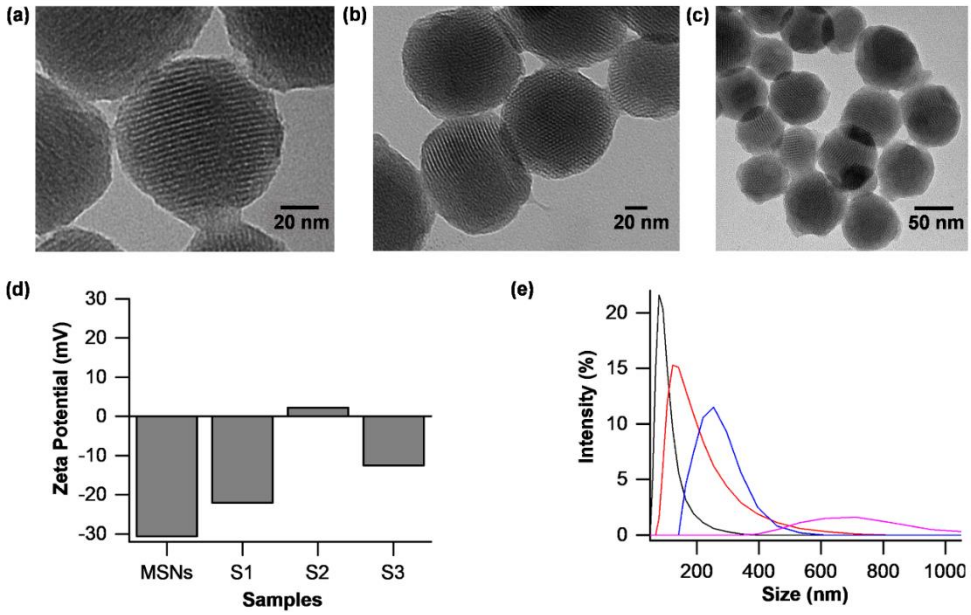

Figure 1. TEM images of (a) calcined MCM-41, (b) **S2** and (c) **S3**, showing both the typical porosity of the mesoporous silica matrix. (d) Zeta Potential for MSNs, **S1**, **S2** and **S3**. (e) Hydrodynamic diameter distribution of calcined MCM-41 nanoparticles (black line), **S1** (red line), **S2** (blue line) and **S3** (pink line) determined by DLS.

The typical hexagonal porosity of the MCM-41 matrix is clearly visualized through TEM images for all solids obtained. MCM-41 (Figure 1a), and solids **S2** and **S3** (Figure 1b and 1c, respectively) are obtained as spherical particles with an average diameter of 108 ± 6 nm (n = 30 particles), confirming that the siliceous matrix structure remains unaltered after the functionalisation process. To complete the characterization, the different steps for the preparation of the nanosensor was evaluated by zeta potential and dynamic light scattering analysis (DLS). The zeta potential shows vales of −30.6, -22.0, 2.25 and -12.5 mV for the starting MCM-41 solid, **S1**, **S2** and **S3**, respectively. Additionally, hydrodynamic diameter values of 171 ± 4, 265 ± 7, 292 ± 14 and 765 ± 10 were found for the starting MCM-41, **S1**, **S2** and **S3** solids, respectively (Figure 1e). Moreover, functionalization of the nanoparticles was also followed by FTIR analysis (Figure S4). FTIR spectrum of

calcined MCM-41 nanoparticles shows typical absorption band at ca. 1100 related to the bond stretching vibrations of Si-O-Si. Moreover, solid **S3** spectrum displays bands at ca. 1629 and 3319 cm^{-1} ascribed to the vibration of peptide bonds and terminal NH_2 and COOH groups from M_2-AChR.

Once the nanoparticles were characterized, we studied rhodamine B released from **S3** (1 mg) in 800 µL of TRIS HCl buffer at pH 8.0 in the absence and in the presence of SCP (see section 3 in SI for details). The obtained payload delivery kinetics are shown in Figure 2a. In the absence of SCP, a low cargo delivery is observed, whereas in the presence of SCP a remarkable release of rhodamine B is found. This cargo delivery agrees with M_2-AChR detachment from the surface of the nanoparticles, due to a displacement of the M_2-AChR induced by the presence of SCP. These results are in accordance with the reported higher affinity constant of the M_2 muscarinic receptor for SCP (0.2 ± 0.1 nM) than for bethanechol (13 ± 4 µM). Affinity of M_2-AChR for bethanechol explains the tight pore closure in **S3**, whereas the larger affinity of M_2-AChR for SCP explains displacement of the former from **S3** and cargo release.[44] Finally, to check the crucial role played by M_2-AChR in the SCP-induced rhodamine B delivery from **S3**, a release experiment from uncapped solid **S2** in absence and presence of SCP was carried out. In this case, an equal and high uncontrolled release of rhodamine was observed in both cases (Figure S5).

In a further step, the release of rhodamine B from **S3** in the presence of increasing amounts of SCP (from 2.24 to 3150 µM) in TRIS HCl buffer solution at pH 8.0 was evaluated (Figure 2b). The obtained results demonstrate an enhancement of the rhodamine B emission at 572 nm as the SCP concentration increases. From the titration curve, a limit of detection (LOD) of 92 µM is calculated. The maximum oral dosage of SCP for medical purposes is 80 mg in 150 mL of water (264 µM), while 100 mg (330 µM) can be lethal in adults.[45] Hence, the detection limit reached enables the method to reliably identify SCP.

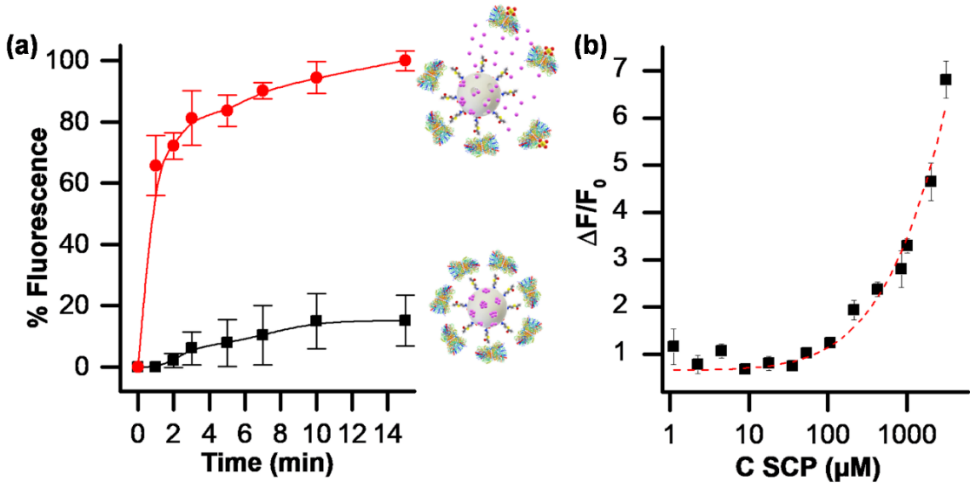

Figure 2. (a) Delivery profiles of rhodamine B from solid **S3** in TRIS HCl buffer at pH 8.0 in absence (black line) and in the presence (red line) of SCP (2.7 mM). (b) Fluorescence intensity of rhodamine B released from solid **S3** in the presence of different amounts of SCP in TRIS HCl Buffer at pH 8.0 after 10 min of addition. Error bars are expressed as 3σ for three independent experiments.

Afterwards, the selectivity of the nanosensor was evaluated in buffer solutions containing others common psychoactive drugs whose consumption is widely spread such as morphine, cocaine, MDMA, heroin and MDPV (Scheme 3). In a typical experiment, the drugs at a concentration of 345 µM were added to suspensions of **S3** and rhodamine B delivery measured after 2 min. The obtained results are shown in Figure 3. Only the presence of SCP induces a remarkable cargo delivery (set as 100% fluorescence) whereas for other drugs rhodamine B release was much less important (less than 30%). The results indicate that **S3** shows a high selectivity towards SCP. Moreover, these findings agree with the poor expected interaction of the tested drugs for the M_2-AChR receptor. Thus, morphine activates the µ opioid receptors or MU receptors involved in pain sensations, whereas cocaine affects the dopaminergic D1 receptor. In addition, MDPV links to the dopamine active transporter (DAT), blocking dopamine reuptake out of the synaptic cleft whereas the principal mechanism of MDMA-induced euphoria is

serotonergic and dopaminergic enhancement. In addition, *in vivo* SCP causes a maximal increase in acetylcholine levels to 10-12-fold over basal values.[46]

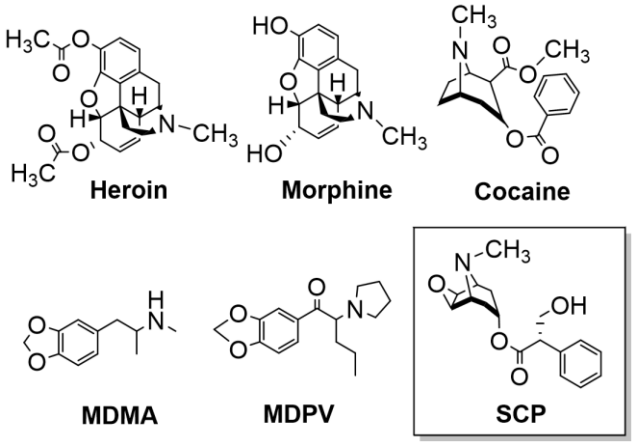

Scheme 3. Structure of different drugs used in the selectivity studies.

We also aimed to demonstrate the feasibility of the nanosensor to detect SCP in complex competitive medium such as saliva. To this end, similar rhodamine delivery studies from **S3** were performed in saliva diluted 30% with TRIS HCl buffer at pH 8.0 spiked or not with SCP. As illustrated in Figure S6, the most significant increase in the fluorescence emission of rhodamine B released from solid **S3** occurs preferentially in the presence of SCP. Furthermore, the sensitivity of **S3** in saliva was measured, showing a detection limit for SCP of 103 µM (Figure S7).

Encouraged by the results above, we moved a step forward with the purpose to obtain a rapid and portable sensor for SCP detection. Modern sectors such as health care, agriculture, environmental monitoring, forensic diagnosis, food safety and in general sensing applications depend heavily on low-cost, point-of-care (POC) tests. Among different technologies LFAs have become increasingly popular as POC diagnostic tool because of their use-friendliness, rapidity, inexpensive nature, and specificity.[47] Besides, this type of assays can be coupled to smartphone read out.[48,49] In fact, integration of mobile phones in (bio)sensing devices is

impacting the POC field in terms of versatility, portability, significant simplification of designs, reduced sizes and costs of the detecting systems.[50]

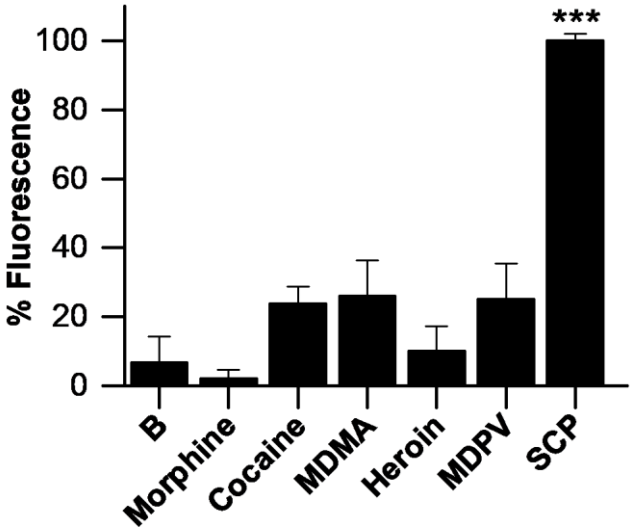

Figure 3. Emission of rhodamine B at 572 nm (λ_{exc} = 565 nm) from a TRIS HCl buffer suspension of solid **S3** in presence of other common drugs (345 µM) 2 minutes after addition. Error bars are expressed as 3σ for three independent experiments (***$p < 0.0001$).

LFAs could help establish a ubiquitous platform for real-time, on-site monitoring. To this end, we proceeded to embed **S3** into a highly selective and sensitive LFA for the direct *in situ* detection of SCP with a smartphone readout. **S3** was thus integrated into glass fiber membranes previously coated with hydrophobic WAX barriers (**S3-WAX-GF**; see experimental details in section 3.1 in Supporting Information) using an absorbent pad after an optimisation process where different materials and conditions were tested. The strip design consists of two zones, zone A in which the sensing material is deposited and zone B in which the fluorescence signal of the released dye dragged in the solvent flow will be collected (Scheme 4). The function of the absorbent pad is to wick the fluid through the membrane through capillary forces, in this way the released dye can be transported through the membrane, allowing the special separation between the sensing material and the released dye. When the strip is immersed in a solution

that does not contain the target analyte, no signal (or a poor signal) would be recorded in zone B since no release of the entrapped dye from the pores occurs. In addition, the nanomaterial remains in zone A without flowing with the solvent. However, when the strip is dipped in a solution with a specific concentration of SCP, the interaction of the analyte with **S3** results in the delivery of the rhodamine B cargo (*vide ante*). The released dye flows with the solvent up to zone B where the fluorescence emission is measured using a smartphone connected with a 3D-printed smartphone case.[51] By means of this device, rhodamine B released is measured using a LED at 522 as excitation source powered by the smartphone via a USB-OTG link and filtered by a short-pass filter (532 nm) while collecting the emission through a long-pass filter (550 nm). Rhodamine B released can be correlated to the amount of SCP present in the sample through extrapolation with a calibration curve.

Following this approach, 2 µL of a **S3** buffer suspension (1 mg/mL) was deposited in the zone A with a micropipette and it was left to dry for 5 minutes. Then, the strip was introduced into 75 µL of a buffered solution in the presence and absence of SCP. After 10 minutes of development and 5 minutes of drying, the test strips were placed in a holder and a picture was taken with the smartphone camera equipped with a 3D-printed smartphone case. The drying step was found to be essential because varying amounts of residual liquid on the strip influence the fluorescence of the dye. Images of the strips were taken with the smartphone camera app under proper light conditions (ISO 100 and exposure time of 1/10 s). The fluorescence intensity of the strips photographs was analysed by extracting the integrated of fluorescence density of the zone B with the software ImageJ.

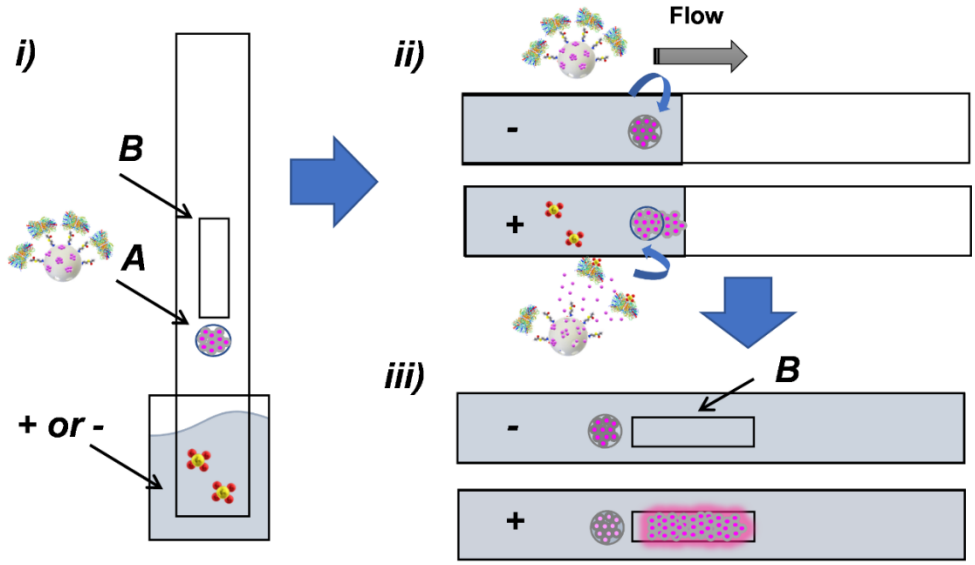

Scheme 4. Design of the lateral flow assay on strip with **S3-WAX-GF** membrane. *i)* Schematic of the integration of **S3** in the zone A of the lateral flow strip immersed in the SCP solution. *ii)* No release occurs in absence of the analyte (negative test), while dye is released in its presence (positive test). *iii)* Rhodamine B released from solid **S3** only in SCP presence is detected in zone B.

Based on the lateral flow experiment designed above, we studied the response of **S3-WAX-GF** membranes as a function of the concentration of SCP in TRIS buffer solution. For this purpose, **S3-WAX-GF** membranes (0.5 x 2.5 cm in size) were prepared and dipped into different solutions with increasing concentrations of SCP (from 9.99 mM to 8.6 µM). As can be seen in Figure S8, when the SCP concentration increases a significant enhancement of the fluorescence emission is observed. From the titration profiles, a detection limit of 0.04 µM was calculated. Finally, **S3-WAX-GF** membranes were tested under more realistic conditions and were able to detect SCP in saliva samples with a limit of detection of 18.7 µM (Figure 4a). In addition, other illicit drugs (200 µM) were also assessed in cross-reactivity studies and the results in terms of selectivity were like those observed by using **S3** in solution (Figure S9).

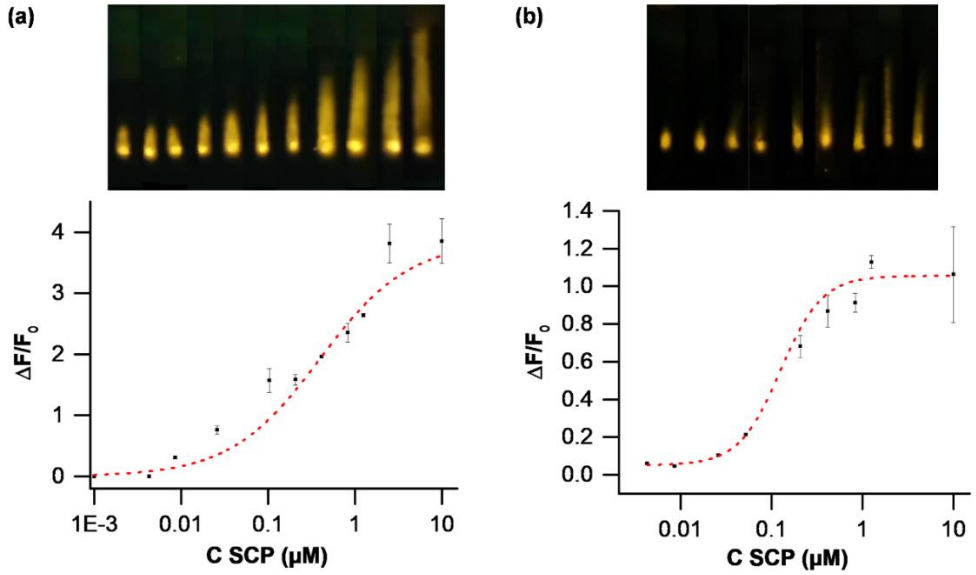

Figure 4. (a) Release of rhodamine B from solid **S3** in the presence of different amounts of SCP in 30% extracted saliva after 10 min of dipping. (b) Release of rhodamine B from solid **S6** in the presence of different amounts of MDPV in 30% extracted saliva after 10 min of dipping. Error bars are expressed as 3σ for three independent experiments. Top: Collage of the photographs registered with the smartphone showing the rhodamine B released in zone B from solid **S3** (a) and solid **S6** (b), shot under proper light excitation.

Having in mind results observed, and considering the modularity of the system, a dual-plex lateral flow assay for the simultaneous detection of SCP and cannibal drug (MDPV) in saliva samples was developed. For the detection of MDPV, the gated MSNs (**S6**) was prepared following procedures previously described by us.[25] **S6** consists of mesoporous silica nanoparticles (MSNs), loaded with a fluorescent reporter (rhodamine B), and functionalized on their external surface with a dopamine derivative (**5**), which specifically interacts with the recombinant human dopamine transporter (DAT), which caps the pores (Scheme 1). Following the same procedure as that described above for SCP, **S6** aqueous suspension (1 mg/mL) were deposited onto **WAX-GF** membranes (0.5 x 2.5 cm size), obtaining as a result **S6-WAX-GF**. These membranes were introduced into different saliva extracted solution (75 µL) with increasing MDPV concentrations (from 9.99 mM to

2.1 µM). From the obtained titration profiles, a LOD of 0.03 µM was calculated (Figure 4b). Moreover, the **S6-WAX-GF** membranes were able to selectively detect MDPV versus MDMA, morphine, heroin, cocaine, MDPV and scopolamine (Figure S10).

Considering the design above, a dual-channel strip was prepared using a similar pattern with the aim to test the presence of both drugs SCP and MDPV simultaneously. **S3** was deposited on the first channel of the strip and the solid **S6** on the second channel under the same conditions as those studied in the individual tests giving rise to **S6@S3-WAX-GF** membranes (Figure S11). The double strip was introduced in different mixed solutions (300 µL) at various concentrations of the two target compounds and the results obtained are depicted in Figure 5. As could be seen, the designed lateral flow assay enables the selective detection of SCP and MDPV in saliva. The studies demonstrated that it possible to develop a lateral flow assay for the simultaneous detection of different drugs which would be of most importance in the areas of health, forensic or drug control and monitoring. In fact, multiplexing features is one of the major challenges in this field. Thus, despite multiplexed detection has been carried out on LFAs, examples to detect small organic molecules are still rare.

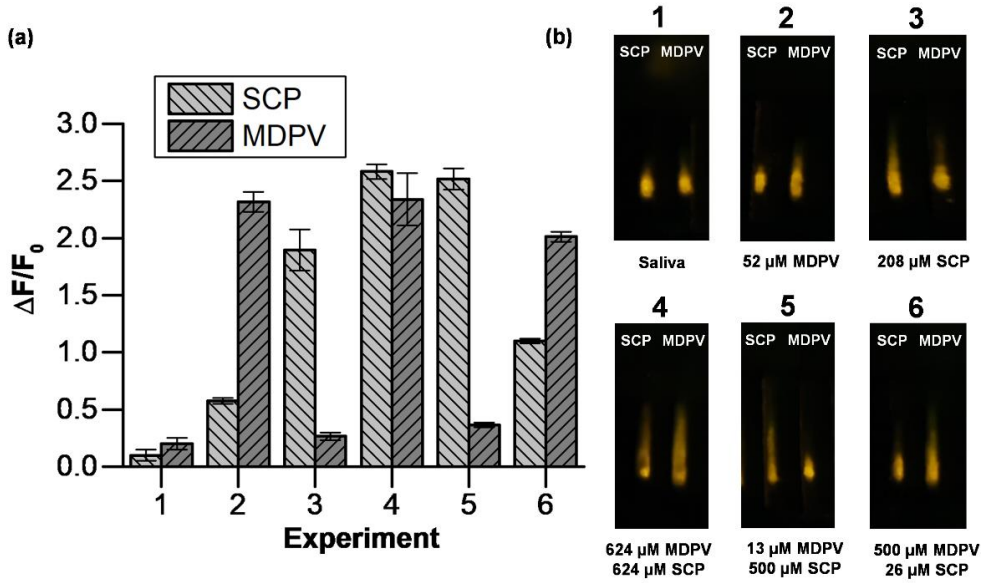

Figure 5. (a) Release of rhodamine B from **S6@S3-WAX-GF** strips in the presence of different amounts of SCP and MDPV extracted saliva after 10 min of dipping. Error bars are expressed as 3σ for three independent experiments. (b) Collage of the photographs registered with the smartphone showing the fluorescence signal of rhodamine B in the detection zone B in the absence and the presence of different concentrations of SCP and cannibal drug in extracted saliva samples.

5.5. CONCLUSIONS

We reported herein the design, synthesis, and characterization of a rapid, highly selective, and sensitive nanosensor for SCP detection in solution and in saliva simulating a realistic environment. The SCP nanosensor consists of MSNs loaded with a fluorescent reporter (rhodamine B) and functionalized on the external surface with a non-selective muscarinic agonist (bethanechol). M_2-AChR interaction with the anchored bethanechol derivative leads to capping of the pores. The sensing mechanism relies on a M_2-AChR-bethanechol recognition inhibition, with subsequent M_2-AChR detachment after its coordination with SCP and cargo delivery. This was confirmed from kinetics release experiments where a remarkable

enhancement in the fluorogenic response is only observed in the presence of SCP, which allows releasing entrapped dye molecules from the pores when M_2-AChR is displaced. Moreover, the probe shows a highly sensitivity in buffer solution (LOD of 92 µM) and in a competitive environment such as saliva (LOD of 103 µM). Other drugs (such as cocaine, heroin, morphine, MDMA and MDPV) induce a negligible cargo release. The material was incorporated into strips for lateral-flow assays coupled to smartphone readout without further treatment or conditioning of the test strips while guaranteeing fast overall assay times of <15 min. The assay fast response times, good selectivity, and exceptional sensitivity, reaching a LOD as low as 0.04 µM in aqueous solution and of 18.7 µM in extracted saliva samples. Finally, a dualplex lateral flow assay capable of detecting *in situ* and *at site* SCP and cannibal drug is developed. Considering the sensitivity and selectivity of the assay, this system provides a highly appealing and reliable approach for the development of portable devices with short assay times and easily handling for the accurate detection of different drugs. Taking into account the versatility of the gated material and the modularity of the assay, it is apparent that this generic approach could be easily transferable to the detection of other drugs from liquid samples without the use of specialized personnel or complex instrumentations.

ASSOCIATED CONTENT

Supporting Information. Supporting information contains materials and methods, synthesis of nanomaterials, additional characterization including powder X-ray diffraction patterns, N_2 adsorption-desorption isotherms, thermogravimetric analysis, and FTIR spectrum. In addition, additional kinetics experiments in buffered solution and lateral flow test with fluorescence read-out protocol was found also in Supporting Information. “This material is available free of charge via the Internet at http://pubs.acs.org.”

Notes

The authors declare no competing financial interest.

ACKNOWLEDGMENTS

This research was funded by the Ministerio de Ciencia, Innovación y Universidades (Spanish Government), the Agencia Estatal de Investigación (AEI) and European Union (projects RTI2018-100910-B-C41 and RTI2018-101599-B-C22-AR (MCIU/AEI/ FEDER, EU) and the Conselleria de Innovación, Universidades, Ciencia y Sociedad Digital, Generalitat Valenciana (Project PROMETEO 2018/024). E. G. is grateful to the Spanish MEC for her FPU grant (FPU16/02464).

5.6. REFERENCES

[1] Renner, U. D.; Oertel, R.; Kirch, W. Pharmacokinetics and pharmacodynamics in clinical use of scopolamine. *Ther Drug Monit* **2005**, *27* (5), 655-665.

[2] García, M. G.; Pérez-Cárceles, M. D.; Osuna, E.; Legaz, I. Drug-facilitated sexual assault and other crimes: A systematic review by countries. *J Forensic Leg Med* **2021**, *79*, 102151.

[3] Hauw, M. E.; Revranche, M.; Kovess-Masfety, V.; Husky, M. M. Sexual and Nonsexual Interpersonal Violence, Psychiatric Disorders, and Mental Health Service Use. *Journal of Traumatic Stress* **2021**, *34*, 416-426.

[4] Kohnen-Johannsen, K. L.; Kayser, O. Tropane Alkaloids: Chemistry, Pharmacology, Biosynthesis and Production. *Molecules* **2019**, *24* (4).

[5] Lakstygal, A. M.; Kolesnikova, T. O.; Khatsko, S. L.; Zabegalov, K. N.; Volgin, A. D.; Demin, K. A.; Shevyrin, V. A.; Wappler-Guzzetta, E. A.; Kalueff, A. V. DARK Classics in Chemical Neuroscience: Atropine, Scopolamine, and Other Anticholinergic Deliriant Hallucinogens. *ACS Chem Neurosci* **2019**, *10* (5), 2144-2159.

[6] Lusthof, K. J.; Bosman, I. J.; Kubat, B.; Vincenten-van Maanen, M. J. Toxicological results in a fatal and two non-fatal cases of scopolamine-facilitated robberies. *Forensic Sci Int* **2017**, *274*, 79-82.

[7] Sáiz, J.; Mai, T. D.; López, M. L.; Bartolomé, C.; Hauser, P. C.; García-Ruiz, C. Rapid determination of scopolamine in evidence of recreational and predatory use. *Sci Justice* **2013**, *53* (4), 409-414.

[8] Drevets, W. C.; Zarate, C. A., Jr.; Furey, M. L. Antidepressant effects of the muscarinic cholinergic receptor antagonist scopolamine: a review. *Biol Psychiatry* **2013**, *73* (12), 1156-1163.

[9] Liu, S.; Shi, D.; Sun, Z.; He, Y.; Yang, J.; Wang, G. M2-AChR Mediates Rapid Antidepressant Effects of Scopolamine Through Activating the mTORC1-BDNF Signaling Pathway in the Medial Prefrontal Cortex. *Front Psychiatry* **2021**, *12* (593), Original Research.

[10] Drevets, W. C.; Bhattacharya, A.; Furey, M. L. The antidepressant efficacy of the muscarinic antagonist scopolamine: Past findings and future directions. *Adv Pharmacol* **2020**, *89*, 357-386.

[11] Oertel, R.; Richter, K.; Ebert, U.; Kirch, W. Determination of scopolamine in human serum by gas chromatography-ion trap tandem mass spectrometry. *J Chromatogr B Biomed Appl* **1996**, *682* (2), 259-264.

[12] Deutsch, J.; Soncrant, T. T.; Greig, N. H.; Rapoport, S. I. Electron-impact ionization detection of scopolamine by gas chromatography—mass spectrometry in rat plasma and brain. *J Chromatogr B Biomed Appl* **1990**, *528*, 325-331.

[13] Swaminathan, S. K.; Fisher, J.; Brogden, N. K.; Kandimalla, K. K. Development and validation of a sensitive LC-MS/MS method for the estimation of scopolamine in human serum. *J Pharm Biomed Anal* **2019**, *164*, 41-46.

[14] Chen, H.; Marín-Sáez, J.; Romero-González, R.; Garrido Frenich, A. Simultaneous determination of atropine and scopolamine in buckwheat and related products using modified QuEChERS and liquid chromatography tandem mass spectrometry. *Food Chem* **2017**, *218*, 173-180.

[15] Ribeiro, M. M. A. C.; Barreto, D. N.; Flávio da S. Petruci, J.; Richter, E. M. Simultaneous determination of scopolamine and butylscopolamine in pharmaceutical and beverage samples by capillary zone electrophoresis. *Microchem J* **2022**, *172*, 106985.

[16] Gamal, M. Analytical review: analytical techniques for hyoscine N butyl bromide. *Analyst* **2020**, *145* (6), 2025-2037.

[17] Koczula, K. M.; Gallotta, A. Lateral flow assays. *Essays in biochemistry* **2016**, *60* (1), 111-120.

[18] Parolo, C.; Merkoçi, A. Paper-based nanobiosensors for diagnostics. *Chem Soc Rev* **2013**, *42* (2), 450-457.

[19] Beck, J. S.; Vartuli, J. C.; Higgins, J. B.; Schlenker, J. L.; Roth, W. J.; Leonowicz, M. E.; Kresge, C. T.; Schmitt, K. D.; Chu, C. T. W.; Olson, D. H.; et al. A new family of mesoporous molecular sieves prepared with liquid crystal templates. *J Am Chem Soc* **1992**, (27), 10834.

[20] Díez, P.; Lucena-Sánchez, E.; Escudero, A.; Llopis-Lorente, A.; Villalonga, R.; Martínez-Máñez, R. Ultrafast Directional Janus Pt–Mesoporous Silica Nanomotors for Smart Drug Delivery. *ACS Nano* **2021**, *15*, 4467–4480.

[21] García-Fernández, A.; Sancenón, F.; Martínez-Máñez, R. Mesoporous silica nanoparticles for pulmonary drug delivery. *Adv Drug Delivery Rev* **2021**, *177*, 113953.

[22] Climent, E.; Mandy Hecht, M.; Rurack, K. Loading and Release of Charged and Neutral Fluorescent Dyes into and from Mesoporous Materials: A Key Role for Sensing Applications. *Micromachines* **2021**, *12*, 249.

[23] Lozano-Torres, B.; Blández, J. F.; Sancenón, F.; Martínez-Máñez, R. Chromo-fluorogenic probes for β-galactosidase detection. Anal BioanalChem **2021**, *413*, 2361–2388.

[24] de Luis, B.; Llopis-Lorente, A.; Sancenón, F.; Martínez-Máñez, R. Engineering chemical communication between micro/nanosystems. *Chem Soc Rev* **2021**, *50*, 8829–8856.

[25] Garrido, E.; Alfonso, M.; Díaz de Greñu, B.; Marcos, M. D.; Costero, A. M.; Gil, S.; Sancenón, F.; Martínez-Máñez, R. A Sensitive Nanosensor for the In Situ Detection of the Cannibal Drug. *ACS Sens* **2020**, *5* (9), 2966-2972.

[26] de Luis, B.; Llopis-Lorente, A.; Rincón, P.; Gadea, J.; Sancenón, F.; Aznar, E.; Villalonga, R.; Murguía, J. R.; Martínez-Máñez, R. An Interactive Model of Communication between Abiotic Nanodevices and Microorganisms. *Angew Chem Int Ed* **2019**, *58* (42), 14986-14990.

[27] de Luis, B.; Morellá-Aucejo, Á.; Llopis-Lorente, A.; Godoy-Reyes, T. M.; Villalonga, R.; Aznar, E.; Sancenón, F.; Martínez-Máñez, R. A chemical circular communication network at the nanoscale. *Chem Sci* **2021**, *12* (4), 1551-1559.

[28] de Luis, B.; Llopis-Lorente, A.; Sancenón, F.; Martínez-Máñez, R. Engineering chemical communication between micro/nanosystems. *Chem Soc Rev* **2021**, *50* (16), 8829-8856.

[29] Garrido, E.; Alfonso, M.; Díaz de Greñu, B.; Lozano-Torres, B.; Parra, M.; Gaviña, P.; Marcos, M. D.; Martínez-Máñez, R.; Sancenón, F. Nanosensor for Sensitive Detection of the New Psychedelic Drug 25I-NBOMe. *Chem Eur J* **2020**, *26* (13), 2813-2816.

[30] Climent, E.; Gröninger, D.; Hecht, M.; Walter, M. A.; Martínez-Máñez, R.; Weller, M. G.; Sancenón, F.; Amorós, P.; Rurack, K. Selective, Sensitive, and Rapid Analysis with Lateral-Flow Assays Based on Antibody-Gated Dye-Delivery Systems: The Example of Triacetone Triperoxide. *Chem Eur J* **2013**, *19* (13), 4117-4122.

[31] Sancenón, F.; Pascual, L.; Oroval, M.; Aznar, E.; Martínez-Máñez, R. Gated Silica Mesoporous Materials in Sensing Applications. *ChemistryOpen* **2015**, *4* (4), 418-437.

[32] Bezinge, L.; Suea-Ngam, A.; deMello, A. J.; Shih, C. Nanomaterials for molecular signal amplification in electrochemical nucleic acid biosensing: recent advances and future prospects for point-of-care diagnostics. *Mol Syst Des Eng* **2020**, *5*, 49–66.

[33] Parolo, C.; Sena-Torralba, A.; Bergua, J.F. Tutorial: design and fabrication of nanoparticle-based lateral-flow immunoassays. *Nat Protoc* **2020**, *15*, 3788–3816.

[34] Cai, Q.; Luo, Z.-S.; Pang, W.-Q.; Fan, Y.-W.; Chen, X.-H.; Cui, F.-Z.; Dilute Solution Routes to Various Controllable Morphologies of MCM-41 Silica with a Basic Medium. *Chem. Mater.*, **2001**, *13*, 258–263.

[35] Valla, A.; Cartier, D.; Zentz, F.; Labia, R.; Atypical Oxidation Reaction by Thionyl Chloride: Easy Two-Step Synthesis of *N*-Alkyl-1,4-dithiines. *Syn. Commun.* **2006**, *36*, 3591-3597.

[36] Largy, E.; Liu, W.; Hasan, A.; Perrin, D. M.; Base-Pairing Behavior of a Carbocyclic Janus-AT Nucleoside Analogue Capable of Recognizing A and T within a DNA Duplex. *ChemBioChem* 2013, *14*, 2199-2208.

[37] Armbruster, D. A.; Pry, T.; Limit of Blank, Limit of Detection and Limit of Quantitation. *Clin. Biochem. Rev.*, **2008**, *29* Suppl 1, S49-S52.

[38] Costa, E.; Climent, E.; Gawlitza, K.; Wan, W.; Weller, M. G.; Rurack, K.; Optimization of analytical assay performance of antibody-gated indicator-releasing mesoporous silica particles. *J. Mater. Chem. B*, **2020**, *8*, 4950-4961.

[39] Moreno-Galindo, E. G.; Alamilla, J.; Sanchez-Chapula, J. A.; Tristani-Firouzi, M.; Navarro-Polanco, R. A. The agonist-specific voltage dependence of M2 muscarinic receptors modulates the deactivation of the acetylcholine-gated K^+ current (IKACh). *Pflug Arch Eur J. Physiol* **2016**, *468* (7), 1207-1214.

[40] Katayama, K.; Suzuki, K.; Suno, R.; Tsujimoto, H.; Iwata, S.; Kobayashi, T.; Kandori, H. Ligand Binding-Induced Structural Changes in the M2 Muscarinic Acetylcholine Receptor Revealed by Vibrational Spectroscopy. *J Phys Chem Lett* **2019**, *10* (22), 7270-7276.

[41] Cai, Q.; Luo, Z.-S.; Pang, W.-Q.; Fan, Y.-W.; Chen, X.-H.; Cui, F.-Z.; Dilute Solution Routes to Various Controllable Morphologies of MCM-41 Silica with a Basic Medium. *Chem. Mater.*, 2001, 13, 258–263.

[42] Valla, A.; Cartier, D.; Zentz, F.; Labia, R. Atypical Oxidation Reaction by Thionyl Chloride: Easy Two-Step Synthesis of N-Alkyl-1,4-dithiines. *Synth Commun* **2006**, *36* (23), 3591-3597.

[43] Largy, E.; Liu, W.; Hasan, A.; Perrin, D. M. Base-pairing behavior of a carbocyclic Janus-AT nucleoside analogue capable of recognizing A and T within a DNA duplex. *Chembiochem* **2013**, *14* (16), 2199-2208.

[44] Moreno-Galindo, E. G.; Alamilla, J.; José A. Sanchez-Chapula, J. A.; Tristani-Firouzi, M.; Navarro-Polanco, R. A. The agonist-specific voltage dependence of M2 muscarinic receptors modulates the deactivation of the acetylcholine-gated K^+ current (I_{KACh}). *Pflug Arch Eur J. Physiol* **2016**, *468*, 1207–1214.

[45] Corallo, C. E.; Whitfield, A.; Wu, A. Anticholinergic syndrome following an unintentional overdose of scopolamine. *Ther Clin Risk Manag* **2009**, *5*, 719-723.

[46] Johnson, D. E.; Nedza, F. M.; Spracklin, D. K.; Ward, K. M.; Schmidt, A. W.; Iredale, P. A.; Godek, D. M.; Rollema, H. The role of muscarinic receptor antagonism in antipsychotic-induced hippocampal acetylcholine release. *Eur J Pharmacol* **2005**, *506* (3), 209-219.

[47] Climent, E.; Biyikal, M.; Gröninger, D.; Weller, M. G.; Martínez-Máñez, R.; Rurack, K. Multiplexed Detection of Analytes on Single Test Strips with Antibody-Gated Indicator-Releasing Mesoporous Nanoparticles. *Angew Chem Int Ed* **2020**, *59* (52), 23862-23869.

[48] Jin, B.; Yang, Y.; He, R.; Park, Y. S.; Lee, A.; Bai, D.; Li, F.; Lu, T. J.; Xu, F.; Lin, M. Lateral flow aptamer assay integrated smartphone-based portable device for simultaneous detection of multiple targets using upconversion nanoparticles. *Sens Actuators B Chem* **2018**.

[49] Xiao, W.; Huang, C.; Xu, F.; Yan, J.; Bian, H.; Fu, Q.; Xie, K.; Wang, L.; Tang, Y. A simple and compact smartphone-based device for the quantitative readout of colloidal gold lateral flow immunoassay strips. *Sens Actuators B Chem* **2018**, *266*, 63-70.

[50] Climent, E.; Rurack, K. Combining Electrochemiluminescence Detection with Aptamer-Gated Indicator Releasing Mesoporous Nanoparticles Enables ppt Sensitivity for Strip-Based Rapid Tests. *Angew Chem Int Ed* **2021**, *60,*26287–26297.

[51] Costa, E.; Climent, E.; Ast, S.; Weller, M. G.; Canning, J.; Rurack, K. Development of a lateral flow test for rapid pyrethroid detection using antibody-gated indicator-releasing hybrid materials. *Analyst*, **2020**, *145*, 3490–3494.

5.7. SUPPORTING INFORMATION

1. EXPERIMENTAL PROCEDURES

1.1. Materials and methods

General techniques: Powder X-ray diffraction (PXRD), thermogravimetric analysis (TGA), elemental analysis, transmission electron microscopy (TEM), Fourier transform infrared (FTIR), dynamic light scattering (DLS) and N_2 adsorption-desorption isotherms were employed to characterize synthesized materials. PXRD measurements were taken on a D8 Advance diffractometer using Cu Kα radiation (Bruker, Massachusetts, United States). Thermogravimetric analyses were carried out on a TGA/SDTA 851e balance (Mettler Toledo, Columbus, OH, USA) in an oxidizing atmosphere (air, 80 mL min^{-1}) with a heating rate program between 393-1273 °C at 10 °C min^{-1}, followed by an isothermal heating step at 1273 °C for 30 min. TEM images were taken with a 100 kV CM10 microscope (Philips). FTIR measurements were taken on a Tensor 27 (Bruker, Massachusetts, United States). DLS experiments were performed using a ZetaSizer Nano ZS (Malvern). N_2 adsorption-desorption isotherms were recorded with a Tristar II Plus automated analyser (Micromeritics, Norcross, GA, USA). The samples were degassed at 90 or 120 °C under vacuum overnight. Specific surface areas were calculated from the adsorption data within the low-pressure range using the Brunauer-Emmett-Teller (BET) model. Pore size was determined following the Barrett-Joyner-Halenda (BJH) method. Fluorescence spectroscopy measurements were taken on a Fluoromax4 from HORIBA Scientific. For the smartphone-based approach, a 3D-box was printed with black PLA using an Ultimaker 3 printer. LEDs and optical filters were purchased from Thorlabs. Photographs were taken with a Samsung Galaxy S7 and values retrieved from images via the integrated density with the software ImageJ, i.e., the

product of mean grey value $\bar{G}$, $\bar{G}$ = (red + green + blue)/3, and the selected area a (in square pixels).

Solvents: All solvents were ACS reagent grade or better quality and were used without any further purification. Ethanol and 1,4-Dioxane were purchased from Scharlab S.L.

Chemicals reagents: Tetraethyl orthosilicate (TEOS), *n*-cetyltrimethylammonium bromide (CTABr), sodium hydroxide, (3-aminopropyl) triethoxysilane, succinic anhydride, benzoic anhydride, zinc chloride ($ZnCl_2$), carbamyl-β-methylcholine chloride (bethanechol chloride), rhodamine B, tris(hydroxymethyl)aminomethane, 3,4-methylenedioxypyrovalerone hydrochloride (MDPV) and scopolamine hydrobromide (SCP) were purchased from Sigma Aldrich química (Madrid, Spain). Magnesium chloride hexahydrate ($MgCl_2 \cdot 6H_2O$) was purchased from Acros Organics. Recombinant human muscarinic acetylcholine receptor 2/CM2 protein was purchased from Abcam PLC. Glass fibre strips were obtained from Whatman™. Other drugs tested, morphine, cocaine, heroin and MDMA were kindly provided by "Agencia Española de Medicamentos y Productos Sanitarios" (AEMPS).

1.2. Synthesis and chemical characterization of nanomaterials

Synthesis of 4-(2-((tert-Butoxycarbonyl)amino)ethyl)-1,2-phenylene bis((3-(triethoxysilyl)propyl)carbamate) (5): Precursor **5** was prepared using a procedure reported by us previously.[1]

Synthesis of S4[1]: In a typical synthesis, a mixture of calcined mesoporous silica nanoparticles (100 mg) and rhodamine B (38.3 mg, 0.08 mmol) were suspended in anhydrous CH_3CN (5 mL) and purged with Argon. The suspension was stirred at room temperature for 24 h in order to load the mesopores. Then, compound **5** (191.5 mg, 0.26 mmol) was added, and the final suspension was stirred

at room temperature for 5.5 h. Finally, the resulting pink solid was filtered and then dried under vacuum overnight, giving rise to **S4** (195 mg).

Synthesis of S5[1]**:** Solid **S4** (10 mg) was suspended in anhydrous CH_2Cl_2 (2 mL) and purged with Argon. The suspension was then cooled to 0 °C, and TFA (0.1 mL, 1.31 mmol) was added for *N*-Boc deprotection. The mixture was stirred at room temperature for 10 min, and the solid was isolated by centrifugation, washed with CH_2Cl_2 (2 × 8 mL), and dried overnight at 37 °C.

Synthesis of S6[1]**:** Solid **S5** (1 mg) was suspended in TRIS HCl buffer (300 µL, 20 mM of TRIS and $MgCl_2{\cdot}6H_2O$, pH 8.0), and then the recombinant human transporter dopamine protein (150 µL, 0.017 µg/µL) was added. The mixture was stirred in a thermo-shaker at 4 °C overnight. Then, the suspension was centrifuged at 12,000 rpm for 5 min. **S6** was then washed with TRIS HCl buffer (300 µL) to eliminate the non-encapsulated dye and the unattached protein.

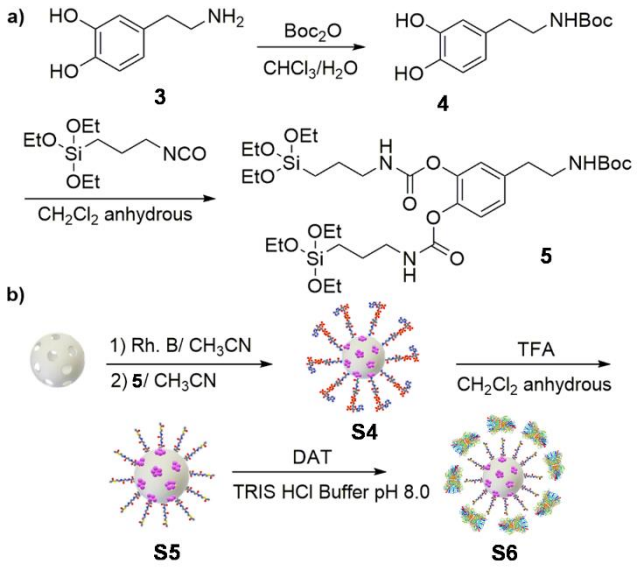

Scheme S1. a) Synthetic route followed for the preparation of the precursor **5**. b) Synthetic route for the synthesis of solid **S6** in the presence of dopamine active transporter (DAT).

2. CHARACTERIZATION OF THE PREPARED MATERIALS

The MCM-41 scaffold and mesoporous solids **S1**, **S2** and **S3** were characterized following standard techniques, including transmission electron microscopy (TEM), powder X-ray diffraction (PXRD), N_2 adsorption/desorption analysis, dynamic light scattering (DLS) and FTIR. On the other hand, content of recombinant human muscarinic acetylcholine receptor M_2-AChR protein in solid **S3** was determined from BCA protein assay[2] whereas bethanechol derivative and rhodamine B on the nanoparticles were determined from thermogravimetric and elemental analysis.

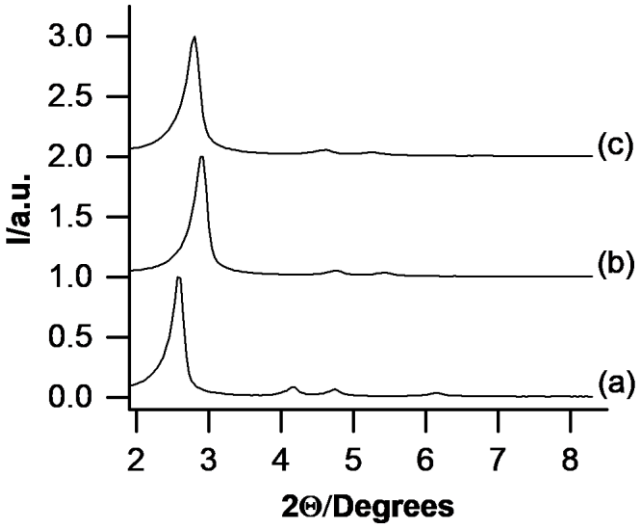

Figure S1. Powder X-ray diffraction (PXRD) patterns of solids (a) as-synthesized MCM-41, (b) calcined MSNs and (c) solid **S2**. Diffractograms are y-shifted for clarity.

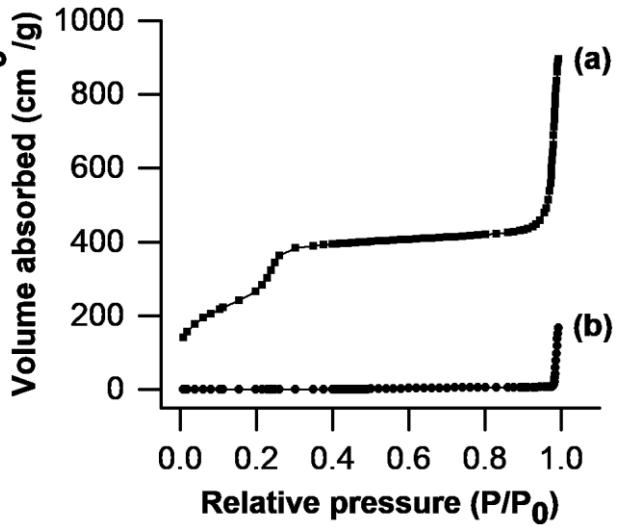

Figure S2. N_2 adsorption-desorption isotherms for (a) calcined MCM-41 nanoparticles and (b) **S2** material.

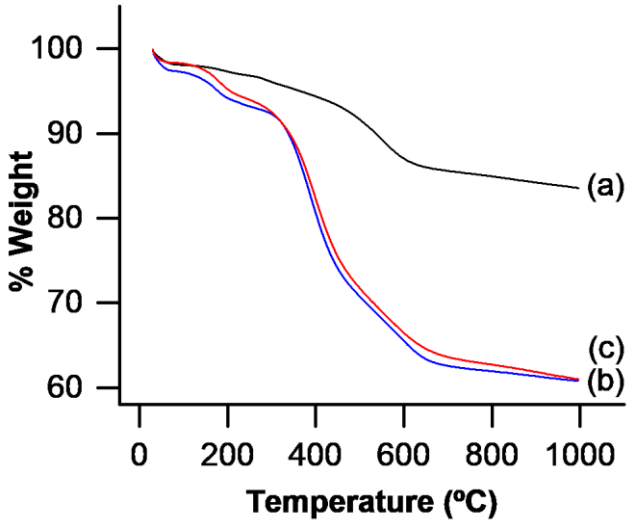

Figure S3. Thermogravimetric analysis for (a) calcined MCM-41 nanoparticles loaded with rhodamine B, (b) **S1** material and (c) **S2** material.

FTIR spectrum of functionalized solid **S1** shows typical absorption bands at ca. 1100, 1500 and 3400 cm^{-1} related to the bond stretching vibrations of Si-O-Si, C=O and of O-H and N-H groups, respectively. Moreover, the spectrum showed the stretching vibrations of C=O groups at 1711 cm^{-1}, which is present in FTIR spectrum

of solid **S2** whereas the O-H band is reduced because of the reaction between **2** and bethanechol. Finally, solid **S3** displays a broad band of N-H, C=O and O-H groups at ca. 1629 and 3319 cm^{-1} ascribed to the vibration of peptide bonds and terminal NH_2 and COOH groups from M_2-AChR.

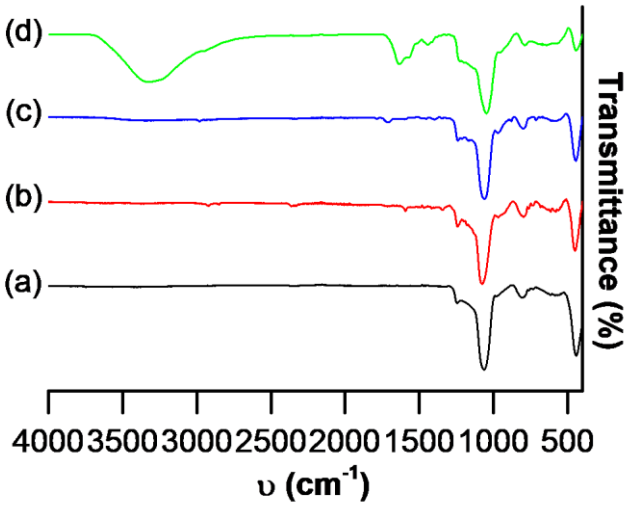

Figure S4. FTIR spectrum of (a) calcined MCM-41 nanoparticles, (b) **S1** nanoparticles, (c) **S2** solid and (d) **S3**. Spectra are y-shifted for clarity.

3. RESULTS AND DISCUSSION

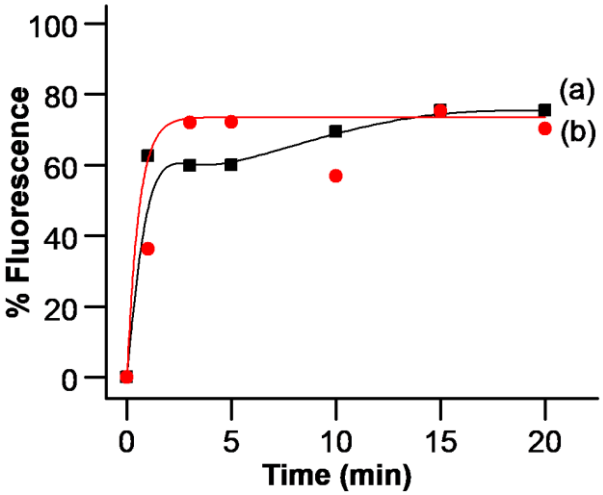

Figure S5. Release profiles of rhodamine B from TRIS HCl buffer suspensions of solid **S2** at pH 8.0 (a) in absence and (b) in the presence of SCP (2.7 mM).

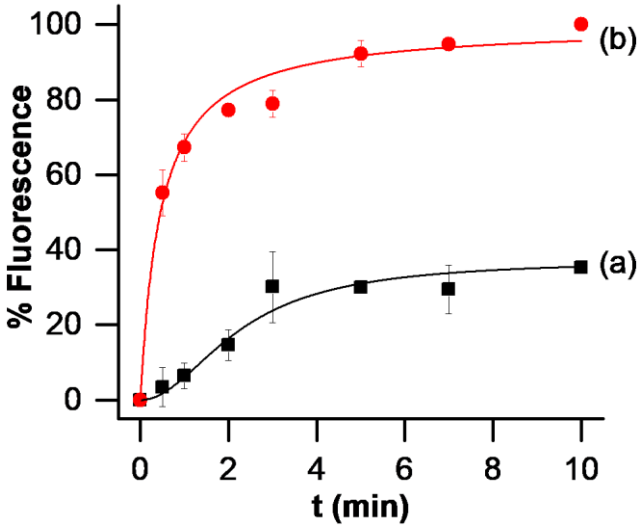

Figure S6. Release profiles of rhodamine B from 30% extracted saliva suspensions of solid **S3** (a) in the absence and (b) in the presence of SCP (2.7 mM). Error bars are expressed as 3σ.

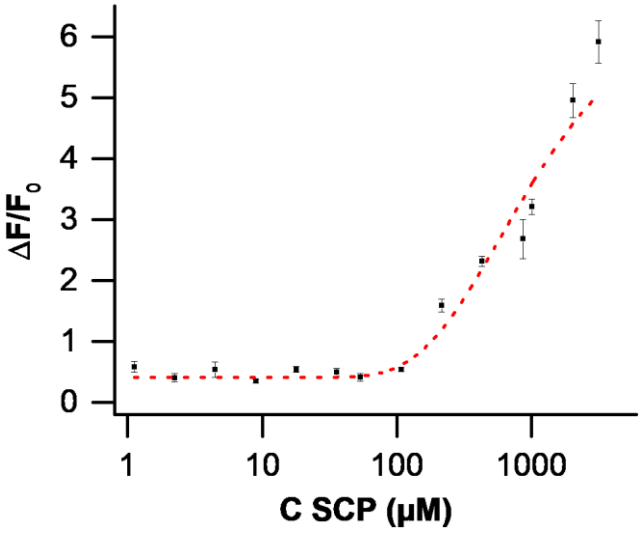

Figure S7. Release of rhodamine B from solid **S3** in the presence of different amounts of SCP in 30% extracted saliva after 10 min of addition. Error bars are expressed as 3σ.

3.1. Lateral flow tests with fluorescence read-out protocol.

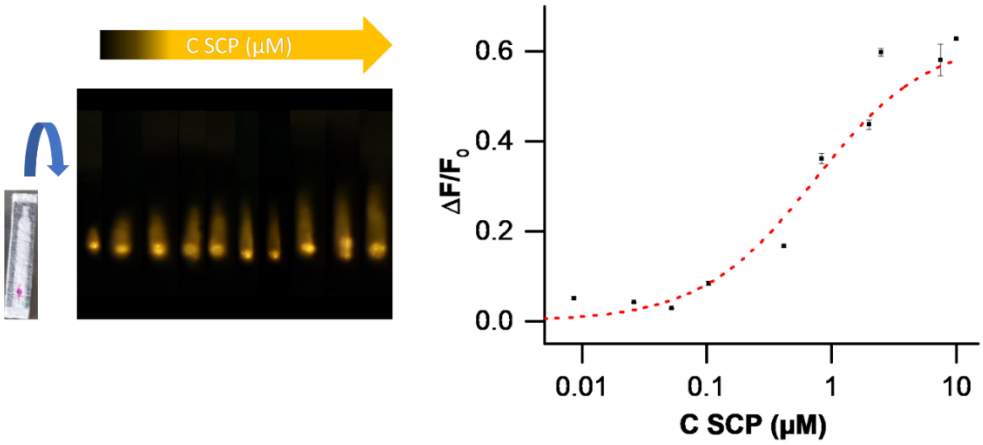

Figure S8. Left: Collage of the photographs registered with the smartphone showing the rhodamine B released in zone B from solid **S3**, shot under proper light excitation. Right: Release of rhodamine B from solid **S3** in the presence of different amounts of SCP in TRIS HCl buffer at pH 8.0 after 10 min of dipping. Error bars are expressed as 3σ for three independent experiments.

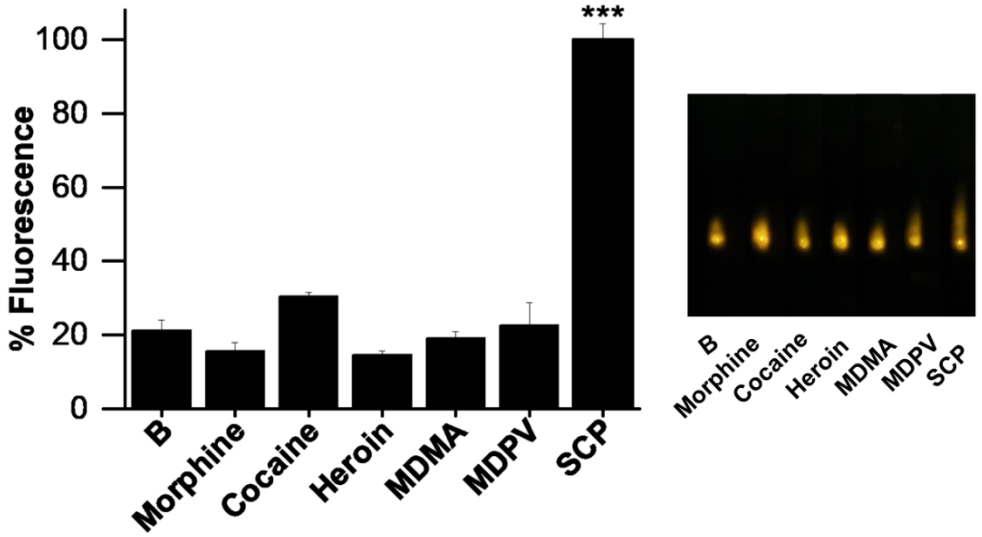

Figure S9. Effect of the indicated drugs (200 µM) on the relative rhodamine B release in GF-strips from solid **S3** in 30% extracted saliva 10 min after dipping. Error bars are expressed as 3σ for three independent experiments.

3.2. Lateral flow assay for the detection of illicit drugs MDPV.

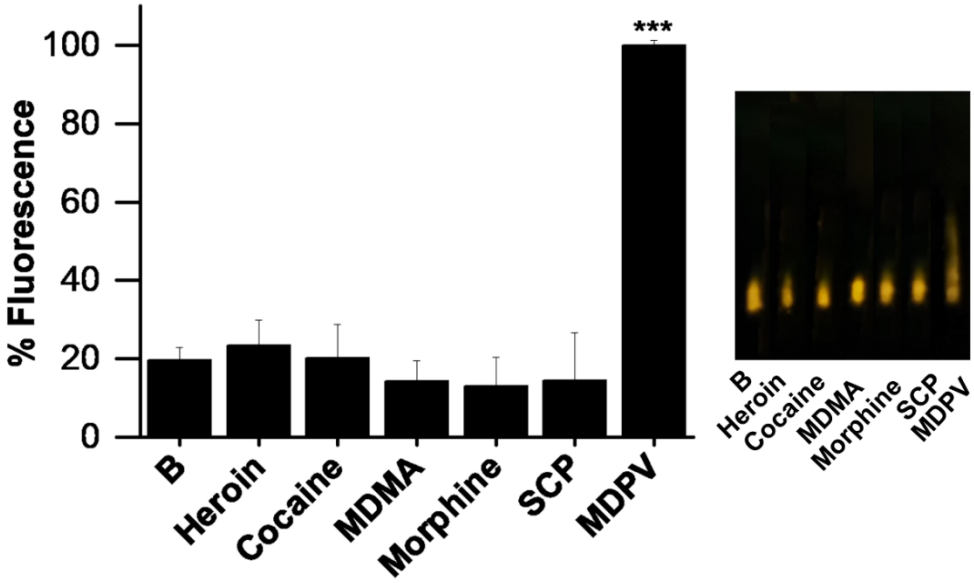

Figure S10. Effect of the indicated drugs (200 μM) on the relative rhodamine B release in **S6-WAX-GF** strips from solid **S6** in 30% extracted saliva 10 min after dipping. Error bars are expressed as 3σ for three independent experiments.

3.3. Duplex lateral flow assay for the detection of illicit drugs MDPV and SCP.

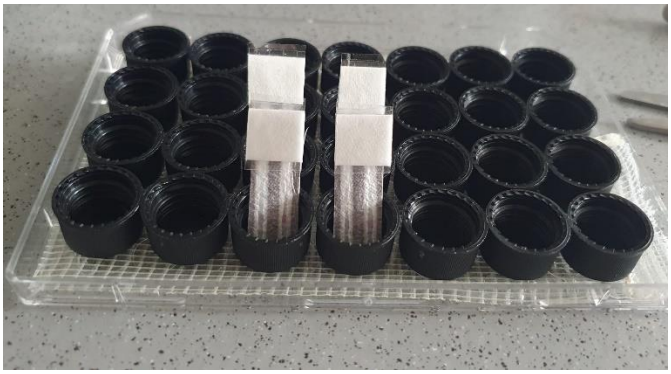

Figure S11. Elution process illustration of a dual-channel strip with **S6@S3-WAX-GF** membranes.

4. REFERENCES

[1] Garrido, E.; Alfonso, M.; Díaz de Greñu, B.; Marcos, M. D.; Costero, A. M.; Gil, S.; Sancenón, F.; Martínez-Máñez, R.; A Sensitive Nanosensor for the In Situ Detection of the Cannibal Drug. *ACS Sens.* **2020**, *5*, 2966−2972.

[2] He, F. BCA (bicinchoninic acid) protein assay. **2011**, Bio-101 e44.

CHAPTER 6

GHB SENSING IN STRIPS BY LATERAL FLOW TEST USING A DYE-DISPLACEMENT ASSAY

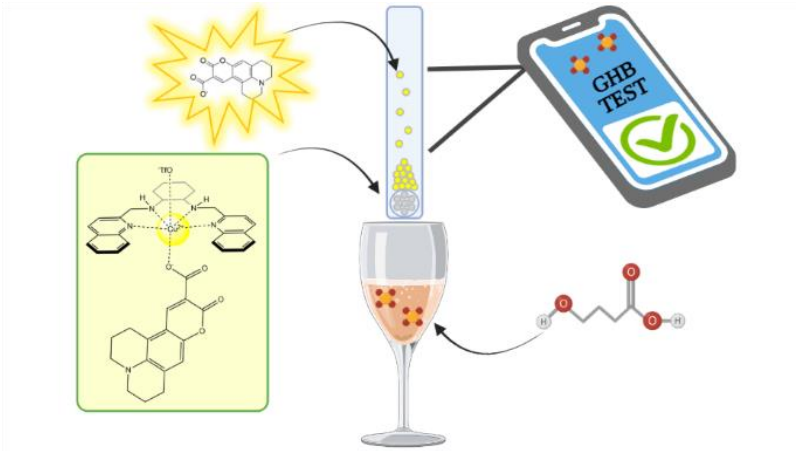

GHB SENSING IN STRIPS BY LATERAL FLOW TEST USING A DYE-DISPLACEMENT ASSAY

Eva Garrido,[†,‡,¥,§] Guillermo Hernández-Sigüenza,[†,§] Estela Climent,[Δ] M. Dolores Marcos,[†,‡,¥,§] Knut Rurack,[Δ] Ana M. Costero,[†,‡] Félix Sancenón,[*,†,‡,¥,§] Vicente Martí-Centelles,[*,†,§] and Ramón Martínez-Máñez[*,†,‡,¥,§]

[†] Instituto Interuniversitario de Investigación de Reconocimiento Molecular y Desarrollo Tecnológico (IDM), Universitat Politècnica de València, Universitat de València, Spain.

[‡] CIBER de Bioingeniería, Biomateriales y Nanomedicina (CIBER-BBN).

[¥] Unidad Mixta de Investigación en Nanomedicina y Sensores. Universitat Politècnica de València, Instituto de Investigación Sanitaria La Fe, Valencia, Spain.

[§] Unidad Mixta UPV-CIPF de Investigación en Mecanismos de Enfermedades y Nanomedicina, Universitat Politècnica de València, Centro de Investigación Príncipe Felipe, Valencia, Spain.

[Δ] Bundesanstalt für Materialforschung und -prüfung (BAM), Richard-Willstätter-Str. 11, 12489 Berlin, Germany.

Submitted

6.1. ABSTRACT

The use of gamma-hydroxybutyric acid (GHB) as a date rape drug has risen because of its availability as a salt which makes it highly soluble in aqueous solutions and alcoholic beverages being necessary to develop rapid detection procedures. In this regard, the development of portable testing methods based on lateral flow strip assays capable of detecting trace concentrations of target analytes has become increasingly important and holds enormous potential for the detection of drugs. Using this strategy, here we report a rapid, low cost, easily handleable and highly sensitive test strips for lateral-flow assay based GHB analysis employing a smartphone for fluorescence readout. The sensing ensemble is based on a Cu^{2+} complex with a tetradentate ligand and the fluorescent dye coumarin 343, that can detect GHB through an indicator displacement assay (*IDA*) with a detection limit of 0.06 µM in aqueous solution. This system when incorporated in a test strip in lateral flow assay shows a detection limit as low as 0.03 µM for GHB in MES buffer solution and its able to detect GHB at concentration as low as 0.1 µM in soft drinks and alcoholic beverages in less than 1 minute.

KEYWORDS: *Colorimetric sensor, dye displacement assay (IDA), Gamma-hydroxybutyric acid (GHB), lateral-flow assay, test strip, smartphone readout.*

6.2. INTRODUCTION

Gamma-hydroxybutyric acid (GHB) is a naturally occurring metabolite found in many living species. Besides, GHB has also been used as date rape drug and as drug-facilitated sexual assaults (DFSA) as it can be easily manufactured in a simple one-step from available precursors. DFSA defines sexual assault without consent of the victim unable to provide approval because of administration psychoactive substances. DFSA has acquired greater relevance worldwide and social impact due to the significantly increase in cases in recent years.

GHB is colorless and odorless, soluble in aqueous/alcoholic drinks making it practically undetectable. Additionally, GHB is rapidly eliminated and its detection in urine samples is only possible within 6-12 h after ingestion.[1,2] It is reported that a 0.5 g dose of GHB produces relaxation and disinhibition, a 1 g dose produces a euphoric effect and a 2-3 g dose produces a deep sleep.[3] Assuming dose is on a 150–200 mL drink, the minimum concentration of GHB in a spiked beverage producing sedative effect is ca. 10 mg/mL (96 mM).

Owing to the increasing use of GHB in rape-assaults, a need has arisen to develop simple and in situ efficient assays for its identification. Detection of GHB can be achieved using a wide range of techniques such as GC-MS and HPLC-UV,[1,4,5] however these procedures are highly specialized and cannot be used for *in situ* GHB detection. As an alternative, several examples have been reported recently based on the use of chromo-fluorogenic probes. For instance Baumes et al reported GHB detection with a limit of detection (LOD) of 100 µM in aqueous solutions using a colorimetric sensing array, based on supramolecular host-guest complexes of cucurbiturils with fluorescent dyes.[6] In addition, Chang and co-workers prepared a fluorescent BODIPY derivative which exhibited a moderate emission quenching in the presence of GHB allowing it detection at concentrations as low as 29 mM in water.[7] Besides, some of us used non-emissive oxazole derivatives to detect GHB through color changes and marked emission enhancements in mixed aqueous solutions allowing detection GHB in soft drinks and alcoholic beverages (LOD of 0.12 µM).[8] Gold nanoparticles bi-functionalized with oxazole and phenanthroline derivatives have also been reported for the colorimetric detection of GHB in water.[9] However, some of these probes still show certain drawbacks for an effective use aiming GHB detection, such as the use of organic solvents, the application of screening techniques, high detection limits in aqueous solution and difficult handling. In the end, methods for the simple, rapid, and *in situ* detection of GHB in

aqueous or alcoholic drinks necessary to prevent drug-facilitated sexual assaults are still to come.

Based on the above, we report herein an indicator displacement assay (*IDA*) for GHB detection using the sensing ensemble **1**, formed by the interaction of the Cu^{2+}complex **3** and coumarin 343 (Figure 1a). The sensing paradigm relies on a preferential coordination of GHB by Cu^{2+} in **1** that induces displacement of coumarin 343 thus restoring its fluorescence (Figure 1b). Figure 1a also shows the synthesis of the tetradentate ligand **4**.[10,11] Besides, *IDA* probe **1** was incorporated into a coated PEG-glass fiber (**PEG-GF**) membrane to obtain a highly robust and sensitive lateral flow assay, that allows detection of GHB in soft drinks and alcoholic beverages in less than 1 min using a simple smartphone fluorescence readout.

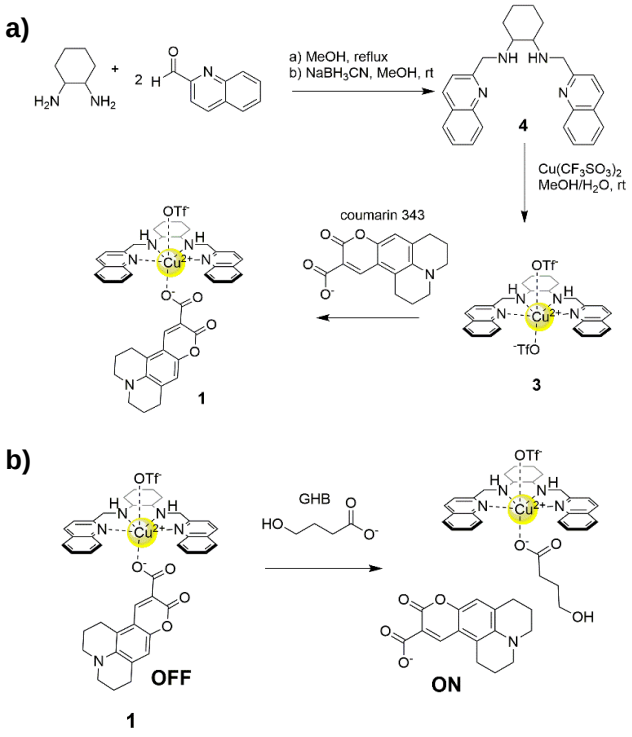

Figure 1. a) Synthesis of tetradentate ligand **4**, Cu^{2+} complex **3** and GHB sensing ensemble **1** (formed between complex **3** and coumarin 343). b) *IDA* assay for fluorescent GHB detection using sensing ensemble **1**.

6.3. EXPERIMENTAL SECTION

Sensing ensemble **1**[10] and N,N-bis(quinolin-2-ylmethylene)-1,2-cyclohexanediamine (**4**)[12,13] were prepared following literature procedures with some changes.

Synthesis of complex 3.[12] To a 50 mL of round bottom flask, **4** (100 mg, 0.252 mmol) was added and dissolved in anhydrous MeOH (20 mL). An aqueous solution of $Cu(CF_3SO_3)_2$ (91.2 mg, 0.252 mmol) in milli-Q water (1.8 mL) was added and the reaction mixture was stirred for 3 h at rt. The solvent was removed under vacuum and the colorless solid obtained was washed with cold MeOH and dried to obtain complex **3** (Figure 1a). HRMS: Calculated for $C_{26}H_{28}CuN_4$ (M^+H^+) 460.08 m/z; measured 460.15 m/z (M^+H^+).

Displacement kinetics in the presence of GHB. In a typical experiment, 2 mL of *IDA* probe **1** in MeOH/H_2O (4:1 v/v) was divided into two aliquots of 1 mL. Then, 50 µL of a 10 mM solution of GHB in MES buffer (50 mM of MES, pH 6.0) were added to one of the aliquots (final concentration of 100 µM), and simultaneously, 50 µL of MES buffer were added to the blank aliquot. Both solutions were stirred at 25 °C and, after certain time, the fluorescence of the displaced coumarin 343 (λ_{exc} = 444 nm, λ_{em} = 494 nm) was measured (Figure 2).

Concentration-dependence studies of *IDA* probe 1 for GHB. To 2 mL of an *IDA* probe **1** solution (prepared by mixing 1.995 mL of a **3** to 212 µM solution and 5 µL of a 40 µM solution of coumarin, giving a final concentration of 0.1 µM) in MeOH/H_2O 4:1 v/v, increasing volumes of a 1 mM solution of GHB in MES buffer (50 mM of MES, pH 6.0) were added. Subsequently, the solution was stirred at 25 °C for 15 second and then the fluorescence of the coumarin 343 (λ_{exc} = 444 nm, λ_{em} = 494 nm) was measured (Figure S1).

Preparation of PEG-coated glass fiber paper (PEG-GF).[14] A mixture of 24 mL toluene and 600 µL 3-(methoxy(polyethyleneoxy)trimethoxy silane was placed in a 50 mL tube containing 15 glass fiber strips of 8 × 2.5 cm. After reaction for 12 h at 25 °C with orbital stirring, the **PEG-GF** strips were washed with ethanol and dried at 37 °C for 2 h.

Concentration-dependence studies of complex 1 for GHB in MES buffer in strip. PEG-GF strips of 4 × 0.5 cm were prepared, and 5 µL of a solution of the *IDA* probe **1** (prepared by mixing 1.995 mL of a 3 to 212 µM solution and 5 µL of a 40 µM solution of coumarin, giving a final concentration of 0.1 µM in MES buffer (50 mM), pH 6.0) were deposited at ca. 1 cm from one end of the strip (zone A). The strips containing *IDA* probe **1** were then dipped into 75 µL of the MES-buffered sample solutions containing different concentrations of GHB and the flow was left to develop for 1 min. Afterwards, the fluorescence emission intensity of the strips was measured using a smartphone readout at 500 nm (λ_{exc} = 465 nm). The amount of dye released for each concentration was calculated according to the ratio of the fluorescence of zone B and the fluorescence of the entire strip (Figure 4).

Concentration-dependence studies of *IDA* probe 1 for GHB in alcoholic beverage in strip. The same procedure described in the section above was carried out in a 50% solution of gin (Figure S3).

Selectivity studies with *IDA* probe 1 in alcoholic beverage in strip. PEG-GF strips of 4 × 0.5 cm were prepared, and 5 µL of a solution of *IDA* probe **1** (prepared by mixing 1.995 mL of a 3 to 212 µM solution and 5 µL of a 40 µM solution of coumarin, giving a final concentration of 0.1 µM in MES buffer (50 mM), pH 6.0) were deposited at ca. 1 cm from one end of the strip (zone A). The strips containing *IDA* probe **1** were then dipped into 75 µL of gin sample solutions containing 1 µM of different drugs (MDMA, morphine, heroin, cocaine, MDPV, scopolamine and GHB). Afterwards, the strips fluorescence was measured using a smartphone

readout at 500 nm (λ_{exc} = 465 nm). The amount of dye released for each concentration was calculated according to the ratio of the fluorescence of zone B and the fluorescence of the entire strip (Figure 5).

6.4. RESULTS AND DISCUSSION

For the preparation of the sensing ensemble, the tetradentate ligand **4** was synthetized by a reductive amination of 1,2-cyclohexyl diamine with 2-quinolinecarboxaldehyde. Structure of **4** was confirmed using ^{1}H and ^{13}C NMR and HRMS and was in agreement with the reported values.[12,13] **4** was then reacted with $Cu(CF_3SO_3)_2$ to obtain the corresponding complex **3**, that was further reacted with coumarin 343 to obtain the final *IDA* probe **1** (Figure 1a).

To assess the proposed *IDA* sensing paradigm for GHB detection, the fluorescence response of **1** in organic-aqueous media (MeOH/H_2O 4:1 v/v) in the presence/absence of GHB was monitored. In a typical experiment, to a solution of **1**, GHB or MES buffer was added and at schedule times, the emission of coumarin 343 at 494 nm (λ_{exc} = 444 nm) is measured. Emission kinetic profiles of **1** in the absence and presence of GHB are displayed in Figure 2. In the absence of GHB, emission of coumarin 343 is highly quenched in **1** due to a photoinduced electron transfer process from the metal center to the fluorophore. In contrast, fluorescence is remarkably enhanced at 494 nm in the presence of GHB, which is ascribed to a preferential coordination of GHB carboxylate group with the copper atom in **1** leading to a displacement of the coumarin 343 molecule. Besides, addition of increasing amounts of GHB to a solution of the sensing ensemble **1** in MeOH/H_2O 4:1 v/v induces a progressive increase in the emission band of coumarin 343 at 494 nm in agreement with a concentration-dependent displacement of the fluorophore from **1** by GHB coordination with Cu^{2+}. From the obtained titration profile (Figure S1) a limit of detection of 0.06 µM for GHB was determined. This value allows detection of a common dose of GHB (2-3 mg) in 150-200 mL (96 mM).

Hence, encouraged by the results obtained above in mixed aqueous buffered solutions we outlined the assembly of complex **1** in PEG-modified glass fiber membranes aiming to develop a low-cost, straightforward, portable, and easy to handle lateral flow assay combined with a smartphone fluorescence readout setup for the *in situ* and *on-site* GHB detection.

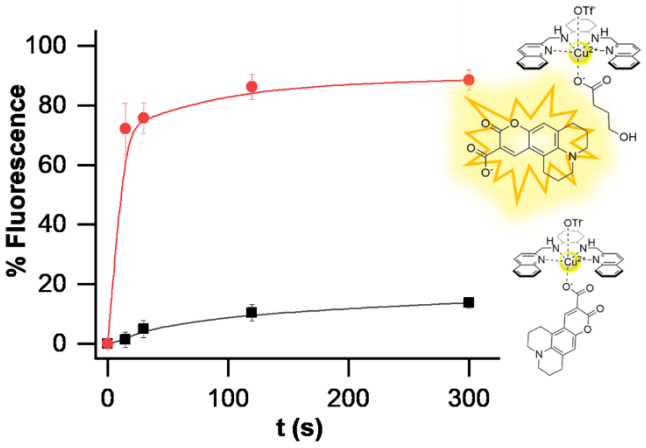

Figure 2. Kinetics of coumarin 343 displaced from *IDA* probe **1** in MeOH/H_2O 4:1 v/v in the absence (black line) and the presence of GHB 100 μM (red line). Error bars are expressed as 3σ for three independent experiments.

Within the field of point of care devices (POC),[15,16,17] lateral flow assays (LFAs)[18] or lateral flow test strips (LFTS)[19] are considered as a striking tools for qualitative, semi-quantitative, and even quantitative detection of various analytes, especially biomarkers,[20,21] toxins,[22] contaminants,[23] and small molecules.[24,25,26] The ASSURED criteria, mentioned by World Health Organization (WHO), insist that all POC devices must provide features including (i) affordable; (ii) sensitive; (iii) specific; (iv) user friendly; (v) rapid and robust; (vi) equipment-free; and (vii) delivered to the end-users. At this respect, LFA technology meets these specifications and has undergone rapid technological advances for various applications in environment, diagnosis, etc. In brief, LFAs tests consists of a liquid sample that runs along the surface of a pad in which different molecules are placed to give finally a visual

output. The sample can drag the analyte without the assistance of external forces (capillary action) through various zones of the strip. The test strip we have developed consists of two different zones; zone A (in which *IDA* probe **1** is deposited) and zone B, which is an area of the strip through which the solvent front travels and in which the signal of the indicator is measured. The presence of GHB is expected to enhance the concentration of free coumarin 343 in zone B (Scheme 1). The amount of coumarin 343 released can be quantified with a digital camera of a mobile communication device with the necessary optical accessories.[27]

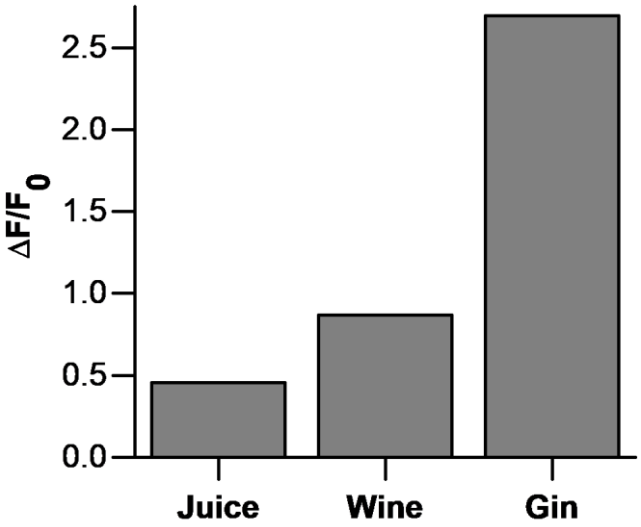

Figure 3. Intensity of fluorescence registered with the 3D-printed smartphone case associated with coumarin 343 displaced from *IDA* probe **1** in zone B of lateral-flow strips after 1 min of developing with adulterated and non-adulterated soft and alcoholic beverages.

Considering this design, we prepared the strips and carried out an optimization in which different materials as membranes were tested. The materials tested were glass fiber (GF), filter paper (PF) and fusion 5 (F5). Moreover, these materials were further modified with a mixture of TEOS and 3-(methoxy (polyethylene-oxy)propyl)trimethoxy silane (Si-PEG and PEG), resulting in the materials PEG-GF, PEG-PF, PEG-F5, Si-PEG-GF, Si-PEG-PF and Si-PEG-F5. Then, a spot

of 5 µL of an *IDA* probe **1** methanolic aqueous solution (4:1 v/v) was deposited on the different materials on zone A leading to dry for 5 minutes. Blanks were introduced into a MES buffer solution at pH 6.0 and simultaneously, others were dipped into a MES buffered solution of GHB (1 mM). After 60 s of development, the test strips were placed in a holder and the fluorescence was measured with a smartphone camera equipped with a 3D-printed smartphone case containing an LED with an excitation wavelength at 465 nm and a long-pass filter to collect the fluorescence emission after 500 nm.[28] Images of the strips were taken with the smartphone camera app under proper light conditions (ISO 400 and exposure time of 0.5 s). The intensity of fluorescence of the photographs of the strips was analyzed, extracting the integrated density of fluorescence of the zone B with the software ImageJ.

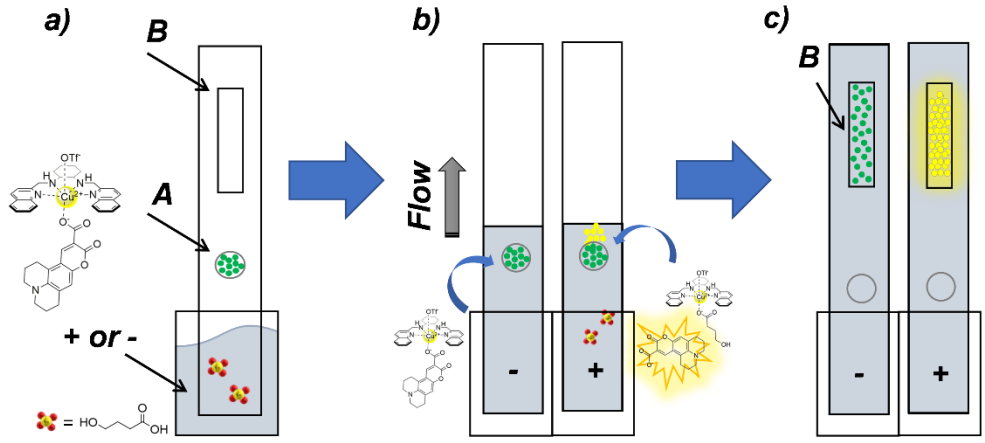

Scheme 1. Design of the lateral flow assay on strip with *IDA* probe **1** integrated into a coated PEG-glass fiber membrane. a) Schematic of the integration of *IDA* probe **1** in the zone A of the lateral flow strip immersed in the GHB solution. b) No release occurs in absence of the analyte (negative test), yet dye is released in its presence (positive test). c) Coumarin 343 displaced from *IDA* probe **1** only in GHB presence is detected in zone B.

Fluorescence intensity of coumarin 343 in the absence and presence of GHB in different materials measured in zone B is shown in Figure S2. The highest

blank/sample difference in emission was observed with the **PEG-GF** strip, which was selected for further assays. Besides, the morphology of the **PEG-GF** strip was studied by SEM and the amount of PEG in **PEG-GF** was calculated from thermo-gravimetric and elemental analysis (Figure S4-S5). A content of 88 ± 0.015 µmol C/g SiO_2 for PEG-GF membranes and 8 ± 0.9 µmol C/g SiO_2 for GF was obtained.

For the **PEG-GF** strip, a low fluorescence of coumarin was recorded in zone B in the absence of GHB, while a remarkable enhancement in the emission was detected in the presence of GHB (Figure 4).

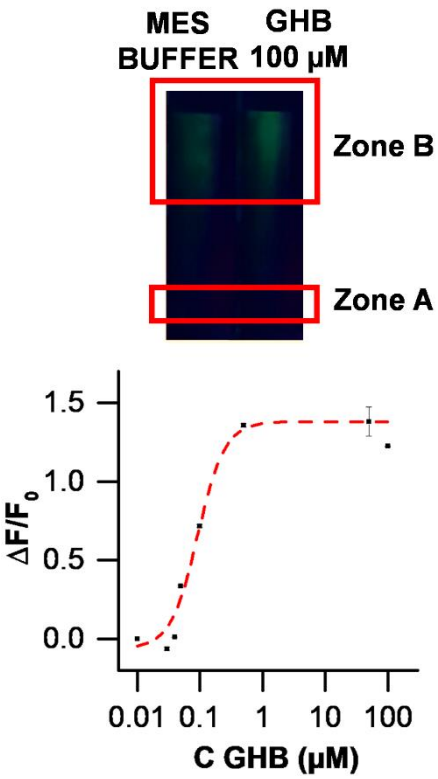

Figure 4. Top: Smartphone readout for the determination of the fluorescence of coumarin 343 displaced from *IDA* probe **1** in the presence and absence of GHB. Bottom: Increase in fluorescence intensity of coumarin 343 displaced from *IDA* probe **1** measured in zone B in the lateral flow assay in the presence of different amounts of GHB in MES buffer (50 mM)

at pH 6.0 after 1 min of dipped. Error bars are expressed as 3σ for three independent experiments.

Based in the procedure detailed above, the response of the LFA as a function of the concentration of GHB in MES buffer solution was studied. For this purpose, **PEG-GF** membranes (4 x 0.5 cm in size) containing **1** were dipped into different solutions with increasing concentrations of GHB (from 0.01 µM to 100 µM). As can be seen in Figure 4, when the GHB concentration increases a significant enhancement of the fluorescence emission is observed. From the titration profile a LOD of 0.03 µM for GHB from complex **1** in **PEG-GF** strips was determined (Figure 4). This limit of detection outperforms LOD reported for other chromo-fluorogenic sensors used for GHB sensing, which are in the millimolar range for aqueous or in the micromolar range for DMSO solutions.

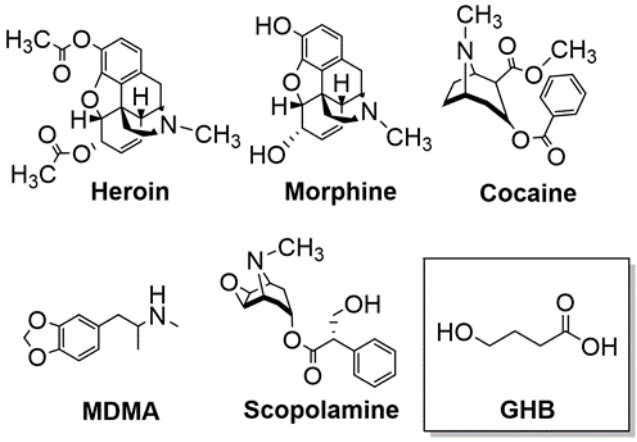

Scheme 2. Chemical structure of the drugs used as interferents for selectivity studies.

We also tested complex **1** integrated into the test strips for the detection of GHB in soft and alcoholic beverages (such as orange juice, wine and gin). For these experiments, we used commercial beverages diluted at 50% with MES buffer that had been either spiked or not with GHB (1 mM). Following a similar procedure as above, the test strips were dipped into 75 µL of the beverages solution. Remarkable differences in the fluorescence emission at zone B was observed between

adulterated and non-adulterated beverages tested, being gin the beverages that shows most significant fluorescence intensity increase in the presence of GHB (Figure 3). Besides, following this procedure the LOD for GHB in gin was as low as 0.1 µM (Figure S3). Overall, the experiments demonstrate the ability of *IDA* probe **1** to identify GHB in alcoholic and soft drinks by using a simple, portable, and rapid (1 minute) assay without the need of trained personnel.

Besides, to demonstrate the selectivity of the system, the fluorogenic response of *IDA* probe **1** in the test strips was evaluated in the presence of other common drugs, such as cocaine, heroin, scopolamine, MDMA, and morphine (Scheme 2). Figure 5 shows the emission of the released coumarin in zone B in the test strip after 1 min from half diluted solutions of gin spiked with the selected drugs (1 µM).

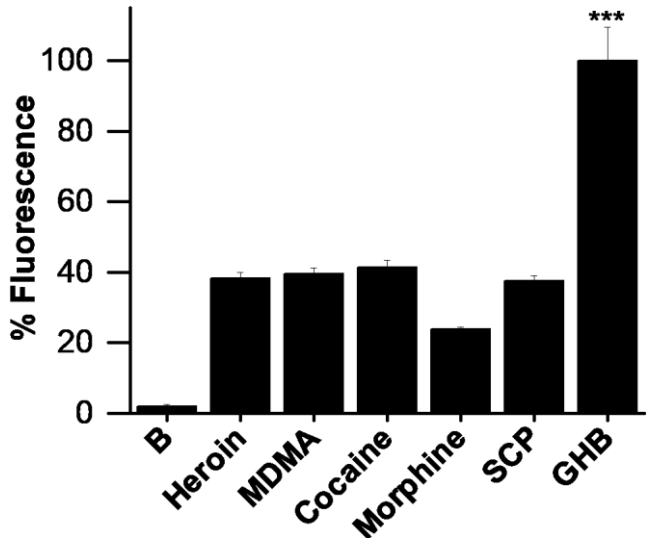

Figure 5. Effect of the indicated drugs (1 µM) on the fluorescence of the coumarin 343 displaced from *IDA* probe **1** in zone B of the test strip in 50% gin solution after 1 min of developing. Error bars are expressed as 3σ for three independent experiments (***p<0.0003).

6.5. CONCLUSIONS

Herein we report the development of a lateral flow assay based on *IDA* probe **1** for the rapid and highly sensitive GHB detection in soft and alcoholic beverages with a fluorescence reader. The sensor consists of a sensing ensemble formed by a Cu^{2+} complex with coumarin 343. The sensing mechanism relies on a displacement of coumarin 343 from the sensing ensemble as a consequence of the higher binding constant between GHB and *IDA* probe **1**. The probe shows a high sensitivity in MES buffer (50 mM, pH 6.0) (detection limit of 0.03 µM). System design and optimization led to straightforward integration into a lateral-flow assay for GHB detection without further treatment or conditioning of the test strips while guaranteeing fast overall assay times of 1 min. Finally, we demonstrated the remarkable robustness of the probe that is able to detect GHB in spiked soft and alcoholic drinks (detection limit of 0.1 µM). The lateral flow assay approach using mobile phones for fluorescence measurements offers a promising methodology for the construction of rapid test kits for practical applications such as roadside drug testing and detection of substances in the workplace or recreational settings.

ASSOCIATED CONTENT

Supporting Information. Materials and methods, determination of binding constants and LOD in MES buffer solution and lateral flow test with fluorescence read-out protocol. “This material is available free of charge via the Internet at http://pubs.acs.org.”

AUTHOR INFORMATION

Corresponding Author

* E-mail: fsanceno@upvnet.upv.es, rmaez@qim.upv.es, and vimarce1@upv.es

Author Contributions

The manuscript was written through contributions of all authors. All authors have given approval to the final version of the manuscript. E.G., G.H., V.M. and

R.M.M. conceived and designed the research, performed most of the experiments, contributed to the experimental designs, data analysis, discussion and writing. E.G., G.H., V.M. and F.S. synthesized and characterized all organic molecules. E.G., G.H. E.C. and V.M. carried out the kinetic studies and determined the sensing features of the molecular sensor. E.G., M.A., F.S. K. R. and R.M.M. analysed the data. Finally, E.G., G.H., V.M., F.S. and R.M.M. wrote the manuscript with feedback from all the authors.

Notes

The authors declare no competing financial interest.

ACKNOWLEDGMENT

This research was funded by the Ministerio de Ciencia, Innovación y Universidades (Spanish Government), the Agencia Estatal de Investigación (AEI) and European Union (projects RTI2018-100910-B-C41 and RTI2018-101599-B-C22-AR (MCIU/AEI/ FEDER, EU) and the Conselleria de Innovación, Universidades, Ciencia y Sociedad Digital, Generalitat Valenciana (Project PROMETEO 2018/024). E. G. is grateful to the Spanish MEC for her FPU grant (FPU16/02464). G. H. thanks to Generalitat Valenciana for his pre-doctoral grant (ACIF/2021/204). V.M.-C thanks the financial support from Generalitat Valenciana (CIDEGENT/2020/031).

6.6. REFERENCES

(1) Xu, W.; Zhai, D.; Chang, Y. T. Detection of GHB by Optical Methods. *Neuropathol. Drug Addict. Subst. Misuse* **2016**, *2*, 529–535.

(2) Ingels, A.-S. M. E.; Wille, S. M. R.; Samyn, N.; Lambert, W. E.; Stove, C. P. Screening and Confirmation Methods for GHB Determination in Biological Fluids. *Anal. Bioanal. Chem.* **2014**, *406* (15), 3553–3577.

(3) Lesar, C. T.; Decatur, J.; Lukasiewicz, E.; Champeil, E. Report on the Analysis of Common Beverages Spiked with Gamma-Hydroxybutyric Acid (GHB) and Gamma-

Butyrolactone (GBL) Using NMR and the PURGE Solvent-Suppression Technique. *Forensic Sci. Int.* **2011**, *212* (1–3), e40–e45.

(4) Gibson, K. M.; Aramaki, S.; Sweetman, L.; Nyhan, W. L.; DeVivo, D. C.; Hodson, A. K.; Jakobs, C. Stable Isotope Dilution Analysis of 4-Hydroxybutyric Acid: An Accurate Method for Quantification in Physiological Fluids and the Prenatal Diagnosis of 4-Hydroxybutyric Aciduria. *Biomed. Environ. Mass Spectrom.* **1990**, *19* (2), 89–93.

(5) McCusker, R. R.; Paget-Wilkes, H.; Chronister, C. W.; Goldberger, B. A.; ElSohly, M. A. Analysis of Gamma-Hydroxybutyrate (GHB) in Urine by Gas Chromatography-Mass Spectrometry. *J. Anal. Toxicol.* **1999**, *23* (5), 301–305.

(6) Baumes, L. A.; Buaki Sogo, M.; Montes-Navajas, P.; Corma, A.; Garcia, H. A Colorimetric Sensor Array for the Detection of the Date-Rape Drug γ-Hydroxybutyric Acid (GHB): A Supramolecular Approach. *Chem. – A Eur. J.* **2010**, *16* (15), 4489–4495.

(7) Zhai, D.; Tan, Y. Q. E.; Xu, W.; Chang, Y.-T. Development of a Fluorescent Sensor for Illicit Date Rape Drug GHB. *Chem. Commun.* **2014**, *50* (22), 2904–2906.

(8) Rodríguez-Nuévalos, S.; Costero, A. M.; Arroyo, P.; Sáez, J. A.; Parra, M.; Sancenón, F.; Martínez-Máñez, R. Protection against Chemical Submission: Naked-Eye Detection of γ-Hydroxybutyric Acid (GHB) in Soft Drinks and Alcoholic Beverages. *Chem. Commun*. **2020**, *56* (83), 12600–12603.

(9) Rodríguez-Nuévalos, S.; Costero, A. M.; Gil, S.; Parra, M.; Gaviña, P. Bifunctionalized Gold Nanoparticles for the Colorimetric Detection of the Drug γ-Hydroxybutyric Acid (GHB) in Beverages. *Chemosens.* **2021**, *9* (7), 160.

(10) Pallavicini, P.; Amendola, V.; Massera, C.; Mundum, E.; Taglietti, A. 'On–off–on' Fluorescent Indicators of PH Windows Based on Three Separated Components. *Chem. Commun*. **2002**, *2* (20), 2452–2453.

(11) Sheykhi, S.; Mosca, L.; Durgala, J. M.; Anzenbacher, P. An Indicator Displacement Assay Recognizes Enantiomers of Chiral Carboxylates. *Chem. Commun*. **2019**, *55* (50), 7183–7186.

(12) Ravikumar, I.; Ghosh, P. Zinc(II) and PPi Selective Fluorescence OFF–ON–OFF Functionality of a Chemosensor in Physiological Conditions. *Inorg. Chem.* **2011,** *50* (10), 4229–4231.

(13) Dengler, J. E.; Lehenmeier, M. W.; Klaus, S.; Anderson, C. E.; Herdtweck, E.; Rieger, B. A One-Component Iron Catalyst for Cyclic Propylene Carbonate Synthesis. *Eur. J. Inorg. Chem.* **2011**, *2011* (3), 336–343.

(14) Costa, E.; Climent, E.; Gawlitza, K.; Wan, W.; Weller, M. G.; Rurack, K.; Optimization of analytical assay performance of antibody-gated indicator-releasing mesoporous silica particles. *J. Mater. Chem. B*, **2020**, *8*, 4950-4961.

(15) Burcu Bahadır, E.; Kemal Sezginturk, M.; Lateral flow assays: Principles, designs and labels. *Trends Analyt. Chem.* **2016**, *82*, 286–306.

(16) Vahid Shirshahi, V.; Liu, G. Enhancing the analytical performance of paper lateral flow assays: From chemistry to engineering. *Trends Analyt. Chem.* **2021**, *136*, 116200-116216.

(17) Sajid, M.; Kawde, A.; Daud, M. Designs, formats and applications of lateral flow assay: A literature review. *J. Saudi Chem. Soc.* **2015**, *19*, 689–705.

(18) Koczula, K. M.; Gallotta, A. Lateral flow assays. *Essays Biochem.* **2016**, *60*, 111–120.

(19) Nguyen, V.; Seungri Song, S.; Park, S.; Joo, C. Recent advances in high-sensitivity detection methods for paper-based lateral-flow assay. *Biosens. Bioelectron.* **2020**, *152*, 112015-112032.

(20) Tohid Mahmoudi, T.; De la Guardia, M.; Baradaran, B. Lateral flow assays towards point-of-care cancer detection: A review of current progress and future trends. *Trends Analyt. Chem.* **2020**, *125*, 115842-115862.

(21) Qin, Z.; Chan, W.; Boulware, D. R.; Akkin, T.; Butler, E. K.; Bischof, J. C. Significantly Improved Analytical Sensitivity of Lateral Flow Immunoassays by Using Thermal Contrast. *Angew. Chem. Int. Ed.* **2012**, *124*, 4434 –4437.

(22) Christopher Pöhlmann, C.; Elßner, T. Multiplex Immunoassay Techniques for On-Site Detection of Security Sensitive Toxins. *Toxins* **2020**, *12*, 727-759.

(23) Costa, E.; Climent, E.; Ast, S.; Michael G. Weller, M. G.; Canning, J.; Rurack, K. Development of a lateral flow test for rapid pyrethroid detection using antibody-gated indicator-releasing hybrid materials. *Analyst*, **2020**, *145*, 3490-3494.

(24) Climent, E.; Rurack, K. Combining electrochemiluminescence detection with aptamer-gated indicator releasing mesoporous nanoparticles enables ppt sensitivity for strip-based rapid tests. *Angew. Chem. Int. Ed.* **2021**, *60*, 2-13.

(25) Climent, E.; Delia Gröninger, D.; Hecht, M.; Walter, M. A.; Martínez-Máñez, R.; Weller, M. G.; Sancenón, F.; Amorós, P.; and

Rurack, K. Selective, Sensitive, and Rapid Analysis with Lateral-Flow Assays Based on Antibody-Gated Dye-Delivery Systems: The

Example of Triacetone Triperoxide. *Chem. Eur. J.* **2013**, *19*, 4117 – 4122.

(26) Climent, E.; Biyikal, M.; Gröninger, D.; Weller, M. G.; Martínez-Máñez, R.; Rurack, K. Multiplexed Detection of Analytes on

Single Test Strips with Antibody- Gated Indicator-Releasing Mesoporous Nanoparticles. *Angew. Chem. Int. Ed.* **2020,** *59*, 23862-23869.

(27) Yu, H.; Tan, Y.; Cunningham, B. T. Smartphone Fluorescence Spectroscopy. *Anal. Chem.* **2014**, *86*, 8805−8813.

(28) Costa, E.; Climent, E.; Gawlitza, K.; Wan, W.; Weller, M. G.; Rurack, K.; Optimization of analytical assay performance of antibody-gated indicator-releasing mesoporous silica particles. *J. Mater. Chem. B*, **2020**, *8*, 4950-4961

6.7. SUPPORTING INFORMATION

1. EXPERIMENTAL PROCEDURE

1.1. Materials and Methods

Chemicals: 2-Quinolinecarboxaldehyde, (±)-*trans*-1,2-diaminocyclohexane, sodium borohydride ($NaBH_4$) were purchased from Sigma Aldrich química (Madrid, Spain). Copper (II) trifluoromethanesulfonate 98% ($Cu(CF_3SO_3)_2$) was purchased from Acros Organics. The drug tested, γ-hydroxybutyric acid (GHB) was kindly provided by "Agencia Española de Medicamentos y Productos Sanitarios" (AEMPS). Saturated sodium chloride (Brine, NaCl sat.) and anhydrous magnesium sulfate ($MgSO_4$) were purchased from Scharlab S.L. 2-(*N*-morpholino)ethanesulfonic acid and tetraethylorthosilicate (TEOS) were purchased from Sigma-Aldrich. Glass fiber and fusion 5 strips were obtained from Whatman™. Filter paper was obtained from Thermofisher Scientific.

Solvents: All solvents were ACS reagent grade or better quality were used without any further purification. Methanol, anhydrous methanol, and anhydrous dichloromethane, were purchased from Scharlab S.L.

General techniques: The reaction progress was monitored by thin-layer chromatography on precoated TLC plates, silica gel on TLC Al foils SIGMA-ALDRICH with fluorescent indicator 254 nm (60 Å medium pore diameter). Spots were visualized under 254 nm UV light and by carrying with phosphomolybdic acid. ^{1}H and ^{13}C NMR spectra were respectively recorded at 400 MHz and 100 MHz on a Bruker 400 Avance III instrument. 2-D COSY and HSQC experiments were carried out to assist in signal assignment. Solutions were used in $CDCl_3$. The chemical shift values are given in parts per million (ppm) from low to high field and referenced to residual solvent. Standard abbreviations indicating multiplicity are used as follows:

s = singlet, d = doublet, t = triplet, q = quartet, m = multiplet. The values of the coupling constant (*J*) are measured in Hz. UV spectrophotometry measurements were recorded using a JASCO V-650 UV/vis spectrophotometer. Fluorescence spectroscopy measurements were taken on a JASCO FP-8300 spectrofluorometer (Hitachi High Technologies). For ESI-TOF-MS mass spectra, 0.1 pM concentrations were used. For the smartphone-based approach, a 3D-box was printed with black PLA using an Ultimaker 3 printer. LEDs and optical filters were purchased from Thorlabs. Photographs were taken with a Samsung Galaxy S7 and values retrieved from images via the integrated density with the software ImageJ, i.e., the product of mean grey value $\overline{G}$, $\overline{G}$ = (red + green + blue)/3, and the selected area a (in square pixels).

2. RESULTS AND DISCUSSIONS

2.1. Determination of LOD in MES buffer solution

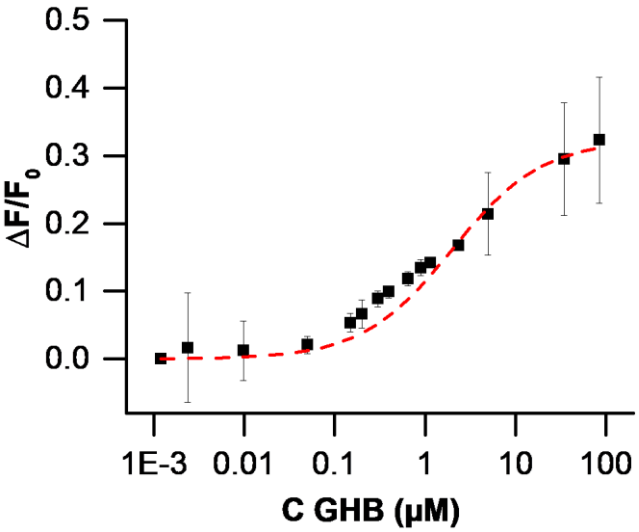

Figure S1. Fluorescence intensity of coumarin 343 displaced from *IDA* probe **1** in the presence of different amounts of GHB in MES buffer (50 mM) at pH 6.0. Error bars are expressed as 3σ for three independent experiments.

2.2. Determination of GHB on lateral flow assays

Preparation of wax-patterned, PEG-coated glass fiber paper (SiO_2-PEG-Materials). A mixture of 3.4 mL Milli-Q water, 7.4 mL ethanol, 2.7 mL TEOS, 300 µL 3-(methoxy (polyethyleneoxy)propyl)trimethoxy silane (PEG) and 180 µL NH_3 (32%) was placed in a 20 ml vial containing 30 glass fiber strips of 8 x 2.5 cm. After reaction for 24 h at room temperature with orbital stirring, the SiO_2-PEG-material strips were washed with ethanol and dried at 37 ºC.

Conditions and materials optimization in lateral flow assay.

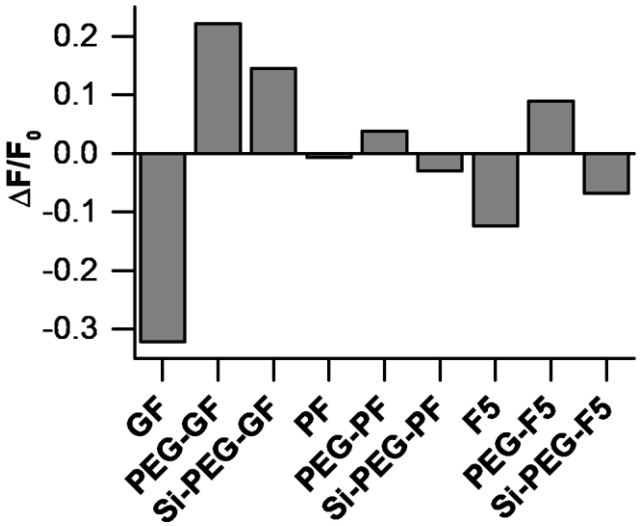

Figure S2. Fluorescence intensity of coumarin 343 displaced from *IDA* probe **1** in different materials measured in zone B in the lateral flow assay in the presence of GHB (1 mM) in MES buffer at pH 6.0 after 1 min of dipped.

2.3. Lateral flow tests with fluorescence read-out protocol

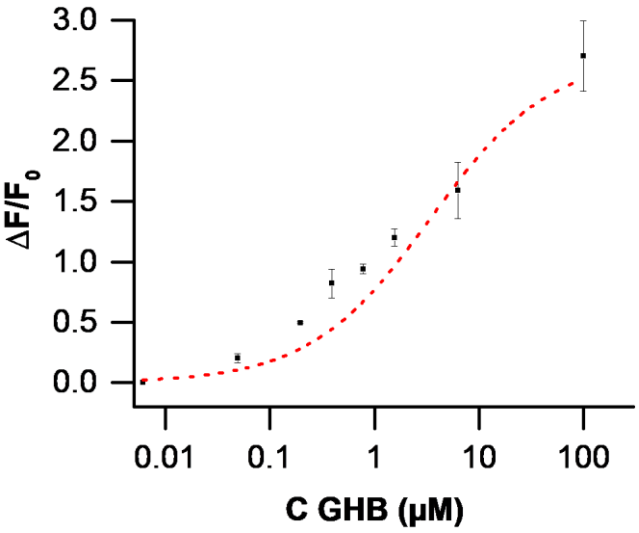

Figure S3. Increase in fluorescence intensity of coumarin 343 displaced from *IDA* probe **1** measured in zone B in the lateral flow assay in the presence of different amounts of GHB in 50% of gin after 1 min of dipped. Error bars are expressed as 3σ for three independent experiments.

3. CHARACTERIZATION OF PEG-GF STRIPS

TGA and EA analysis were also performed to quantitatively estimate the amount of PEG on the modified **PEG-GF** fibers. Figure S6 shows the mass loss as a function of the temperature determined from TGA analysis for the reference membrane GF (black line) and for the modified paper **PEG-GF** (red line). TGA analysis revealed a mass loss of 3.34% of organic matter for **PEG-GF** (curve b) with respect to GF membranes (curve a) corresponding with a content of 88 ± 0.015 μmol C/g SiO_2 for **PEG-GF** membranes and 8 ± 0.9 μmol C/ g SiO_2 for GF.

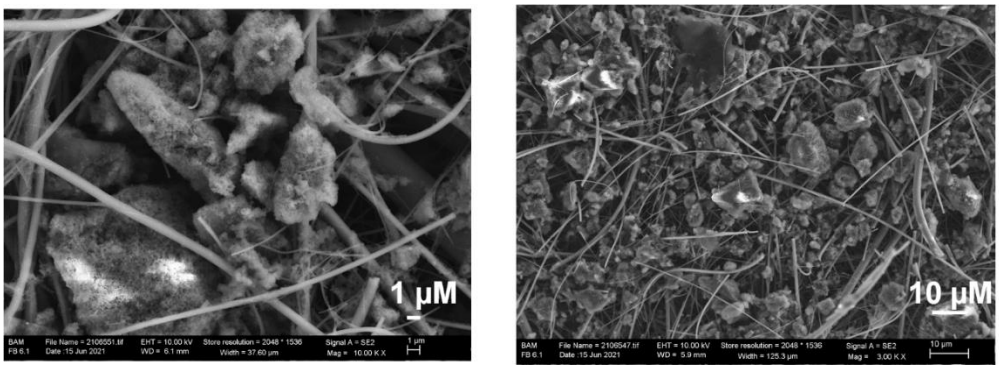

Figure S4. Representative SEM micrographs of the **PEG-GF** fibers.

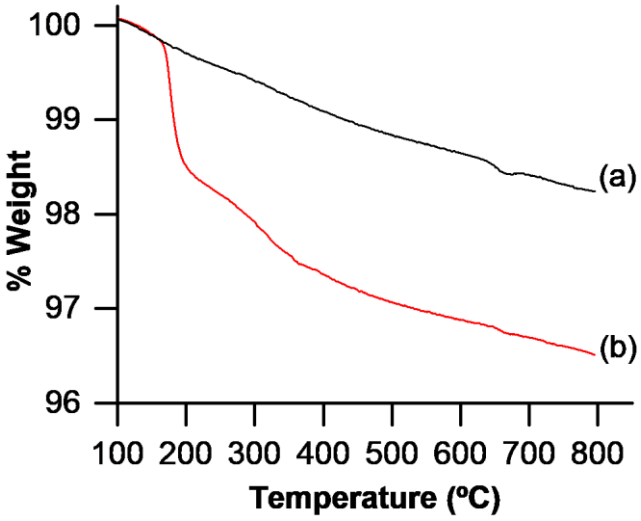

Figure S5. Thermogravimetric analysis for (a) **GF** and (b) **PEG-GF** membranes.

CHAPTER 7

CONCLUSIONS AND PERSPECTIVES

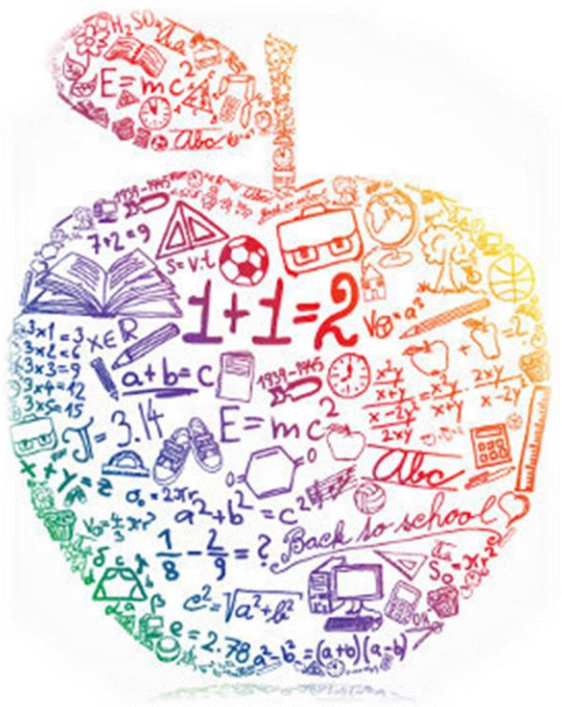

The development of reliable tools for the early and selective detection of drugs of abuse is a current area of attention due to the lack of systems able to generate a quantifiable signal in a short period of time. In this regard, the unique structural features of MSNs facilitates efficient loading of different molecules (such as dyes, fluorophores and drugs) and its subsequent controlled release at the target site or in response to an analyte, enabling its use in several fields such as medicine, agriculture, sensing, among others. Therefore, MSNs have risen to great importance in the field of sensing, as they provide viable alternatives to the continuous challenges related to lower detection limits and non-specific effects. Apart from MSNs, transition metal complexes play a prominent role in the sensing of psychoactive drugs owing to their rich photophysical characteristics. In this context, this PhD thesis has explored the design, characterization, and evaluation of smart biomolecule-gated nanodevices based on MSNs functionalized with various biological moieties as molecular gates and the synthesis of a transition-metal complexes.

The third chapter of this PhD thesis describes a fluorogenic nanosensor based on the incorporation of the 5-HT_{2A} receptor-specific antibody as a capping element in the outer surface of nanoparticles that enable the entrapped dye release only in response to the hallucinogenic drug, 25I-NBOMe. This nanosensor is constructed using MCM-41 type MSNs loaded with rhodamine B (as a model

fluorophore) and functionalized with a serotonin derivative that interacts with the 5-HT_{2A} antibody. The recognition mechanism involves an affinity binding assay where 5-HT_{2A} antibody shows a higher binding affinity for the 25I-NBOMe than has for the anchored serotonin derivative. In the presence of the target analyte, the antibody detachment from the nanoparticles external surface is triggered, leading the release of the encapsulated dye. From titration experiments, the nanodevice showed a detection limit as low as 0.6 µM in buffer solution. A similar behavior was found in artificial saliva with a value of 0.9 µM for the detection limit. In addition, the prepared nanosensor displayed a high selectivity in the presence of other common drugs such as cocaine, heroin, mescaline, lysergic acid diethylamide, MDMA, and morphine. Finally, the sensor is able to distinguish adulterated sweets and thereby detect chemical submission attempts.

The fourth chapter reports a bio-inspired dopamine transporter-capped optical nanomaterials for straightforward and sensitive cannibal drug (MDPV) detection in both saliva and blood plasma. MSNs were loaded with a fluorescent dye that was encapsulated as a result of a selective recognition between the recombinant human dopamine transporter and the dopamine derivative anchored onto the external surface of the MCM-41 material. The synthesized nanodevice is solely responsive to MDPV, even in the presence of other drugs whose use is widespread, with a detection limit of 5.2 µM in aqueous solution. The sensing mechanism relies on displacement of the dopamine transporter from the nanoparticles surface after its preferential coordination with MDPV. The performance of the sensor was evaluated in competitive media displaying a similar response to that observed in buffered solution.

In the fifth chapter, a dual-track strip with smartphone read out for simultaneous MDPV and scopolamine detection in saliva samples was developed. In a first step, the preparation, characterization, and behavior assessment of the nanoprobe for the scopolamine detection was carried out. The design is based on

the filling of the empty MCM-41 pores with a fluorescent dye and subsequent functionalization of the external surface with bethanechol (an agonist of M_2-AChR receptor). Then, the pores were completely capped due to non-covalent interaction of the grafted bethanechol with M_2-AChR. It has been showed payload delivery is only observed in the presence of MDPV and not tuned by other common illicit drugs. Afterwards, it is worth pointing out that the detection limit reached was as low as 92 μM in buffered solution and 103 μM in saliva samples. In a second step, scopolamine and MDPV nanosensors were integrated into WAX-GF membranes and studied their behavior individually in the portable lateral flow assay with smartphone readout in less 10 minutes. These facts demonstrated the ability to a highly selective and sensitive detection of both illicit drugs in saliva samples. Remarkably, experiments with both nanodevices integrated into a dual lateral flow assay enabling to distinguish among different concentrations of each drug in saliva samples. Hence, this system provides a highly appealing and reliable approach for the development of portable devices with short assay times and easily handling for the accurate detection of a large number of analytes in complex matrices.

The sixth chapter describes an indicator displacement assay (*IDA*) for GHB using a sensing ensemble based on a colorimetric Cu^{2+} complex with a tetradentate ligand and the fluorescent dye coumarin 343. The *IDA* assay developed allowed GHB detection in aqueous media with a limit of detection of 0.06 μM. In addition, a simple, rapid and portable lateral flow assay coupled with smartphone readout was developed for the detection of GHB in alcoholic beverages in less than 1 minute. Thus, the design and development of molecular sensor that respond to psychoactive drugs could be an interesting tool in the *in situ* identification of chemical submission cases.

Finally, a general conclusion that can be extracted from this PhD thesis is that the incorporation of antibodies or specific receptors on MSNs allows to prepare sensory nanodevices with a highly selective and sensitive response for a

wide variety of new psychoactive drugs detection which currently lack reliable methods. As well as the synthesis of molecular sensors enables rapid analysis of multiple analytes is a useful tool in the sensing field. On the other hand, the development of portable and easily handled point-of-care tests combined with fluorescent reader via smartphone represent a potential methodology to produce devices that may become powerful tools for new challenging applications such as early chemical submission cases detection. Moreover, because of the long shelf life and the fact that refrigeration is not required for their storage, lateral flow assays are very well adapted for use in developing countries, small ambulatory care settings, at customs by the authorities, pubs and battlefields.

As additional future perspectives, the results achieved in this PhD thesis open and encouraged us to pursue new research opportunities and projects. In this sense, the combination of nanomaterials or molecular complexes with biological molecules in point-of-care processes enhances the selectivity of the current detection methods and can improve the production of nanosensors for more complex and ambitious purposes. In this regard, the inclusion of these systems among police forces, health personnel, in pubs or among young people enable to detect early cases of drug trafficking, illicit drug use or drug facilitated sexual assaults.

Gracias al Ministerio de Educación, Cultura y Deporte por el contrato concedido para realizar esta tesis doctoral.